



**MECHANICS OF A FUNCTIONALLY-
GRADED TITANIUM MATRIX COMPOSITE**

THESIS

G. Brandt Miller, Captain, USAF

AFIT/GMS/ENY/00M-01

DEPARTMENT OF THE AIR FORCE
AIR UNIVERSITY

AIR FORCE INSTITUTE OF TECHNOLOGY

Wright-Patterson Air Force Base, Ohio

APPROVED FOR PUBLIC RELEASE; DISTRIBUTION UNLIMITED.

DTIC QUALITY INSPECTED 4

20000803 140

“The views expressed in this thesis are those of the author and do not reflect the official policy or position of the Department of Defense or the U. S. Government.”

MECHANICS OF A FUNCTIONALLY-GRADED TITANIUM MATRIX

COMPOSITE

THESIS

Presented to the Faculty

Graduate School of Engineering and Management

Air Force Institute of Technology

Air University

Air Education and Training Command

In Partial Fulfillment of the Requirements for the

Degree of Masters of Science in Material Science Engineering

G. Brandt Miller, B.S.

Captain, USAF

March 2000

MECHANICS OF A FUNCTIONALLY-GRADED TITANIUM MATRIX
COMPOSITE

G. Brandt Miller, B.S.

Captain, USAF

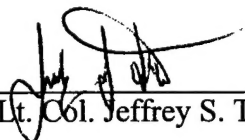
Approved:



Dr. Shankar Mall (Chairman)

3/10/00

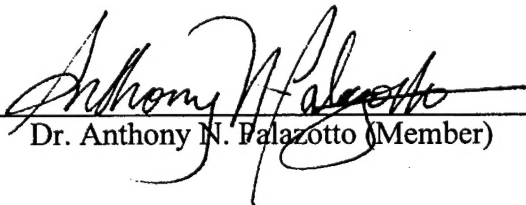
(date)



Lt. Col. Jeffrey S. Turcotte (Member)

10 MAR 2000

(date)



Dr. Anthony N. Palazotto (Member)

10 Mar 2000

(date)

Acknowledgements

I would like to express my appreciation to all of those who have helped me complete this thesis effort. I would like to especially thank the following people for their valuable assistance – without which I could not have found the successful resolution to the numerous setbacks specific to this work and inherent with research in general.. I thank my thesis advisor, Dr. Shankar Mall, for his valuable insights, guidance, and advice. He helped me see the big picture and yet encouraged me to keep focused on the task at hand. The AFIT Machine Shop (Russ and Condi), of their own initiative, found a better machining process which reduced the time to produce test samples by 75 percent. I gained a huge appreciation for skilled technicians and what they can teach me from my association with them. Mr. Ken Goeke of AFRL/ML single-handedly helped me overcome the thorny issue of grip failures during fatigue testing. I appreciate greatly his expertise; he helped me solve in half an hour a problem which had set me back for a month. Ms. Luann Piazza of AFRL/ML was invaluable as an experienced SEM operator who knows the art and science to good imaging. Without her help and patience, I could not have determined the existence and composition of the inclusions which played a key role in this study. I would also like to thank Dr. Daniel Eylon of the University of Dayton for his willingness to review my work and to help me verify the results of my work. Lastly, I would like to thank Rachel for her support and encouragement.

Table of Contents

	Page
List of Figures	viii
List of Tables	x
Abstract	xi
1. Introduction	1
1.1. Background.....	1
1.2. Functionally-Graded Composites: A Possible Solution	2
1.3. Objective.....	3
1.4. Potential Benefits.....	5
2. Previous Works	6
2.1. Introduction	6
2.2. Ti 6-4 Titanium Alloy.....	7
2.3. Titanium Matrix Composites (TMCs).....	8
2.3.1. Fiber/Matrix Interface.....	9
2.3.2. Fatigue.....	11
2.3.3. Monotonic Loading.....	12
2.3.4. Tension-Compression Fatigue	13
2.4. Joint Region – Functionally Graded Titanium Matrix Composite	14
2.4.1. Deformation by Damage.....	15
2.4.2. Deformation by Plasticity	16
2.4.3. Combined Deformation Mechanisms	17
2.4.4. Strain Effects.....	18

2.4.5. Analysis.....	18
2.5. Similar Efforts	19
2.6. Summary.....	20
3. Test Procedures	21
3.1. Objective.....	21
3.2. Description of Test Material.....	21
3.2.1. Fabrication Details	21
3.2.2. Test Panel Description	26
3.2.3. Specimen Dimensions.....	28
3.3. Test Specimen Preparation	30
3.3.1. Machining and Polishing	30
3.3.2. Tabbing Procedure	31
3.4. Testing Method.....	32
3.4.1. Monotonic vs. Interrupted Tension Tests	32
3.4.2. Tension-Tension (TT) Fatigue Testing.....	33
3.5. Test Equipment.....	34
3.5.1. Apparati.....	34
3.5.2. Data Collection	36
4. Results and Discussions	37
4.1. Tensile Testing	37
4.1.1. Discussion of Results (Parent Materials).....	37
4.1.2. Discussion of Results (Functionally-Graded Material)	38
4.2. Tension-Tension Fatigue Testing	41

4.2.1. Introduction.....	41
4.2.2. Discussion of Results (Parent Materials).....	41
4.2.3. Discussion of Results (Functionally-Graded Materials).....	44
4.2.4. Investigation of Premature Failure Source	46
4.2.5. Lessons Learned.....	60
4.3. Determining the Fatigue Life of Functionally-Graded Material	63
4.3.1. Fatigue Life: Lower Bounds (Inclusion-Free Titanium)	64
4.3.2. Fatigue Life: Upper Bounds (Alloy-Clad Titanium Matrix Composite).....	66
4.3.3. Comparison and Discussion of S-N Curves.....	68
4.4. Fracture Toughness.....	71
5. Conclusions and Recommendations.....	74
5.1. Conclusions	74
5.2. Recommendations	75
Appendix A: Additional Graphical Results of Tensile Testing	77
Appendix B: Additional SEM Images of Fracture Surfaces.....	79
Appendix C: X-ray Spectroscopy of Inclusions	85
Appendix D: Comparison of Toughness and Fatigue	89
Vita.....	91
Bibliography	92

List of Figures

Figure 3.1: ARC's lay-up/consolidation process	23
Figure 3.2: Joint Region – Taper Angle Geometries	27
Figure 3.3: Actual-Size Test Specimen	29
Figure 3.4: Overall view of test setup	35
Figure 3.5: Detail view of setup for tensile and fatigue testing	35
Figure 4.1: Specimen #199 stress-strain curve (monotonic tensile test)	38
Figure 4.2: Specimen #204 stress-strain curve (interrupted tensile testing)	38
Figure 4.3: S-N curve for titanium alloy, titanium composite, and both F/G materials. ..	43
Figure 4.4: S-N curve showing consolidated data	45
Figure 4.5: Specimen B3 (F/G, 20:1 taper) fracture surface.....	47
Figure 4.6: Specimen B3 fracture surface (close-up view of flaw)	47
Figure 4.7: Specimen C4 (monolithic alloy) fracture surface.....	49
Figure 4.8: Specimen C4 fracture surface – detail view	50
Figure 4.9: Specimen B2 (20:1 taper) fracture surface.....	52
Figure 4.10: Specimen B2 – detail view.....	53
Figure 4.11: Specimen 200 (4:1 taper) fracture surface	55
Figure 4.13: Specimen 200 (4:1 F/G) – detail view.....	56
Figure 4.14: Specimen A2 (4:1 F/G) fracture surface.	57
Figure 4.15: Specimen A3 (4:1 taper) fracture	61
Figure 4.16: Specimen A3 (4:1 F/G) – detail view.....	62
Figure 4.17: Comparison of the S-N curves derived from Eylon et al.	65

Figure 4.18: Comparison of the S-N curves derived from Ramamurty	67
Figure 4.19: Comparison of S-N curve data by Eylon to data by Ramamurty	69
Figure 5.1: Improved F/G TMC design	76
Figure A.1: Stress-strain curve for the 4:1 taper hybrid (Specimen #199	77
Figure A.2: Stress-strain curve for the 20:1 taper hybrid (Specimen #204).....	78
Figure B.1: Specimen A2 fracture surface.....	79
Figure B.2: Specimen B2 fracture surface.....	80
Figure B.3: Specimen 200 fracture surface.....	81
Figure B.4: Specimen C5 (monolithic alloy) fracture surface	82
Figure B.5: Close-up of flaw on C5 fracture surface.....	83
Figure B.6: Specimen B1 (20:1 taper) fracture surface	84
Figure C.1: Chemical composition of Specimen 200 inclusion (fiber shard).....	85
Figure C.2: Specimen A3 inclusion chemical composition.....	86
Figure C.3: Specimen A3 fiber shard chemical composition	87
Figure C.4: Specimen C5 flaw chemical composition (inclusion reaction zone).....	88
Figure D.1: Scatterband comparison of room temperature fatigue crack growth rate.....	89
Figure D.2: Comparison of fatigue life of Ti-6Al-4V PA, high and low contaminate.....	90

List of Tables

Table 4.1: Tensile Test Results	37
Table 4.2: Tension-Tension Fatigue Test Results ($R=0.1$, 10 Hz, $T \approx 20$ °C)	42

Abstract

Functionally-graded Titanium Matrix Composites (F/G TMCs) combine the ideal properties of titanium matrix composites with the more practical machining qualities of monolithic (unreinforced) alloy. This material shows great promise in application to aerospace structural components – even in parts whose design requirements have defied the use of composite materials in the past. Successful implementation of such a material would lead to enhanced aircraft performance.

However, the basic properties of a functionally-graded titanium matrix composite need to be investigated. The composite/alloy transition region, or joint area, may be less strong than its constituents and therefore determine the overall performance of the material. Therefore, this work studied the properties (modulus of elasticity, failure strength) and mechanical behavior (fatigue and deformation/failure mechanisms) of the joint area as the first step in further testing and future evaluation of this material. The scope of this effort involved tension and fatigue testing. The results of this study found that the transition region was more robust than expected: the joint area shows a combination of the properties for the parent materials and is nearly as strong as the unreinforced alloy. The deformation mechanism of the joint area was determined to be plasticity, and not damage. As a result, the monolithic alloy proved to be the source of failure in fatigue loading. This indicates that strain values in the monolithic alloy play a key role in the fatigue life of the entire material. These findings encourage further evaluation of functionally-graded titanium matrix composites.

MECHANICS OF A FUNCTIONALLY-GRADED TITANIUM MATRIX COMPOSITE

1. Introduction

1.1. Background

Acceptance and implementation of advanced composite materials into both military and commercial aerospace systems has made considerable progress over the last fifteen years. In particular, composite materials (both polymer matrix and metal matrix composites) are desirable for use in high-performance aircraft (such as fighter jets) due to their high strength- and stiffness-to-weight ratios, superior fatigue properties, and crack growth resistance. For components subject to large out-of-plane loading (bending), metal matrix composites (MMCs) have found successful application. Using these new materials has reduced the weight of the airframe, thereby increasing the aircraft's speed, endurance, range, and payload. However, not all aircraft structural components are suited for composites. As considered from a fabrication and functional standpoint, there are many mechanical interfaces (bearing runs, seals, attachment points) in some structural components which are difficult areas for any composite material application. This is because machining or drilling into composite material invariably cuts through fibers,

rendering the material weaker than the matrix material. Currently, the complexity of these components virtually precludes the use of composites and has therefore required the use of monolithic material. This has limited the application (and thus the weight-saving benefits) of advanced composite materials employed in high-performance aircraft.

1.2. Functionally-Graded Composites: A Possible Solution

Titanium matrix composites (TMCs), reinforced with continuous silicon carbide fibers, have many of the attractive properties for composites listed above, including superior environmental resistance. TMCs have been employed successfully in several high-temperature applications in jet aircraft, including turbine blades. However, there are many potential applications in airframe structural components [1]. TMCs could provide an almost two-fold increase in structural efficiency as compared to unreinforced titanium alloys [2]. In terms of depot maintenance alone, a titanium composite landing gear system could save as much as \$900k annually (as compared to a system of high-strength steel), since field experience has shown that TMCs are impervious to corrosion and do not require painting or special plating [3]. The fabrication processes for TMCs are proven and reliable [2]. Research and implementation of this material over the last 20 years demonstrates that this material is technically feasible and “ready to deliver the projected benefits” [2]. However, as mentioned above, one of the major obstacles preventing widespread application of advanced composite materials is that of machining and mechanical interfacing. Past attempts to sidestep this drawback have included

welding (or otherwise bonding) sections of monolithic titanium alloy to TMCs in order to incorporate the benefits of composite material. These attempts met with limited success, but encouraged further investigation of a part composite, part alloy (or “functionally graded”) material that combined the attractive properties of composites with the machineability of metal.

Recently, joining monolithic to composite material has been done using powder metallurgy techniques, in one step, during fabrication. This technique has been successfully applied to incorporate monolithic titanium sections into the ends of TMC landing gear cylinders [3], gas turbine engine shafts, and other components [2, 4] for welding/joining purposes. This new fabrication method could possibly remove the machineability barrier that has limited the application of TMCs (and composites in general) from aircraft structural components. However, there is a complete lack of mechanical characterization of this titanium alloy/composite, functionally graded material. Understanding the basic material properties of such a material is critical before any application can be made.

1.3. Objective

As the first step toward a fundamental understanding of the mechanics and material properties of this material, the integrally fabricated joint connecting the monolithic alloy to the composite should be studied. The objective of this study is to do just that: to compare the properties of the joint interface to those of the monolithic alloy

and pure composite and to make some basic characterizations of this functionally graded, titanium matrix composite (F/G TMC) material. An extensive literature search revealed no previous or current research concerning the properties of integrally fabricated joints between a composite and monolithic alloy. Therefore, the scope of this effort is to investigate the basic, fundamental properties of F/G TMC material under monotonic and fatigue loadings and compare them to those of the parent materials. Further, this study will be limited to room temperature condition, as it is focused to application of this material in aircraft structural components.

This functionally-graded material employs a double scarf joint to transition from composite to monolithic titanium. This study uses scarf joints of two different taper angles to determine its effect on the overall mechanical behavior of the material. It has been theorized that a narrower taper angle will provide a stronger joint. However, a narrow taper angle requires a longer joint section which might not be practical for a small component, might not be feasible on a manufacturing standpoint, or may adversely affect machining/grinding characteristics [2]. Therefore, a tradeoff is involved to find the optimum taper angle resulting in an adequately strong joint that also satisfies functional constraints. This study will investigate two different taper angles as the first step in determining an optimal configuration.

It may be possible to model the mechanics of the joint region in order to better understand and predict its behavior. Past research over the last 30 years has produced several finite element models (FEM) attempting to describe the mechanics of various

composite materials. This study will compare the results of the joint region's behavior to previous models in the hopes that correlation may be found.

1.4. Potential Benefits

This study will establish the basic properties of F/G TMCs. If the findings are encouraging, it will lead to further research and testing. This, in turn, may pay significant dividends towards the larger effort: acceptance and implementation of additional advanced composite materials (such as titanium matrix composites) in aerospace vehicles to increase performance. Therefore, although this work has a narrow, direct focus, it is nevertheless an essential part of a larger effort that may have significant benefits to the Air Force.

2. Previous Works

2.1. Introduction

As explained in the previous section, the key feature (and the biggest unknown) in the functionally-graded titanium matrix composite (F/G TMC) material is the transition area, from composite to monolithic material. This joint region could be the potential “weak link”, and determining its mechanical behavior and properties are essential in future evaluation and acceptance of such a material. In order to characterize the mechanics at the joint, it is first necessary to review previous research efforts in the parent materials, as well as that of the joint region. This section is therefore divided into three categories of previous work: (1) monolithic alloy (especially work done in powder metallurgy), (2) titanium matrix composites (especially the SCS-6/Ti family of materials), and (3) joint characteristics. Although research into the mechanical properties and failure characteristics of alloy-to-composite transition/joint region is practically nonexistent, there are many features of existing theories and past efforts in composite research that may prove insightful to the current work. These past theories and efforts form a foundation for understanding (and perhaps modeling/predicting) the joint characteristics under monotonic and fatigue loading.

2.2. Ti 6-4 Titanium Alloy

The mechanical characteristic and material properties of Ti 6-4, under a variety of different fabrication techniques, are well-documented. Values such as Young's modulus, ultimate and yield strength, Poisson's ratio, and other basic properties have been studied carefully, since both the aviation and the biomechanical industries have used Ti 6-4 in the past as their titanium alloy of choice. The deformation mechanisms and damage modes are understood. Studies involving monotonic loading, fatigue loading (both tensile and compressive), and life prediction methodologies have been conducted since the mid-sixties and refined thereafter. The properties of Ti 6-4 formed by powder metallurgy (PM) techniques are also well-understood and represent an area of study since the early 1980s and beyond. Early fabrication efforts in powder metallurgy were less than desirable since the consolidated material was not 100% dense, meaning that voids were present. These voids led to early crack growth and premature failure when compared to conventional fabrication methods. Later advances with using hot isostatic pressing (HIP) in the late 1980s and mid 1990s were able to produce material with virtually full density [5, 6].

Several studies have compared the mechanical properties [7] and the fatigue life curves [8, 9] of Ti 6-4 using various fabrication methods. Titanium parts fabricated using powder metallurgy techniques typically have a fatigue life curve lower than those parts produced from wrought processing but higher than parts made by casting [10].

2.3. Titanium Matrix Composites (TMCs)

Since the inception of TMCs in the eighties, “considerable development and progress have occurred towards their characterization, evaluation, and application in aircraft engines and structures” [11]. In terms of advances in fabrication and manufacturing, significant improvements have been made in the mechanical properties of TMCs when compared with material produced in the early 1980s [12]. For the most part, these advancements have led to a reduction in the number of defects such as matrix porosity and fiber distribution inhomogeneities.

The mechanical behavior of TMCs is significantly different than for the monolithic alloy and has been the subject of intense study since early in this decade. There have been numerous studies of TMCs involving both experiments and analyses [11]. Research efforts include: tension-compression fatigue testing in cross-ply configuration [13], fatigue behavior at elevated temperatures under strain control [17], high temperature tension-compression fatigue [14], the effect of frequency on fatigue [15], the effect of elevated temperatures on fatigue [15], the effect of thermal cycling [16], and fatigue behavior in a cross-ply configuration [17]. These efforts have contributed to well-defined life prediction models for the class of TMCs using Ti 6-4 alloy reinforced with monofilament silicon carbide fibers.

Research has shown that TMCs are sensitive to ply orientation. For example, a 90°-ply TMC (where fibers are oriented perpendicular to the loading direction) have a lower fatigue life than does unreinforced titanium [13]. For this reason, most TMCs

employ 0°-ply laminates only. The possible significance of this finding toward the current work will be discussed later in this section.

2.3.1. Fiber/Matrix Interface

Jeng, Yang, and Yang studied the nature and properties of the fiber/matrix interface and determined it plays a “critical role in the performance and failure behavior of the composite” [18]. They conducted experiments in order to quantify the interfacial properties of several TMCs, including SCS-6/Ti 6-4 (which is similar to the material used in this effort). They found that the fiber/matrix interface reaction products were mostly TiC, with the other alloying elements (vanadium and aluminum) not involved in the reaction. This TiC-rich reaction “zone” surrounds the fiber and its extent into the matrix varies, from roughly 0.5 to 4 microns into the matrix. Their work found that the fiber strength decreases rapidly as a function of increasing reaction zone thickness, with the maximum allowable thickness being 0.93 microns without significantly degrading fiber strength. This relationship between fiber strength and reaction zone thickness is attributed to the formation of notches on the fiber surface. These notches are created by premature fracture in the reaction zone. The larger the reaction zone, the higher the occurrence of these fracture sites. They determined that this premature reaction zone fracture is influenced by such factors as fiber surface chemistry, matrix alloy composition, and residual stresses at the interface [18]. Clyne and Watson also report that a thick reaction layer in TMCs impairs composite performance [12], and other

research also shows that the crack initiation energy decreases as the reaction zone increases [19].

Jeng et al. found that this TiC-rich reaction zone between the SCS-6 fiber and the titanium matrix is weaker and more brittle than the matrix. They found a large reaction zone not only weakens the fiber but also the tensile strength of the reaction zone. This is because “the probability of finding strength-limiting flaws increases as the thickness of the reaction zone increases” [20]. They also determined that the interfacial bonding strength affected the stress-strain response, damage initiation and growth, and the fracture behavior of the composite. Damage growth occurs from microcracks originating in the brittle reaction layer. They found that, for a tough matrix and high interfacial bonding strength (such as in the case of SCS-6/Ti 6-4), matrix microyielding leads to blunting of the crack. In such case, if the adjacent fiber is strong, the crack will not propagate along the fiber and cause debonding. The fracture of the composite is most likely caused “by fiber fracture, which occurs randomly throughout the composite because of the statistical scatter of the fiber strength” [20]. Previous studies show that the strength of TMCs with this type of failure mechanism is determined by the critical fiber length and stress concentration factor of the remaining intact fibers on the plane [21, 22].

Jeng et al. found that the critical defect size required to initiate brittle fracture of the SCS-6/Ti 6-4 composite is on the order of a few fiber diameters [20]. The failure of several adjacent fibers in the same plane may be sufficient to initiate failure of the composite.

2.3.2. Tension-Tension Fatigue Behavior

The loading-unloading response of the material can provide valuable insights into the mechanics of deformation mechanisms and constitutive response of TMCs – not only because this behavior has been well documented, but also since this type of loading closely parallels most operating conditions [11]. Factors which affect fatigue life include ply orientation, loading type, temperature/environment, fiber volume fraction, and interface properties [23].

Studies for tension-tension fatigue testing of 0-ply laminates at room temperature conditions revealed that failure is either matrix-dominated, fiber-dominated, or due to fiber-matrix interfacial debonding/cracking [24]. Many researchers have described the failure mechanisms of TMCs by dividing the fatigue life diagram into distinct regions according to these three failure modes [13, 14, 17, 23, 25, 26, 40]. These regions can be classified as follows: matrix-dominated damage (below 1300 MPa maximum stress loading), fiber-matrix interfacial failure (between 1300 and 2200 MPa), and fiber-dominated damage (above 2200 MPa). Low-cycle fatigue life is controlled by several important mechanisms: crack initiation at the reaction layer or surface defects, crack propagation rate in the matrix, and fiber strength. High-cycle fatigue life is controlled by matrix properties such as matrix toughness, as well as crack initiation in the reaction zone. Beneath a certain loading, the material exhibits “infinite life” (greater than 10^6 cycles) and will not fail even though it is saturated with matrix cracks. In this condition, the fibers essentially carry the entire load, since the matrix is virtually cracked completely through the cross section [25]. After the onset of matrix cracking, cracks nucleate and

grow throughout the matrix. However, the fibers act to retard crack growth by “bridging” both sides of the crack surface, preventing cracks from linking up. During fatigue crack growth, the TMC specimen will fracture if the maximum stress carried by the bridging fibers reaches the ultimate strength of the fiber (as determined by the *in situ* fiber bundle strength). If the fiber fracture criterion is not met, eventually the cracks will link up to the point that the merged cracks span the entire cross-section of the area, and the fibers are completely carrying the entire load [40].

Johnson, Lubowinski, and Highsmith, determined that heat treatment (16 hours, 482°C) increased the yield strength, ultimate strength, and stiffness of the matrix. This heat treatment also caused a chemical reaction between the fiber and the matrix; they were among the first to term it the “reaction zone” [24]. However, further heat treatment is detrimental in that this reaction zone is more brittle than the matrix and can initiate cracks in both the fiber and the matrix. Jeng et al. report that the biggest factor in improving the fatigue life is to eliminate surface defects and to control the thickness of this reaction layer to be as small as possible [25].

2.3.3. Monotonic Loading Behavior

Monotonic tensile loading can be viewed as the extreme case of low-cycle fatigue: failure mechanisms are similar; both exhibit fiber-dominated failure. Once enough fibers fail in roughly the same plane perpendicular to loading, fracture will occur.

Although the matrix plays little role in carrying the load as monotonic loading progresses towards failure, observing its deformation behavior may be important to the

present effort. During monotonic loading, matrix plasticity can occur before fiber-matrix debonding, with the region of highest plasticity located near the fiber-matrix interface as well as the expected region in front of matrix cracks [26]. However, cracks in the reaction zone form prior to matrix plasticity, and play a role in causing matrix plasticity [27].

2.3.4. Tension-Compression Fatigue Behavior

Studies have investigated the effects of cyclic response at varying load ratios and frequencies. On a maximum stress (σ_{\max}) basis, TMCs subjected to tension-tension fatigue testing have longer lives than for tension-compression [13, 14, 28]. On the other hand, using an overall stress range ($\sigma_{\max} - \sigma_{\min}$) basis, tension-compression specimens have longer lives than that of tension-tension specimens. These divergent results are due to two different means of evaluating material characteristics. Tension-tension testing has a higher mean stress value and thus would be expected to have a shorter life based on this criterion, whereas tension-compression testing causes additional damage and plasticity when viewed on a maximum stress criterion [13]. The reduction in fatigue life in tension-compression over tension-tension testing (based on a maximum stress range) can be attributed to the creation of additional damage and plasticity sites caused by the loading conditions [13].

Dennis conducted tension-compression fatigue testing employing strain-controlled loading instead of the stress-controlled case on unidirectional TMC specimens. Such testing showed that the stress-strain curve exhibits three distinct regimes, very

similar to the behavior of crossply laminates. Similar to that of stress-controlled loading, the fatigue curve (strain versus number of cycles) showed three similar regimes of fracture mechanisms: fiber failure dominated the first regime, followed by matrix cracking and matrix fatigue for the next two regimes [17]. Dennis reports that, for a higher strain loading, the strain-controlled specimens had a longer fatigue life than that of stress-controlled specimens at roughly the same loading [17].

2.4. Joint Region – Functionally Graded Titanium Matrix Composite

Although no research has been conducted specifically on the interface region of F/G TMCs, other studies provide valuable insights. The effect of the joint should be the same as a fiber end or discontinuity in a composite. Micromechanical analysis of TMCs identifies two main deformation/failure mechanisms: damage and plasticity. Damage mechanisms consist of cracks, either in the matrix, the fiber, or along the interface between them. Plasticity involves slip-band formation, dislocations, and void coalescence [23]. Several researchers have investigated both mechanisms. As will be shown, these mechanisms might be more pronounced at the fiber ends in the joint region. In addition, strain in the unreinforced alloy may be important to the fatigue life. Finally, there are several analytical models which may offer insights into the mechanical behavior at the joint.

2.4.1. Deformation by Damage

Reaction Zone Effects: As mentioned previously, Jeng, Yang, and Yang studied the nature and properties of the fiber/matrix interface (or reaction zone) and its critical role in the performance and failure behavior of the composite [18]. They found that the reaction zone was much more brittle than the matrix: both the reaction zone and fiber strength decrease rapidly with increasing reaction zone thickness, since “the probability of finding strength-limiting flaws increases as the thickness of the reaction zone increases.” Their work determined that damage growth occurs from microcracks originating in this brittle reaction layer. Therefore, it is possible that damage may occur along the fiber ends.

Fiber Direction Effects: As mentioned previously, cross-ply TMCs have a much shorter fatigue life than unidirectional TMCs – or even monolithic titanium. In such a case, the fibers set perpendicular to the loading axis acts to weaken, and not reinforce, the material. Thus, TMC fatigue life is very sensitive to the loading direction [13]. This has a potential impact on the current effort. Laminates containing off-axis plies are subjected to premature failure along the fiber/matrix interface [29]. This occurs since the cracks in the brittle reaction zone in off-axis components are more in a Mode I (opening) fracture mechanism rather than a Mode II (sliding) mechanism (as in the case for fibers aligned with the loading axis). The fiber ends in the joint region may prove to have a similar (if not as magnified) effect as an off-axis ply, in that the reaction zone not only surrounds the fiber length, but the fiber ends as well. This reaction zone “cap” covering the fiber end would experience a Mode I (opening) mechanism should crack growth occur there.

2.4.2. Deformation by Plasticity

Continuously-Reinforced TMCs: Majumdar and Newaz investigated whether plasticity or damage is the dominant mode of permanent (or inelastic) deformation in TMCs with continuous fiber reinforcement. Using such models as compliance changes (by loading beyond the elastic region, and then noticing any change in elastic modulus and residual stress), changes in Poisson's ratio, metallurgical evaluation, and finite-element modeling, they determined that matrix plasticity dominates inelastic deformation in unidirectional TMCs. They also found that reaction zone cracks played an important role in nucleating this matrix plasticity. For this reason, they stressed the importance of "optimizing the fiber-matrix interface, to retard the formation of reaction-zone cracks" [30].

Discontinuously-Reinforced TMCs: Several researchers have investigated crack propagation effects from fiber ends of TMCs with discontinuous (or chopped) fiber reinforcement. Studies involving the discontinuous (or chopped) fiber reinforcement are valuable in determining the effects of fiber ends in the matrix. Many micromechanical studies have been undertaken over the last several decades to determine the stress concentration and strain effects of discontinuous fibers in the matrix. Clyne and Watson determined that for most short-fiber MMCs "under most loading configurations, high tensile stresses build up at the fiber ends, and these can cause interfacial cavitation" [12]. This is especially true if the fiber is aligned parallel to the direction of loading. They report that, although it is uncertain how critical plastic strain is affected by different fiber

sizes, most researchers investigating this behavior are in agreement that “the fiber ends are the preferred location” for plastic strain and have used FEM computations in an attempt to model it [31]. The onset of failure in MMCs “is frequently provoked by cavitation linkup in the matrix adjacent to a fiber ends” [12]. It is thought that this cavitation at the fiber ends may lead rapidly to failure at the taper joint of the material used in this study by growth and link-up of these cavities. Whereas crack growth in the reaction zone parallel to the loading axis leads to debonding cracks analogous to Mode II fracture mechanics (sliding), cavitation in the reaction zone at the fiber ends leads to voids and cracking similar to Mode I fracture mechanics (opening) [12].

2.4.3. Combined Deformation Mechanisms

The deformation/failure mechanism occurring in TMC material (damage versus plasticity) depends on the applied stress level, but may show interdependence: The formation of slip bands may nucleate cracks, or pre-existing matrix cracks can cause localized plasticity [23]. This finding of interdependence is especially important for a composite/monolithic joint, where damage in the composite and plasticity in the unreinforced alloy (due to higher strain values) may combine to make the joint region the weakest section of the test specimen.

2.4.4. Strain Effects

The work of Majumdar and Newaz on varying the fiber volume has one incidental finding that may prove important to the present study. By testing samples with different fiber volume fractions, they found that strain range controls the fatigue life in the matrix-dominated failure region (Region II). This work verifies that the fatigue life of unreinforced (monolithic) metals is strain range-dependent [23]. During testing of F/G TMCs, the strain range will change significantly from the monolithic to the composite sections. This strain gradient over the joint region might affect its strength and fatigue life.

2.4.5. Analysis

Finite element modeling (FEM) has been used to predict the effect of the interface region [30]. Aveston and Kelly pioneered some of the earliest work in modeling the mechanics of discontinuous fiber-reinforced materials nearly 30 years ago. They developed a model that sought to account for the bonding strength between the fiber and matrix, and investigated load transfer between these two elements. Their model was one of the first to capture debonding effects and the phenomenon of fiber bridging in their finite element model. They were among the earliest to document the effects of matrix cracking [32]. A shear-lag model has shown promise for predicting the stress-strain behavior of unidirectional ceramic matrix composites and could prove useful for TMC analysis as well [33]. Other important composite models include: Aboudi's continuum model [34, 35], the Ahmad-Nicholas model [35, 36], the Dvorak/Bahei-el-Din/Zuiker

model [37], the Hopkins-Chamis multi-cell model [38], the vanishing fiber diameter model [35, 38], and the concentric cylinder model [38].

2.5. Similar Efforts

Joining Dissimilar Alloy: In the early 90's, Anoshkin, Gelman, and Pavlov recognized the importance of joining dissimilar titanium materials to take advantage of the relative strengths and pursued research to that end [39]. Although their work consisted of joining unreinforced titanium alloys, it recognized the critical nature of the joint region and the potential benefits of linking materials to take advantage of their combined attractive qualities.

Cladded TMCs: A somewhat similar research effort delved into the mechanisms of plasticity and damage in selectively reinforced composites. Ramamurty conducted research on Ti 6-4 TMC panels clad on both faces with a layer of monolithic alloy [40]. This arrangement varies distinctly with the material used in the current study; nevertheless, his work provides potential insights to the mechanics of the tapered joint region. Ramamurty also recognized the advantages of having a pure titanium region in a TMC component in order to simplify machining and joining to other materials, albeit his material had a surface layer of pure titanium (selective reinforcement) instead of a functionally graded material. He found that the performance and fatigue life characteristics of cladded TMC panels were "far inferior" to those of uncladded panels. The cladded metal served as a seedbed for early crack initiation when compared to all-

TMC panels. Cracks formed in the clad alloy and grew large enough to suppress matrix cracking: all of the fracture energy went into the propagation of a single large crack that eventually caused complete fracture of the specimen. In other words, the larger the cladding thickness, the more fatigue life degrades. Ramamurty found that cladding had no effect on monotonic loading [40], since the fiber properties dominate the material under low-cycle fatigue.

2.6. Summary

The research conducted into the mechanical properties and behavior of the “parent materials” (both monolithic titanium and for titanium matrix composite) is extensive and therefore provides valuable insights into the possible properties and behavior of the functionally-graded material. Applying past efforts to the current study indicates that the fiber ends in the joint region may have a detrimental effect on the overall strength of functionally-graded TMCs, whether by damage or plasticity. It is important to determine which of these mechanisms (or what combination of them) is dominant in order to characterize the F/G TMC material.

It is not clear which deformation mechanism will be the primary cause of failure by comparing research on both mechanisms alone. Therefore, the test method for this study will seek to determine which of these failure/deformation mechanisms defines the behavior of F/G TMCs.

3. Test Procedures

3.1. Objective

The previous chapter identified two possible deformation modes: damage and plasticity. The current study seeks to determine the mechanical properties (yield and ultimate strength, elastic modulus) and the mechanical behavior (fatigue life, permanent deformation/failure modes) of functionally-graded titanium matrix composites as the first step in evaluating the material for future use. To this end, the tests described in this chapter were conducted. To understand the reasoning behind the testing method, it is first necessary to describe the test material in adequate detail.

3.2. Description of Test Material

3.2.1. Fabrication Details

Fabrication of a functionally-graded titanium matrix composite with the desired taper angle in the joint region is not a straightforward matter. Atlantic Research Corporation (ARC) has developed an innovative method for one-step fabrication of such a material. The process is proprietary and still immature, but follows many of the tried and proven methods for powder metallurgy. An informative description of the fabrication method is essential to this research effort.

Parent Materials: Titanium alloy Ti 6-4 is composed of 90% weight titanium, 6% weight aluminum, and 4% weight vanadium. Ti 6-4 is an $\alpha + \beta$ dual-phase alloy typically fabricated by forging and/or cold-rolling with subsequent annealing to reduce residual stresses from working the metal. Grain sizes are of either three or ten microns in size, depending on the annealing treatment and selected according to the eventual function of the part. ARC used alloy with less interstitial content than commonly-used Ti-6-4 ELI (extra-low interstitial) material. The material was heat treated to the “dead soft” condition (annealed + slow furnace cool) [41]. For this study, the metal was fabricated by using the gas atomized process to render the bulk alloy into powder, and then consolidating the powder into the final product through the hot isostatic press (HIP) method. Powder metallurgy (PM) is an ideal method for fabricating parts made out of titanium. The ingot material (IM) is separated into powder particles 200-400 microns in diameter. This separation process is conducted in an inert medium such as nitrogen to prevent contamination. The powder is then transferred to a hopper where controlled amounts can be inserted and consolidated until the desired shape and thickness of the titanium part is obtained [5, 6, 7]. Titanium fabricated in such fashion typically has a modulus of elasticity of 110 GPa (16.0 Msi), an ultimate strength of 980 MPa (142 ksi), a yield strength of 883 MPa (128 ksi) a maximum strain value of 14%, and a density of 4.43 g/cm³ (0.160 lb/in³).

The Trimarc 1 fiber is very similar to the SCS-6 fiber used in previous studies. The overall diameter is 130 microns (5.07 mil). The silicon carbide is formed around a tungsten filament 18 microns (0.7 mil) in diameter through chemical vapor deposition.

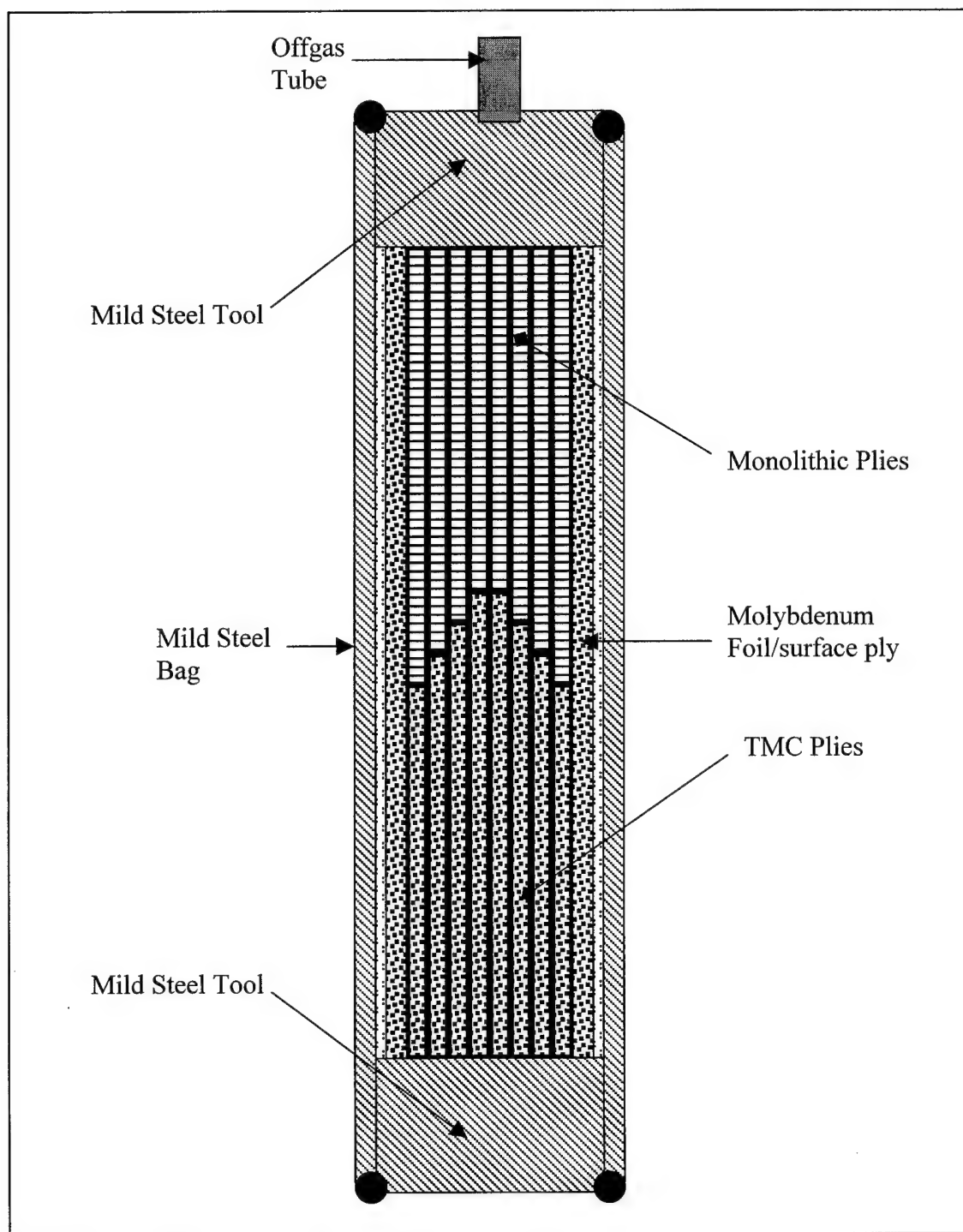


Figure 3.1: ARC's lay-up/consolidation process for the panels used in this study (provided courtesy of ARC)

To finish fabrication of the Trimarc 1 fiber, it is coated with a carbon shell 2-3 microns (0.08-0.12 microns) thick to enhance fiber/matrix compatibility. The fiber has a modulus of elasticity of 420 GPa (61 Msi), an ultimate strength of 3447 MPa (500 ksi), maximum strain value of 0.8%, with a density of 3.15-3.24 g/cm³ (0.114-0.117 lb/in³).

Composite Panel Fabrication: ARC fabricated the composite material using their tapecast method. The specifics are proprietary, but the basic method is as follows [42]. The starting materials are Trimarc 1 fibers (5.07 mil diameter silicon carbide fiber) and gas-atomized titanium powder in "green form" (before consolidation). The tapecast method uses a large diameter drum as the key to ensuring proper fiber alignment. The drum is wrapped in aluminum foil and the foil is coated with polyisobutylene (PIB) adhesive. The adhesive keeps the fibers in place during subsequent operations and handling. A single Trimarc 1 fiber is wound around the drum (fiber traverses at fixed speed while drum rotates) so that there are 125 windings per inch. Once the overall winding width on the spool reaches the desired ply width, the fiber is cut perpendicular to the winding direction along the entire length of the drum. This results in a mat of fibers, each fiber aligned parallel to one another and of the same length.

The mat of fiber mat and aluminum foil, still held together by the adhesive, are removed from the drum and laid flat. This fiber mat has the same fiber spacing as on the drum: 125 fibers per inch. More PIB adhesive is applied to the mat, and a layer of dry Ti-6-4 powder is spread on its surface. The adhesive not only helps ensure proper fiber alignment but also helps bind the alloy to the fibers. The alloy and mat are then coated with layer of polymethylmethacrylate (PMMA). The PMMA coating does not dissolve in

the PIB adhesive; its purpose is to keep fiber/powdered alloy in place during subsequent powder application. This application of PIB adhesive, alloy powder, and PMMA coating are repeated until the resultant tapecast mat fiber volume fraction is 37 percent (the overall fiber volume for the consolidated lay-up panel is 35 ± 1 percent).

The fiber mat/powdered alloy sheet is then cut into appropriately sized plies, the foil is removed and the plies are placed in the lay-up tool. The total lay-up consists of eight plies, with a Ti 6-4 foil placed on the top and bottom surfaces of the lay-up. To prevent the lay-up panel from bonding to the mild steel lay-up tool, the inside surface of the cover sheets and inside walls are coated with boron nitride stop-off. Once the lay-up panel is in place inside the lay-up tool, the tool is then made airtight (hermetic seal) so that it will not leak when evacuated.

The lay-up and tool assembly is then evacuated and heated at control ramp rates up to 450°C (850 F). The assembly is held at this state until all binders (PIB and PMMA) are driven off ("outgassed"). A residual gas analyzer (RGA) and mass spectrometer analyze the effluent species to verify complete removal of the PIB and PMMA. The eight ply lay-up panel is then consolidated using the hot isostatic press (HIP) method: the panel is heated to 900°C (1650 F) and pressurized at 100 MPa (15 ksi) for 2 hours. Afterwards, the lay-up panel is removed from the tool and the panel is trimmed to size.

Monolithic Panel Fabrication: The monolithic alloy panels were made similar to the composite panels, in that it consists of eight plies consolidated in the lay-up tool. The internal plies are cast similar to tapecast plies: titanium powder layers are cast on to aluminum foil until desired metal loading is achieved. However, the surface sheets are

molybdenum foil instead of titanium, and the layers are laid up directly in the tool. The purpose of the molybdenum and titanium foils is to prevent the monolithic lay-up from reacting with the lay-up tool during consolidation (these foil layers will be nitric etched and chemically milled afterwards to remove the molybdenum and molybdenum-titanium interaction zone, respectively). The PIB and PMMA binders are removed in the same manner as described previously, and HIP consolidation uses the same values as before. Afterwards, the molybdenum zone is removed from the panel and the panel is trimmed to size.

Functionally Graded Material: The plies were formed as described above, but this time the positioning of the fiber ends in each ply was carefully controlled to create the desired scarf joint transition region between the monolithic section (see Figure 3.1 and Figure 3.1). ARC used a proprietary method to ensure that the monolithic section would have the same cross-sectional area as the composite section after consolidation.

3.2.2. Test Panel Description

As stated in Chapter 1, the objective of this effort is to characterize the alloy/composite functionally graded material (especially the transition/joint region) and compare it to the parent materials. To meet this objective required test specimens from four different panels. Panel A consisted of $[0]_8$ Trimarc/Ti 6-4 titanium matrix composite (TMC) transitioning into monolithic Ti 6-4 alloy using a double-scarf joint with a 4:1 taper angle (see Figure 3.1). Panel B also consisted of the same TMC transitioning into pure alloy, but with a 20:1 taper angle. Specimens cut from monolithic Ti 6-4 alloy

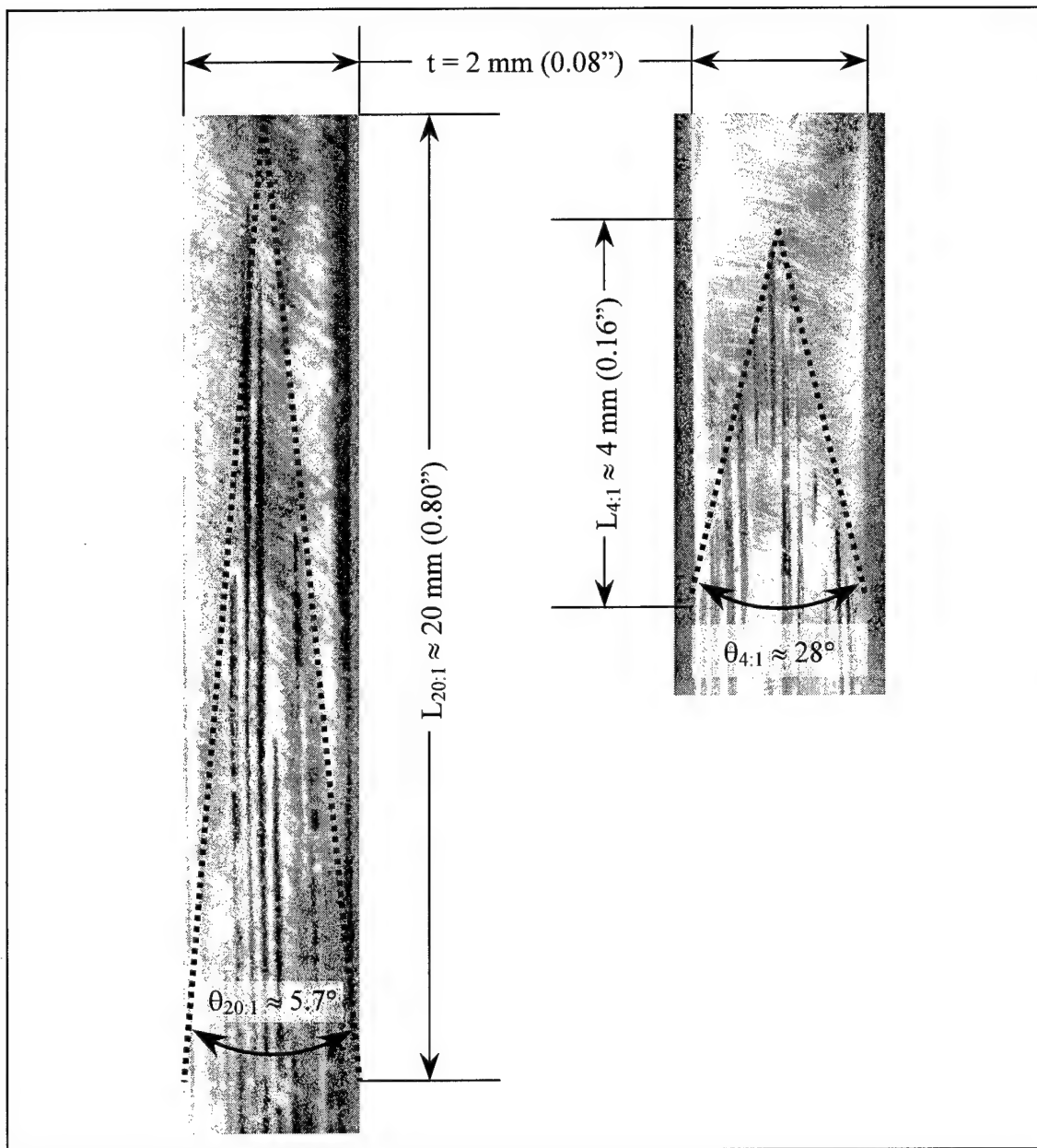


Figure 3.1: Joint Region – Taper Angle Geometries

(Panel C) and from monolithic $[0]_8$ Trimarc/Ti 6-4 composite (Panel D) were also tested at the same levels as Panels A and B. Conducting the same monotonic and fatigue tests on all-alloy or all-composite specimens allowed for direct comparison of results with specimens cut from the functionally graded (F/G) material.

3.2.3. Specimen Dimensions

The dimensions of the specimens depended not only on the type of material but also on the type of test (see Figure 3.1). For monotonic and tension-tension fatigue testing of the functionally graded material (Panels A and B), straight-sided specimens were considered appropriate, since the specimens were expected to fail in the transition region (scarf joint). However, specimens cut from monolithic alloy or composite (Panels C and D) required samples with a wider grip area than the gage area (this type of specimen profile is commonly referred to as a “dogbone” due to its shape). This profile is necessary to ensure fracture occurs at the gage section, and not in the grip area: the compression on the gripped material may create a biaxial stress field in the grip area whose magnitude is larger than the axial stress in the gage area. Decreasing the gage area (and thus increasing the axial stress in this area) prevents premature failure at the grip.

The exact radius used to transition from the gage to the grip width is a matter of importance. Monolithic composite specimens are very sensitive to shear stresses in the shoulder region. To prevent premature failure in the shoulder region of TMCs due to shear stress, Majumdar and Newaz determined that the ratio of shear stress to axial stress must be 0.06, and that a radius of curvature of 317.5 mm (12.5”) in the shoulder region

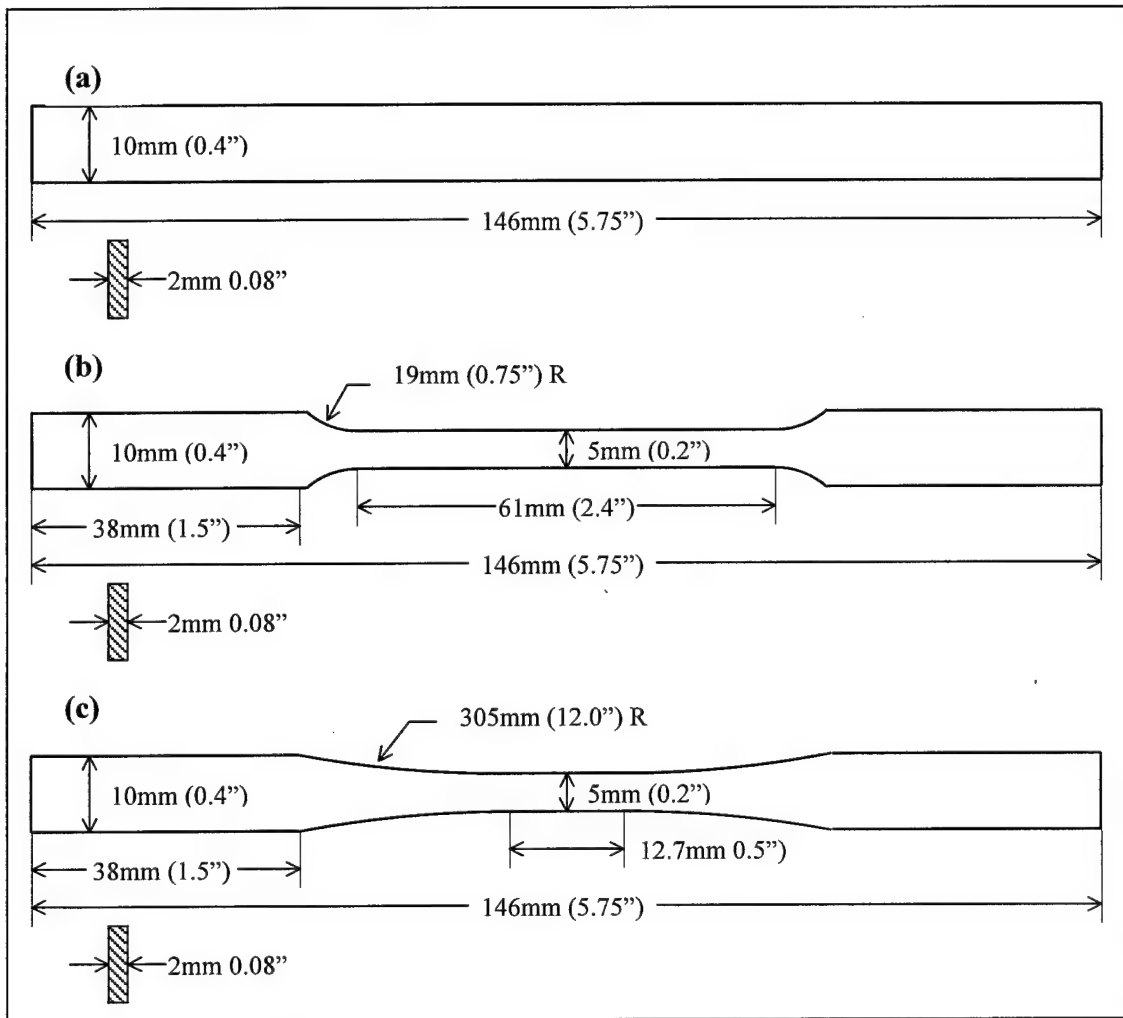


Figure 3.1: Actual-Size Test Specimen Dimensions for (a) tension-compression tests (from F/G material, 4:1 taper), (b) F/G material (both 4:1 and 20:1 taper), (c) Ti 6-4 alloy, and (d) Trimarc/Ti 6-4 composite

ensures this ratio. They arrived at this value through previous experience using specimens of varying notch radii [23]. Meeting these criteria for a test specimen requires a difficult balance. As stated by Kraabel, "The key to designing the dogbone specimen is to achieve maximum reduction in area within the gage length while maintaining a large enough radius of curvature so that failure does not occur in the shoulder region due to high shear stresses" [14]. The TMC samples used in this study had a radius of 305 mm (12") as the optimum balance between large radius of curvature and sufficient straight section for the grip area. For monolithic alloy specimens, a radius as small as 19 mm (0.75") in the shoulder region is acceptable: the alloy is not as sensitive to notching as the composite.

3.3. Test Specimen Preparation

3.3.1. Machining and Polishing

Since the functionally graded (F/G) material specimens do not require a dogbone profile, all specimens were cut from Panels A and B into strips 8mm (0.3") wide using a diamond-encrusted blade (except for the tension-compression test specimens as explained previously). In order to cut all of the dogbone specimens to the required dimensions, an arc-wire cutter was used since a diamond blade has difficulty in machining curved specimens. Regardless of the machining process, all specimens used in this study were polished along the machined surfaces to remove any resulting burrs, pitting, or scratches due to cutting. It was important to remove these defects as they may provide crack initiation points and would thus skew the test results. Polishing was accomplished using a

Stewers radial polisher, first with a 120-grit abrasive pad and followed by a 240-grit finish. To prevent rounding of the specimen edges during polishing, the samples were sandwiched between Aluminum samples with identical dimensions as the samples and secured in a vise at the grip end area.

3.3.2. Tabbing Procedure

Initial fatigue testing revealed that Ti 6-4 is very sensitive to fretting. Early attempts at testing functionally graded (F/G) specimens resulted invariably with premature failure in the grip section on the pure alloy end. Similar results occurred for specimens cut from the pure Ti 6-4 alloy (Panel C) as well. Subjecting the grips to diagnostic alignment tests proved that the grips were adequately aligned; therefore, the failure was not caused by grip-induced bending moments. Observing the gripped surface of the tested specimens under an optical microscope led to the suspicion that fretting was the factor. Consulting with technician Ken Goeke of AFRL/ML, appropriate tab fixtures were constructed to test this hypothesis. The tab fixtures consist of a lay-up of 0.025" brass shim and plumber's cloth (both with the same dimension as the specimen grip area) placed between the brass and the specimen. This prevented localized stress raisers on the alloy grip surface, while yet providing enough friction so that the specimen did not slip. (The tab fixture was only placed on the alloy end of the F/G specimen and not the TMC end, since TMC material has a much higher tolerance for fretting). This tabbing method remedied the problem: Not a single F/G or pure alloy specimen failed in the grips after this method was implemented.

3.4. Testing Method

3.4.1. Monotonic vs. Interrupted Tension Tests

Monotonic Testing: Monotonic tension tests on specimens of each material (Panels A through D) were conducted first to measure the overall failure strength and elastic modulus specific to the parent materials. All tests were conducted in room temperature conditions, as dictated by the scope of this research (see Chapter 1). Obtaining these values for the failure strength and elastic modulus were important, in that they established (1) a baseline for later testing and comparison of the F/G TMC specimens, and (2) the maximum stress levels used in the fatigue tests. For the monolithic alloy and all-composite (Panels C and D) specimens, the test profile was monotonic, or the typical “pull to failure” tests usually conducted, with loading rate of 4.45 kN/min (1000 lbf/min).

Interrupted Testing: The tension test profile of the functionally graded material (Panels A and B) specimens used a “interrupted” profile which deserves explanation. The test profile first applied 20% of the expected ultimate strength for Ti 6-4 at a rate of 4.45 kN/min (1000 lbf/min). The profile then proceeded to 30% of the ultimate strength again at 4.45 kN/min (1000 lbf/min) and then back to the 20% level at the same loading rate. Then the profile increased the load to 40% and again returned to a 20% loading level in the same manner. The profile continued in like fashion to the 50% level, 60% level, 70% level, and so forth (each time returning to the 20% level), until the specimen

failed. The reason for conducting tests with such a "interrupted" profile was twofold. This test would both compare the elastic modulus of the joint before and after deformation, as well as capture any progression of damage in the fiber ends of the joint area. After each loading increment, the test returned to the 20% loading level and paused there long enough to permit a remote microscopic image (50x to 200x magnification) of the alloy/composite interface region in the order to document any crack growth from the fiber ends. In addition to the interrupted tests, two standard monotonic tension tests were conducted on F/G samples of both taper angles in order to compare the results. These monotonic tests were used to determine the yield and fracture strength of the F/G samples.

3.4.2. Tension-Tension (TT) Fatigue Testing

After the tensile tests were conducted on the all-composite, all-alloy, and both types of F/G specimens, several specimens of all four panels were fatigue tested at values ranging from 80 to 33 percent of the respective ultimate strength values. These tests took place at room temperature conditions using an R-value of 0.1: that is, the ratio of the maximum stress to the minimum stress equaled 0.1 for each cycle. The test used a sinusoid profile alternating between the minimum and maximum load at 10 Hz. A remote microscopic imaging system (Questar camera) captured images of the interface region of many of the samples as the fatigue tests progressed. Pictures of the fiber ends were taken at 10^3 , 10^4 , and 10^5 cycles (and every set of 10^5 cycles thereafter for the high-cycle tests) in an effort to capture and document any crack growth in the joint area.

3.5. Test Equipment

3.5.1. Apparati

The Material Test System (MTS) 810 unit, equipped with a 100 kN (22 kip) load cell, served as the servo-hydraulic test stand for all test cases. This test stand works in conjunction with the MTS TestStar IIs controller, with the related test and interface software loaded on an IBM-compatible computer with a Pentium ® processor (see Figure 3.1). The test stand/controller/computer assembly (the test system) was capable of performing all the load profiles required in this study, as well as collecting the necessary output data from the extensometers and strain gages.

Capturing the strain measurements at the interface region of the F/G specimens required two different types of extensometers, depending on the taper angle. A specimen with 4:1 taper angle has a transition region of about 4 mm (0.16"), whereas a specimen with a 20:1 taper angle has a transition region of roughly 20 mm (0.8"). Therefore, to measure the *average* strain at the joint region, an extensometer with an 8 mm (0.3") gage length was used for the 4:1 taper angle specimens, and one with a 25 mm (1.0") gage length for the 20:1 taper angle specimens. Note that extensometer placement on the joint area is a sensitive matter, in that the strain value varies over the length of the joint, as it transitions from alloy to TMC. Therefore it is only possible to measure the average strain at the joint. For the tensile tests of the F/G samples, strain gages were attached in both

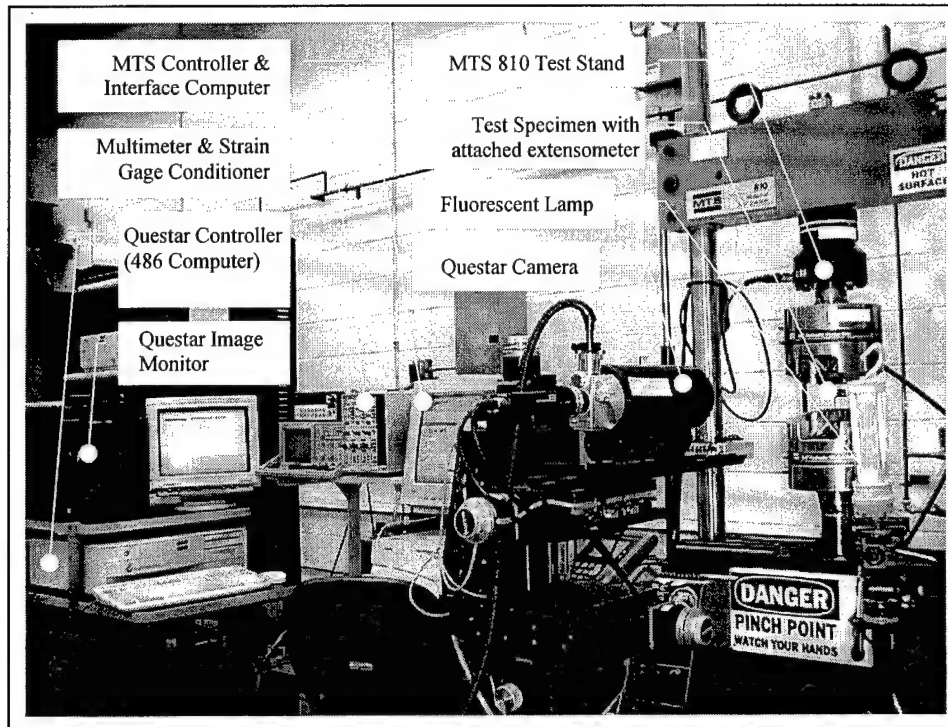


Figure 3.1: Overall view of test setup

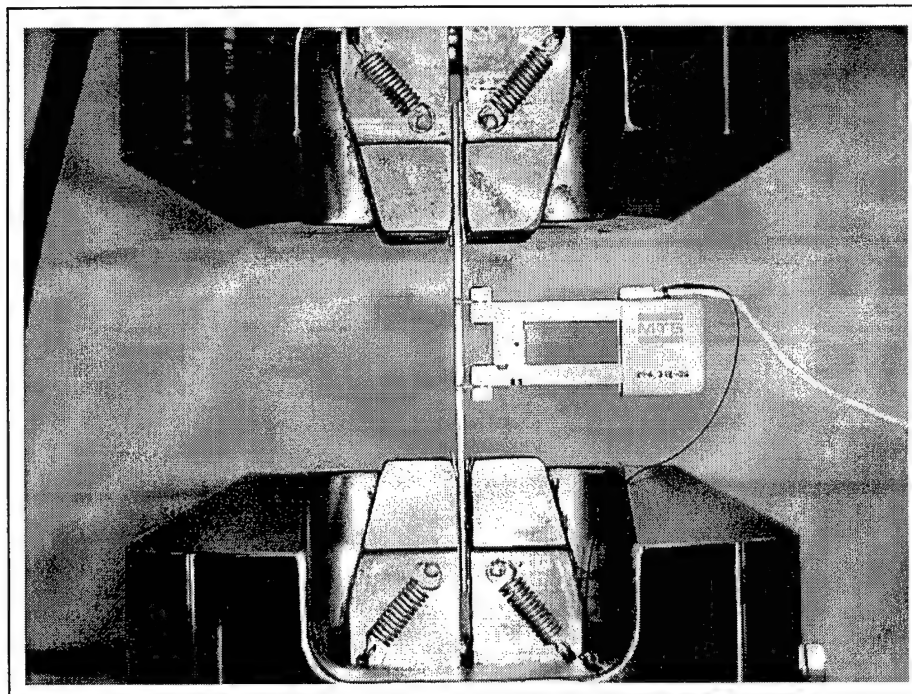


Figure 3.2: Detail view of setup for tensile (monotonic and interrupted) testing and tension-tension (TT) fatigue testing

the pure alloy and pure TMC regions in order to compare the strain values in the monolithic material to that of the interface region (see Figure 3.2).

The Questar remote microscope imaging system includes a 50x optical lens housing with a digital camera, an IBM-compatible 486 computer with related software as the controller and data collector, and a black-and-white monitor to show the real-time image from the camera. A fluorescent lamp was used to enhance the quality of the image. After failure, a Scanning Electron Microscope (SEM) was used to inspect the fracture surface of most specimens in order to determine the fracture mechanisms involved.

3.5.2. Data Collection

During each test, the MTS controller collected the load value (every 0.1 sec for the tensile tests, or every 5 sec for the fatigue tests), the corresponding strain voltage (as well as the cycle number for fatigue tests), and stored this data as a text file in the attached computer. These data were converted to stress and strain values, respectively, and graphed using the Microsoft Excel spreadsheet software. Image data was taken during testing using the Questar imaging system and saved at various stages during both the interrupted tensile tests and the fatigue tests. Each image was stored as a TIFF file on the computer dedicated to the Questar camera. The SEM Image data for the fracture surfaces was also saved using the TIFF format.

4. Results and Discussions

4.1. Tensile Testing

A summary of the results of tensile testing is listed below.

Table 4.1: Tensile Test Results

Spec #	Type of Material	Modulus of Elasticity (E)	Failure Strength (σ_f)	Fracture Location
A5	F/G (4:1)	157 GPa (22.8 Msi)*	965 MPa (140 ksi)	Joint Area (tip)
199	F/G (4:1)‡	156 GPa (22.6 Msi)*	960 MPa (139 ksi)	Joint Area (tip)
203	F/G (20:1)	146 GPa (21.2 Msi)*	945 MPa (137 ksi)	Joint Area (tip)
204	F/G (20:1)‡	150 GPa (21.8 Msi)*	920 MPa (133 ksi)	Joint Area (midsection)
C2	Alloy	110 GPa (16.0 Msi)	1000 MPa (146 ksi)	Gage Area
D4	TMC	210 GPa (30.5 Msi)	1655 MPa (240 ksi)	Gage Area

‡ Denotes interrupted tensile test * Denotes modulus at the joint area

4.1.1. Discussion of Results (Parent Materials)

The moduli values and the ultimate strength for the alloy are similar to other researchers' findings for Ti 6-4 produced via powder metallurgy [7, 8, 9, 10, 43, 44, 46, 47, 48]. In like manner, the values for the composite specimens are in agreement with past research [1, 11, 19, 20, 40]. This set of findings is not important in and of itself. Its purpose is only to verify that the experimental data matches other independent findings. This correlation in turn lends confidence to the experimental data collected for the F/G specimens, since the parent specimens were fabricated in the same way in order to perform a direct comparison between these materials.

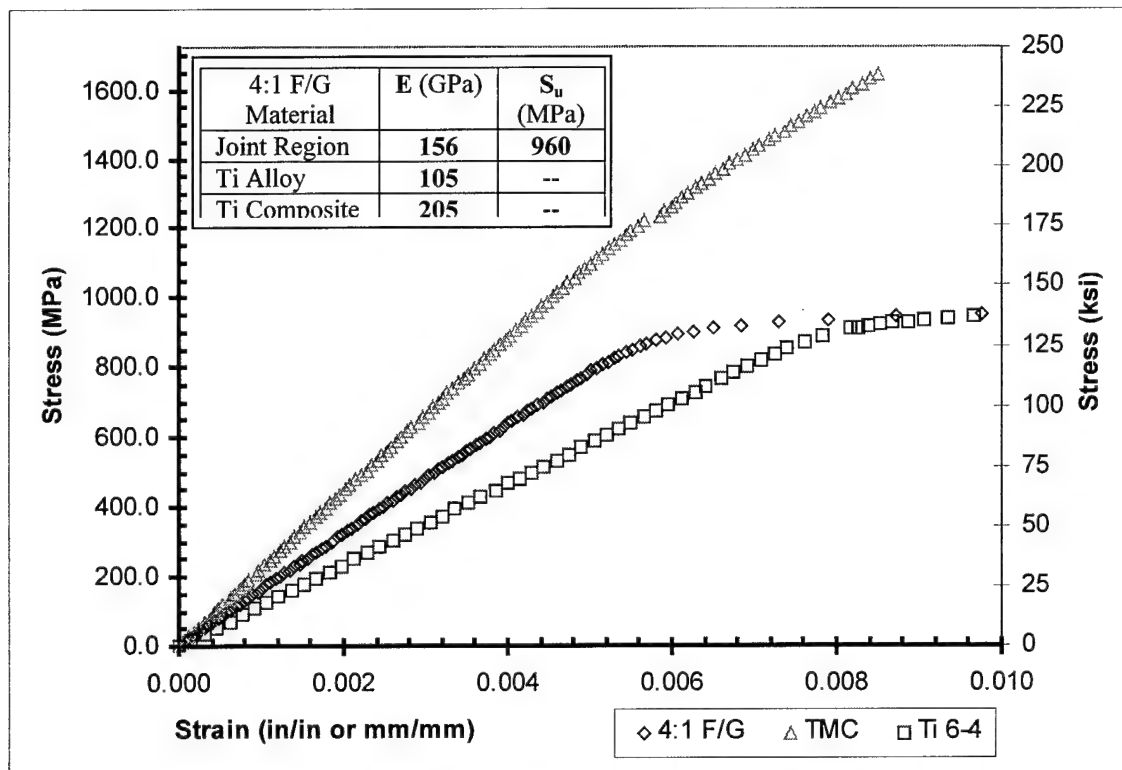
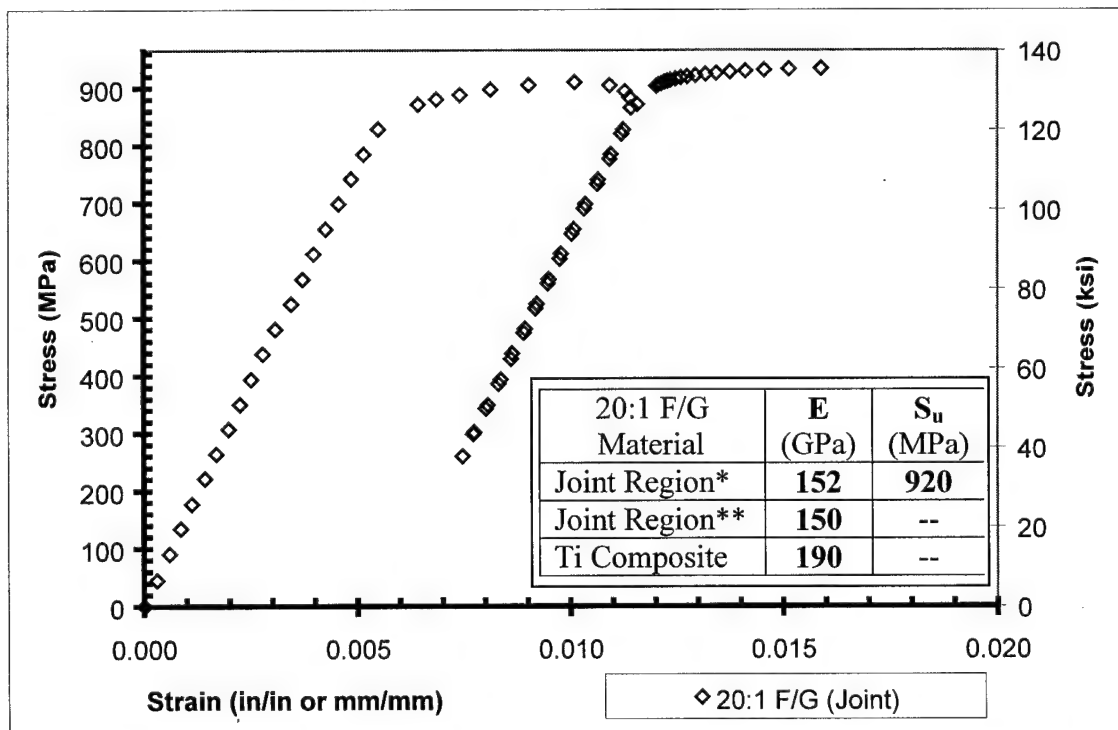


Figure 4.1: monotonic tensile test results for 4:1 taper F/G vs. TMC and alloy material



* Denotes original elastic modulus, before deformation ** Denotes modulus after deformation but before failure

Figure 4.2: Specimen 204 (20:1 taper F/G) stress-strain curve (interrupted tensile testing)

4.1.2. Discussion of Results (Functionally-Graded Material)

Fracture Location: The F/G specimens invariably failed at the “tip” of the joint area (the bottom of the “V” created by the taper angle). However, the fracture surface did not follow the taper angle: it failed from the tip of the joint and out through the unreinforced alloy at an angle of 45° from the loading axis. In addition, the fiber ends showed no sign of cracks developing when viewed by the remote microscope.

Strength Values: The F/G specimens with both tapers failed at nearly the same stress level: 920 MPa (139 ksi). This value only slightly below the failure strength of the monolithic Ti 6-4 alloy from monotonic test: 1000 MPa (146 ksi). The joint strength under tensile testing is much more robust than expected (see Figure 4.1 and Figure 4.2)

Strain Values: From Figure 4.1 and Figure 4.2, the strain values for specimens of both taper angles are nearly the same: elastic strain has a value of 0.006, and failure strain is roughly 0.012.

Elastic Modulus: The modulus for the joint area was expected to be the average of the parent materials, or 155 GPa (22.5 Msi), based on the following modified rule of mixtures formula:

$$E_{joint} = c_a E_a + c_c E_c = c_a E_a + c_c (v_f E_f + v_m E_m)$$

Where E_a and E_c are the moduli and c_a and c_c are volume correction factors for the monolithic alloy and composite, respectively. Since the modulus of elasticity for the matrix is the same as for the alloy ($E_m = E_a$), the equation simplifies to

$$E_{joint} = (c_a + c_c v_m)E_m + (c_c v_f)E_f$$

For a double scarf joint (regardless of taper angle), the volume for both the alloy and composite sections are both one-half of the total volume. Therefore the values for c_c and c_a are 0.5 in this study (note that the sum of the volume correction factors is always unity, similar to the volume fractions). By using the composite material values (fiber and matrix volume fractions and respective moduli) and the parent material values (volume correction factors and moduli of elasticity), the modulus value for the joint roughly matches the experimental value.

As for the elastic moduli of the all-alloy and all-composite sections of the F/G specimens, the strain gages mounted on the specimens give values of 110 GPa (16 Msi) and 210 GPa (30 Msi), respectively. These values are similar to the ones found for specimens from the parent, as would be expected

Deformation Mechanism: From the stress-strain curves of the monotonic tensile test, it is evident that deformation in the joint area occurs at the same load as plastic deformation in the alloy section of the material, even though their moduli are different. This finding indicates that plasticity is the deformation/failure mechanism. Apparently, even if damage mechanisms nucleated cracks from the fiber ends, plasticity in the matrix/monolithic alloy caused yielding and then eventual failure. As further evidence, the interrupted tensile test for the 20:1 taper angle material (Specimen #204) captures the initial elastic modulus and the modulus after deformation but before failure (see Figure 4.2). Note that these values are both roughly the same: 150 GPa (21.8 Msi). According to Majumdar and Newaz, this is one of the ways to determine that plasticity is the

deformation mode: damage would result in a significantly lower modulus if cracking had been the failure mode [30].

Summary: These results would indicate that, although the joint area initiated failure under tensile testing, its strength is nearly that of the unreinforced alloy. The joint area elastic modulus is the average of the moduli for the parent materials. It appears that deformation occurs through plasticity, and not damage.

4.2. Tension-Tension Fatigue Testing

4.2.1. Introduction

In contrast to the tensile testing results, the results of fatigue testing were more complex and unexpected. As a result, this section will require much more detail to describe what the results were, why they were unexpected, and what insights the results provide. Although the results were not as expected, they nevertheless provide an increased understanding of the mechanical behavior for F/G TMC material.

4.2.2. Discussion of Results (Parent Materials)

As was expected, the composite S-N curve is substantially higher than the S-N curve for the alloy specimens, and matches the values given by others [40]. However, the S-N curve for the alloy specimens has values lower than expected and do not match what others have typically found for Ti 6-4 fabricated by powder metallurgy techniques.

Table 4.1: Tension-Tension Fatigue Test Results (R=0.1, 10 Hz, T≈20 °C)

Spec #	Type of Material	Loading σ_{\max} (MPa)	Cycles to Failure	Fracture Location	K_I (MPa\sqrt{m})
200	F/G (4:1)	450	71,629 cycles	Interface	31
201	F/G (4:1)	540	30,071 cycles	Alloy region	11
A1	F/G (4:1)	225	2,000,000 cycles	(no fracture)	--
A2	F/G (4:1)	360	469,699 cycles	Interface	8.6
A3	F/G (4:1)	630	10,536 cycles	Alloy region	9.2
B1	F/G (20:1)	360	100,941 cycles	Alloy region	7.6
B2	F/G (20:1)	450	28,485 cycles	Alloy region	12
B3	F/G (20:1)	540	31,631 cycles	Alloy region	10
C3	Alloy	360	226,917 cycles	Gage Area	8.7
C4	Alloy	450	39,297 cycles	Gage Area	9.6
C5	Alloy	540	29,368 cycles	Gage Area	11
D3	TMC	1075	5,808 cycles	Shoulder	--
E1	TMC	1240	3,839 cycles	Gage Area	--
E2	TMC	580	1,000,000 cycles	(No failure)	--
E3	TMC	910	57,575 cycles	Gage Area	--
E4	TMC	745	114,623 cycles	Gage Area	--

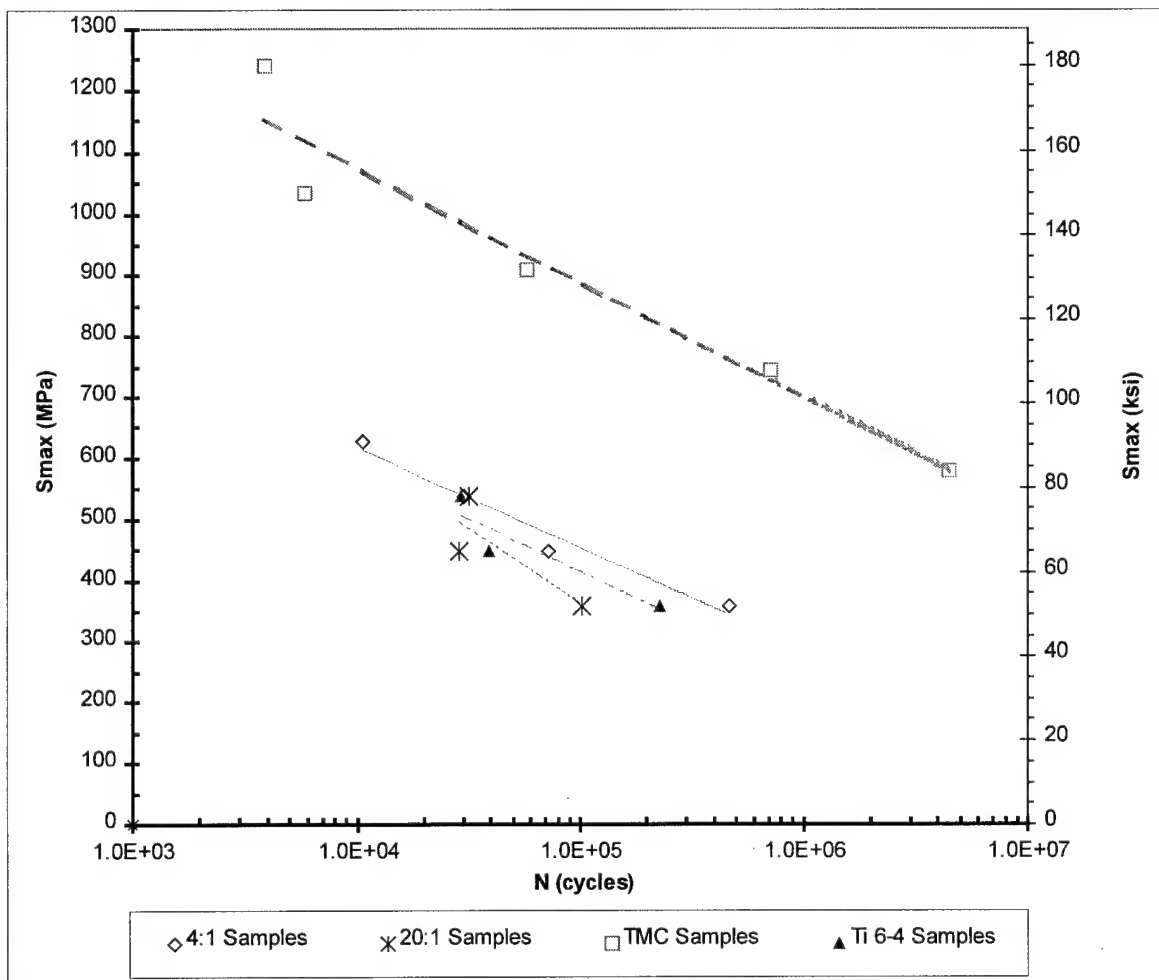


Figure 4.1: S-N curve for titanium alloy, titanium composite, and both F/G materials.

These lower values are not due to differences in fabrication or heat treatment of the material. Testing F/G samples provided even more unexpected results.

4.2.3. Discussion of Results (Functionally-Graded Materials)

Fracture Location: Except on two occasions, the F/G specimens failed in the alloy section of the material in apparently random locations. Two of the specimens failed at the joint area, but this difference will be discussed later.

Fatigue Life: The S-N curves for the F/G specimens were nearly identical (regardless of taper angle) and fall within the same band of values as the monolithic alloy samples. The S-N curves for the functionally graded specimens were expected to be even lower than for the monolithic alloy due to the inherently weaker joint section. Instead, the S-N curve for the functionally graded material is not significantly different than for the alloy (see Figure 4.1). The 20:1 taper angle functionally graded material was predicted to have a longer life since the steeper taper angle supposedly does not facilitate void link-up and crack growth as much as the 4:1 taper angle samples.

Summary: The F/G samples did not break at the joint area, the expected weak section of the material. Instead, the fractures were randomly distributed throughout the alloy section. The fatigue curves for the F/G samples were much lower than expected, were independent of the taper angle, and closely matched the S-N curve for the alloy samples. In Figure 4.1, the S-N curves for the F/G and monolithic specimens are combined to show that, allowing for statistical scatter, they all fall on the same curve.

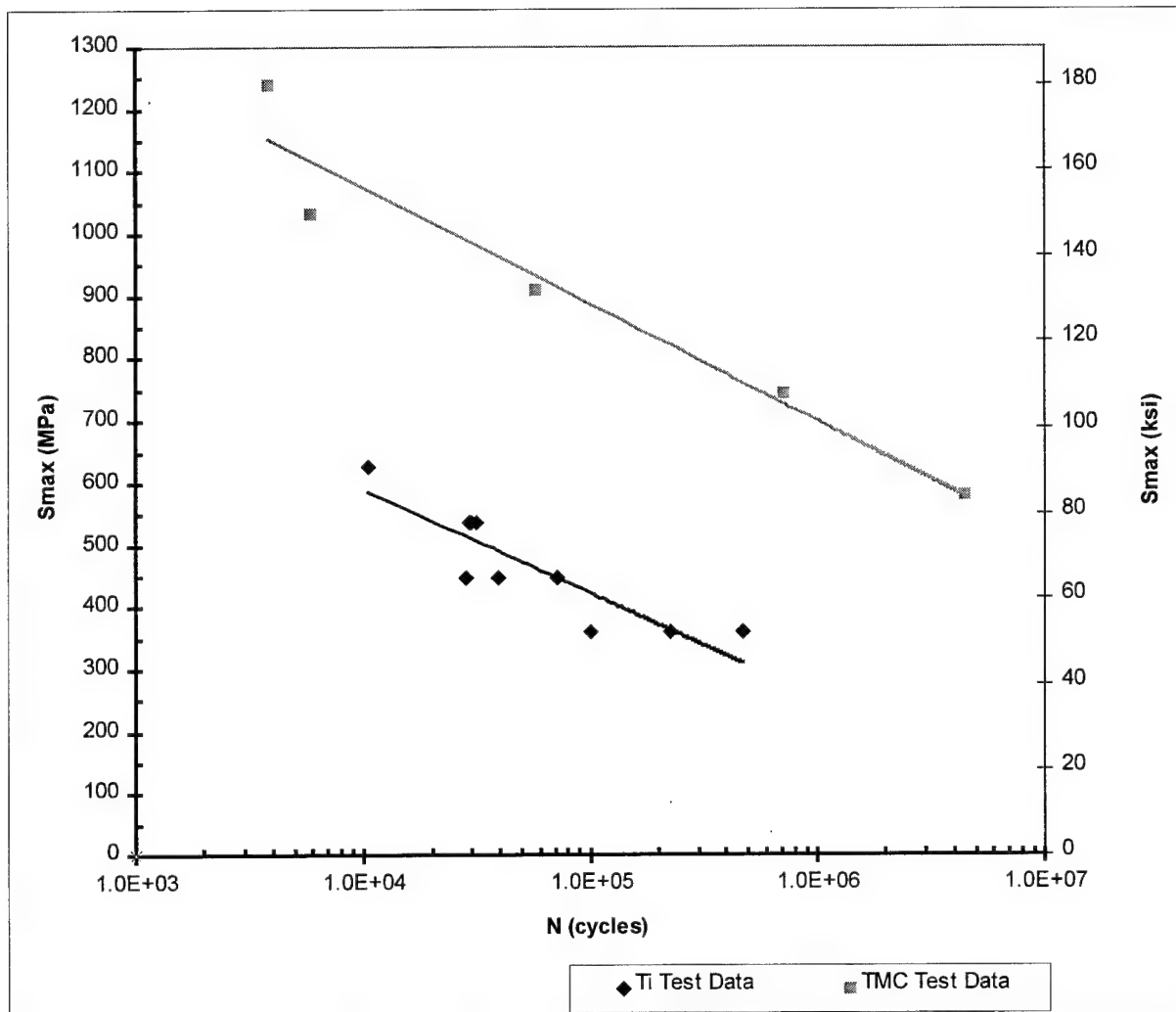


Figure 4.1: S-N curve showing consolidated data from the Ti 6-4 samples (including both 4:1 and 20:1 F/G materials since they failed in the alloy section) and from the TMC samples. These S-N curves form the upper and lower bound for the fatigue life of inclusion-free F/G TMCs.

Considering these unusual results led to the suspicion that something was causing the samples to experience premature failure.

4.2.4. Fracture Surface Inspection

Microscopic Imaging: Inspection of the fracture surfaces using a low-power optical microscope identified possible flaws in the functionally-graded material (see Figure 4.1). No such impurities were identified on the composite specimen fracture surfaces. Inspection of the monolithic alloy specimen fracture surfaces, however, identified impurities very similar to those in the F/G samples. This would indicate that the fracture mechanics for the functionally graded material are the same as for the all-alloy material and would explain the F/G materials having the same S-N curve as for the alloy.

Electron Imaging: Using a secondary electron microscope (SEM) confirmed the existence of inclusions on the fracture surface which initiated crack growth. The fracture surfaces were examined using SEM and backscattered electron imaging. All of the fracture surfaces in the alloy section contained inclusions that initiated crack growth and eventual fracture (see Figure 4.1). These inclusions were surrounded by a reaction zone of part impurity, part titanium, which confirmed that they were present during consolidation of the material, and not a subsequent deposit on the fracture surface. Also, the fracture centered on the inclusion, showing crack growth radiating from the impurity. This indicates that the inclusion was present at the time of material consolidation and not deposited after the specimen fractured. The inclusions varied in length from 20 to 200

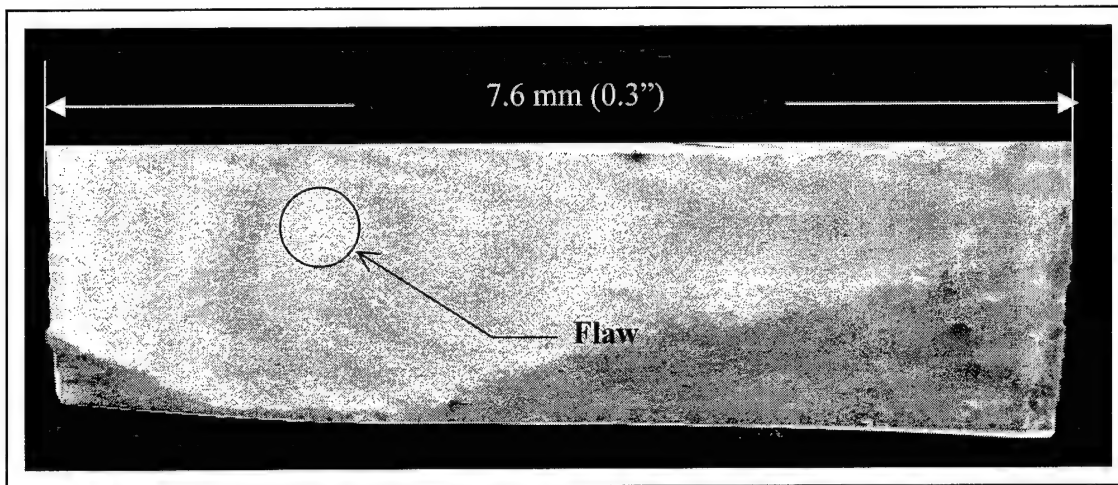


Figure 4.1: Specimen B3 (F/G, 20:1 taper) fracture surface: fatigue testing at 540 MPa (78 ksi). Note flaw at center of surface. Failure occurred at 31.6k cycles

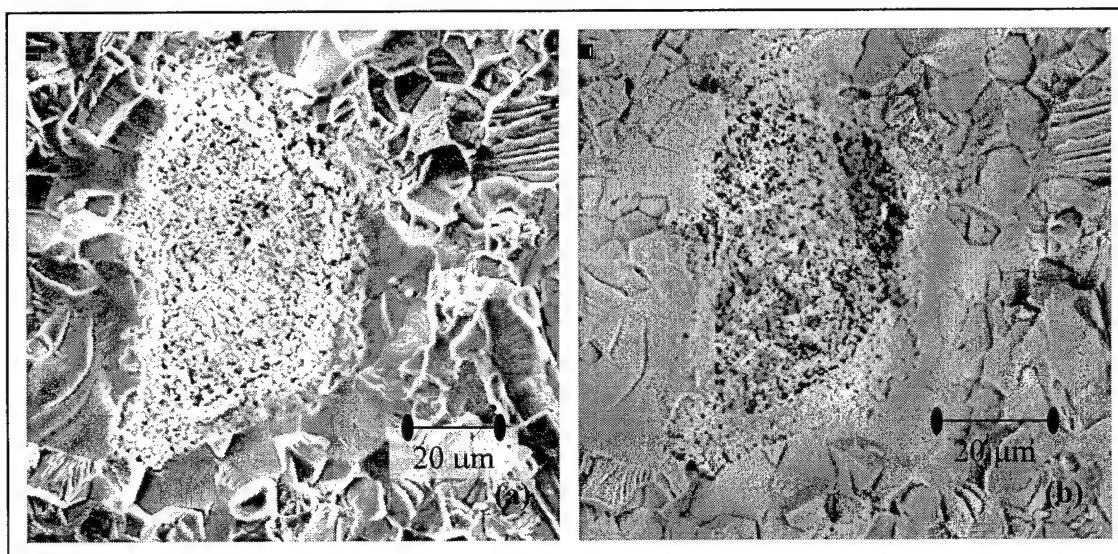


Figure 4.2: Specimen B3 fracture surface (close-up view of flaw) using (a) secondary (SEM) and (b) backscattered (RBS) electrons. The flaw consists of a calcium, silicon, and magnesium compound.

microns, with 100 microns being the average size (see Figure 4.2). As for the two samples which did fail at the joint region, the fiber ends did not cause fracture. In both cases, SEM imaging showed that fiber shards (lying perpendicular to the loading axis, similar to a crossply fiber) initiated cracks and caused specimen failure. For a complete review of all the fracture surfaces, please refer to Appendix B.

Effect of Calcium Inclusions in the Alloy: The fracture surface for Specimen C4 (monolithic alloy) shows the debilitating effect of these tiny inclusions (see Figure 4.3). Failure occurred after fatigue testing at 450 MPa (65 ksi) for 39k cycles. It is evident from the images that the failure-causing crack propagated from the inclusion. A close-up view of the flaw on the Specimen C4 fracture surface using (b) secondary (SEM) and (c) backscattered (RBS) electron imaging reveals the overall geometry of this flaw. Note that the RBS image shows the inclusion as the white area (calcium-based material). At this magnification it is evident that the inclusion is shaped like a flake, with the surface perpendicular to the axis of loading, maximizing its potential for crack propagation. Its closeness to the specimen surface put the inclusion in a plane stress condition, further aggravating crack growth. Higher magnification of the calcium-based inclusion on the Specimen C4 fracture surface flaw reveals its brittle nature (see Figure 4.4). Note the cracks in inclusion (white area), part of which has chipped away to expose the reaction zone with the titanium alloy (dark, rough area) underneath.

Effect of Magnesium Inclusions in the Alloy: The fracture surface for Specimen B2 (20:1 taper F/G) shows the effect of another type of inclusion. This specimen failed after fatigue testing at 450 MPa (65 ksi) and failure at 28.5k cycles. Note flaw at center

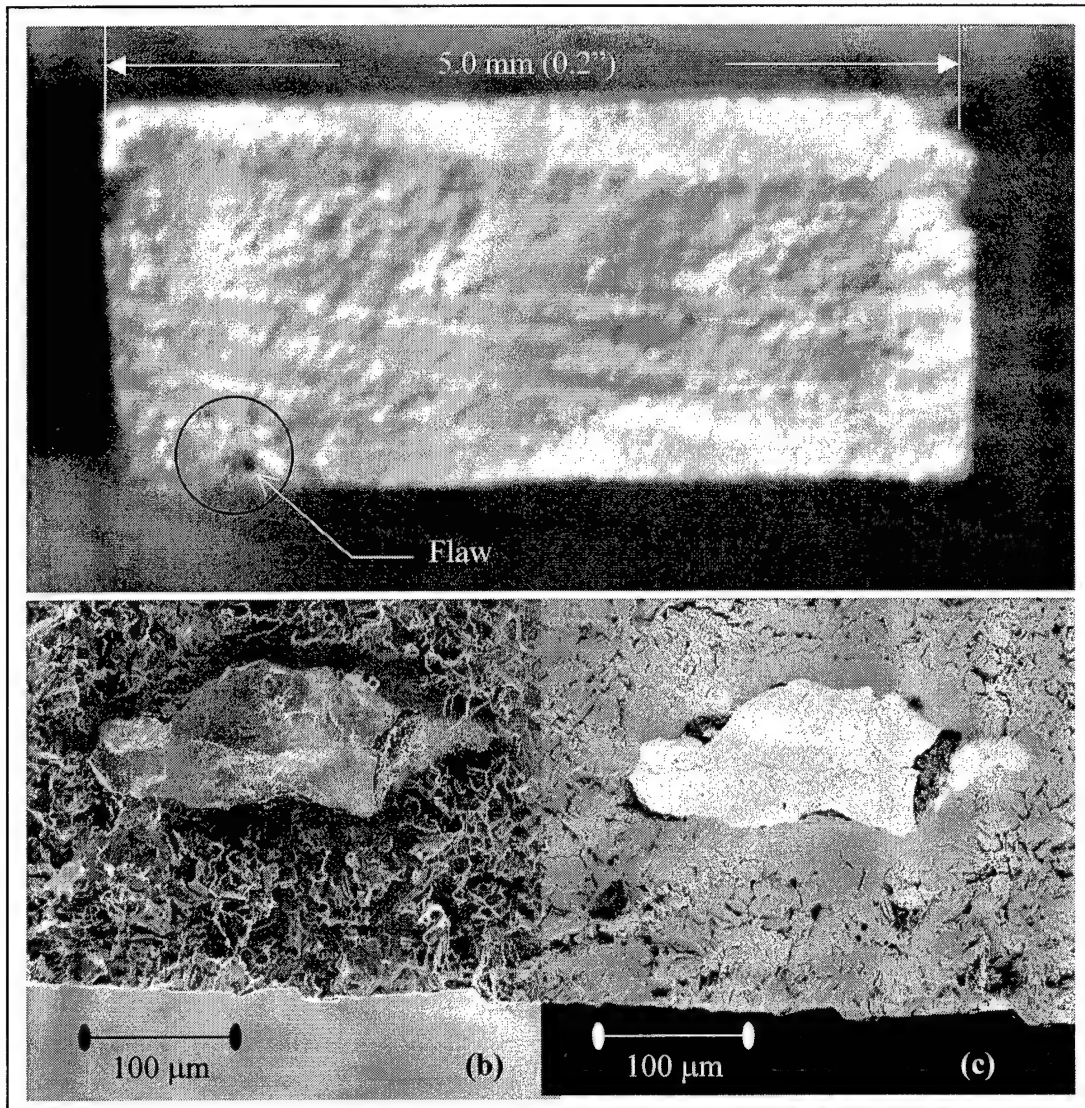


Figure 4.3: Specimen C4 (monolithic alloy) (a) complete view of surface, plus (b) secondary (SEM) and (c) backscattered (RBS) electron imaging of the inclusion

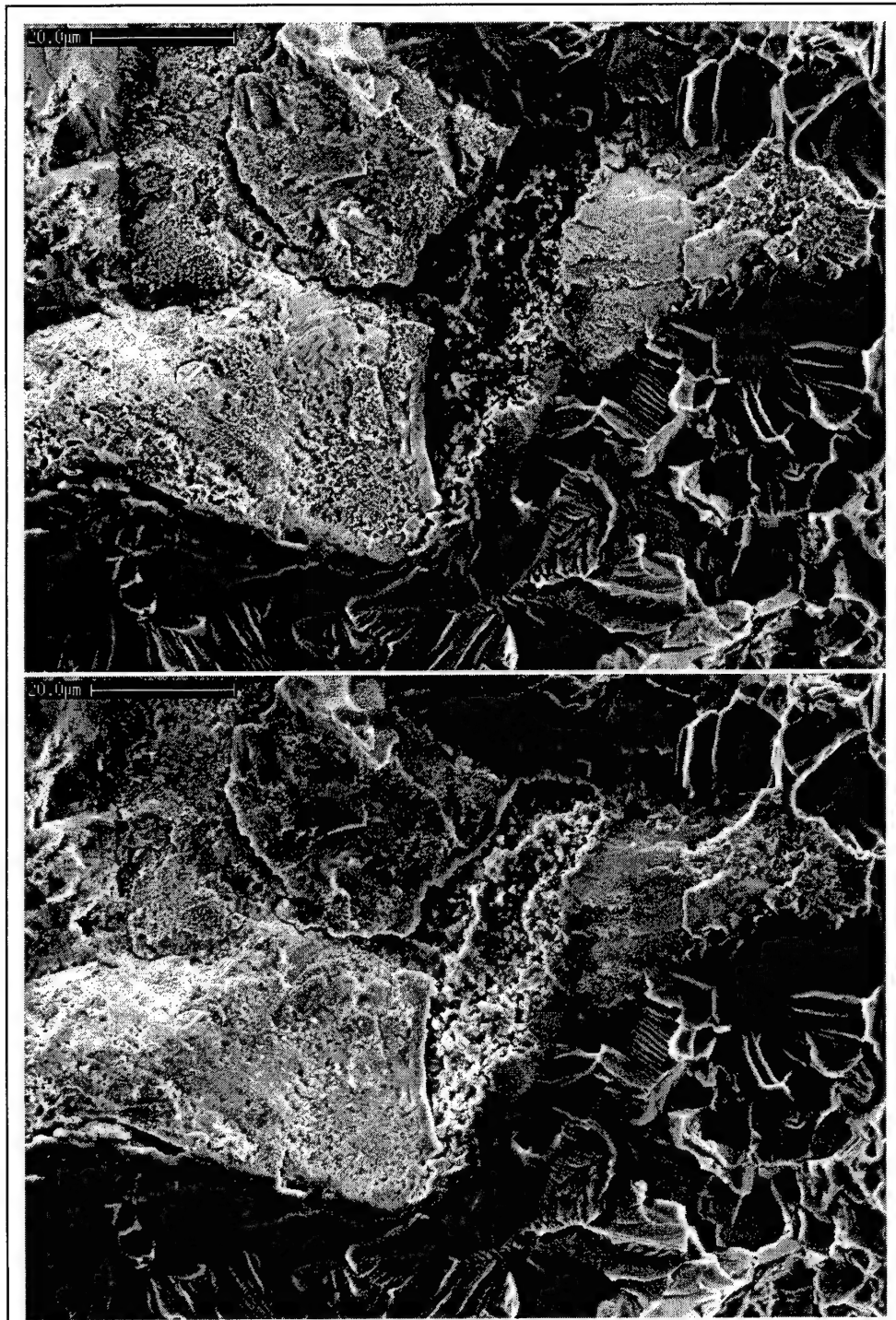


Figure 4.4: Specimen C4 fracture surface – detail view of the calcium-based inclusion using SEM (above) and RBS (below) imaging.

of surface as shown in Figure 4.5. The inclusion is shown in greater detail in SEM and RBS imaging as well. This type of inclusion was very rough, porous, and granular. The reaction zone between the inclusion and the matrix was full of voids, which probably help initiate the cracks leading to fracture (see Figure 4.6).

Effect of Fiber Shards at the Joint Area: The fracture surface for Specimen 200 (4:1 taper F/G) shows that failure occurred in the joint area (see Figure 4.7). However, close inspection shows that the fiber ends did not cause fracture. Complete and detail view of after fatigue testing. The specimen was subjected to 450 MPa (65 ksi) fatigue testing and failed after 71.6k cycles. Note the smooth section in lower left of specimen. This shows crack nucleation near the surface of the specimen face and propagation through the monolithic section and into the fiber section. The tilted view of the same surface (centered on the flaw) shows the terrain features of the fracture. Note how the large smooth crack started in the alloy and grew until it linked up with matrix cracking in the upper section. Note how this matrix cracking occurred on a different plane than the large crack. Also note fiber bridging effects, in that the large crack did not extend into the monolithic section at the top of the image. A close-up of the crack initiation site shows that the inclusion in this case is a fiber shard measuring 200 microns long (see Figure 4.8 and Figure 4.9). This was evidently a fiber remnant that was deposited during fabrication. It shows that fibers, if placed perpendicular to the loading direction, causes the material to have a shorter fatigue life than unreinforced titanium alloy.

Specimen A2 (4:1 F/G) was the only other specimen to fail at the joint area; again, this was most likely caused by fiber shards. This specimen was subject to fatigue

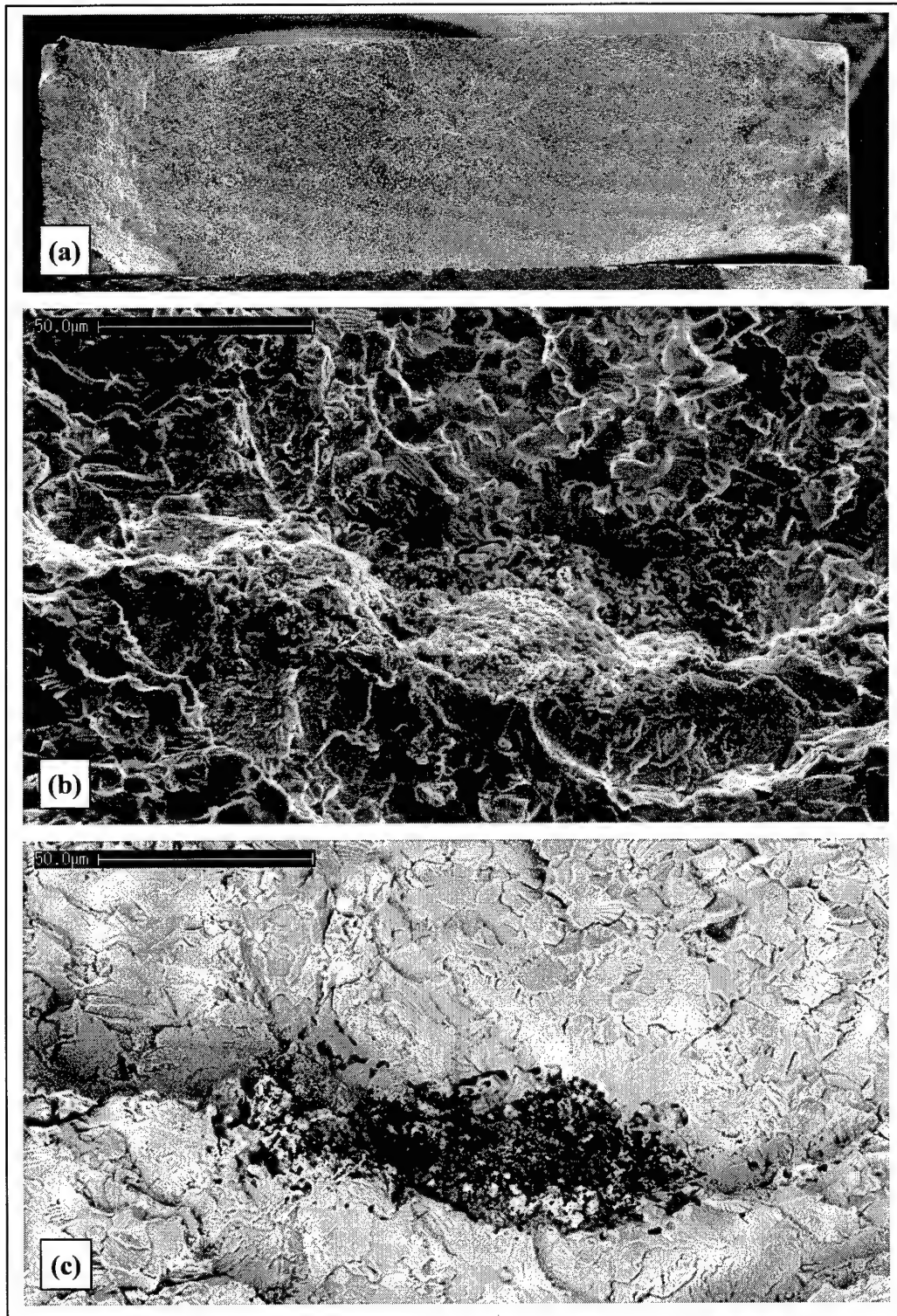


Figure 4.5: Specimen B2 (20:1 taper) fracture surface (a) Complete view, note flaw at center of surface, shown in greater detail in (b) SEM and (c) RBS imaging

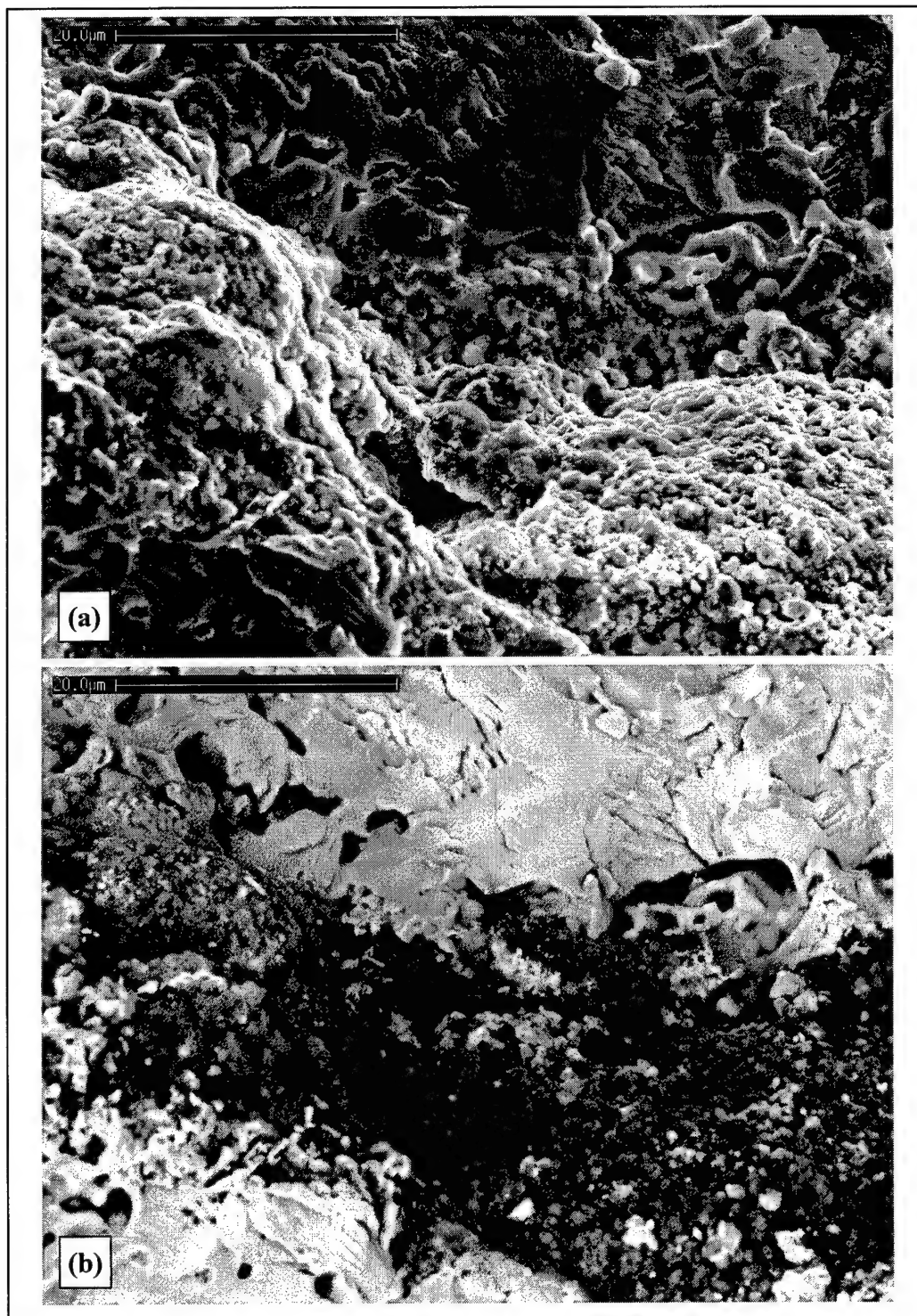


Figure 4.6: Specimen B2 – detail view of the magnesium-based inclusion using (a) SEM and (b) RBS imaging

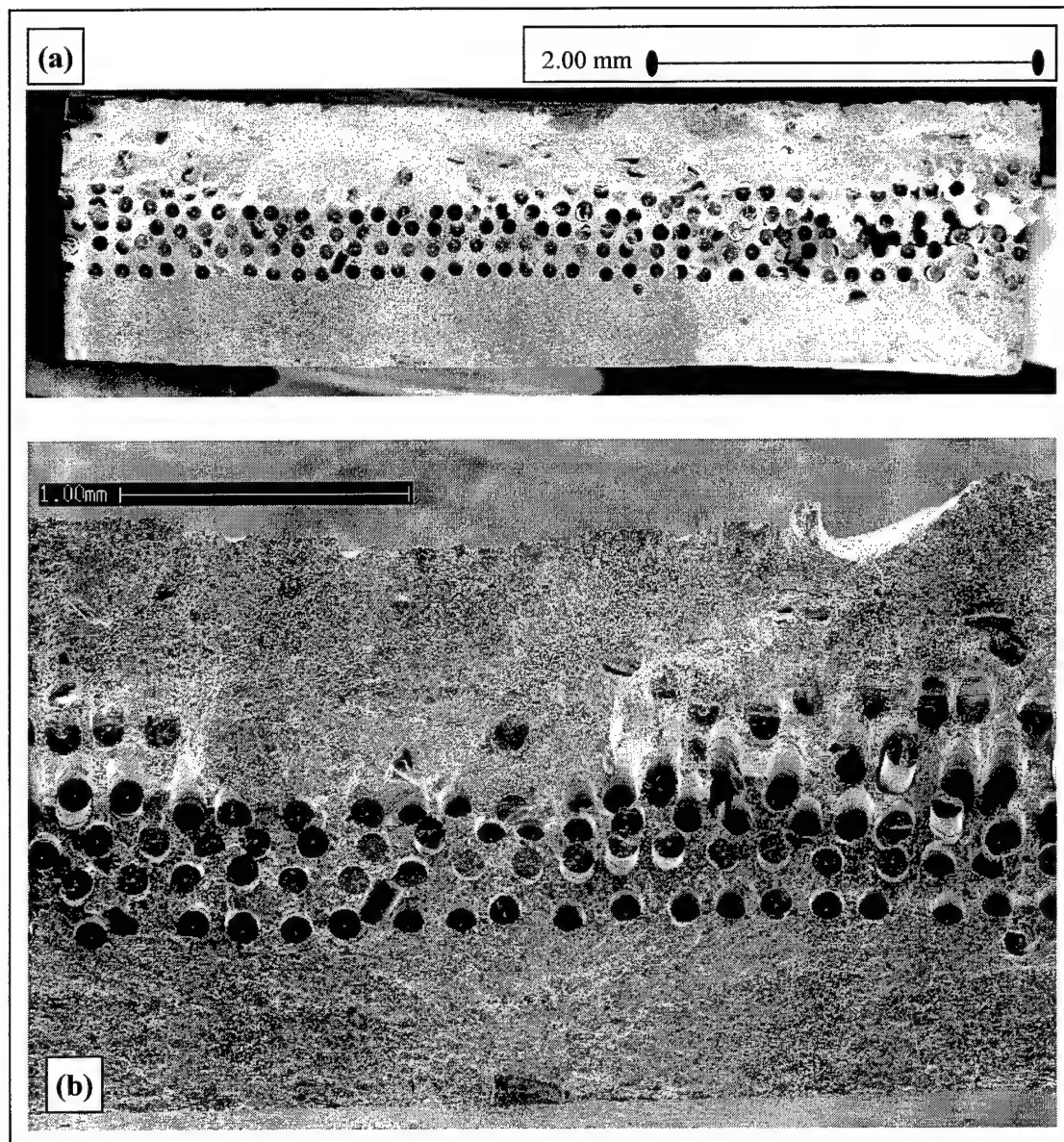


Figure 4.7: Specimen 200 (4:1 taper) fracture surface (a) complete view (b) tilted view of the same surface, centered on flaw, to show the terrain features of the fracture

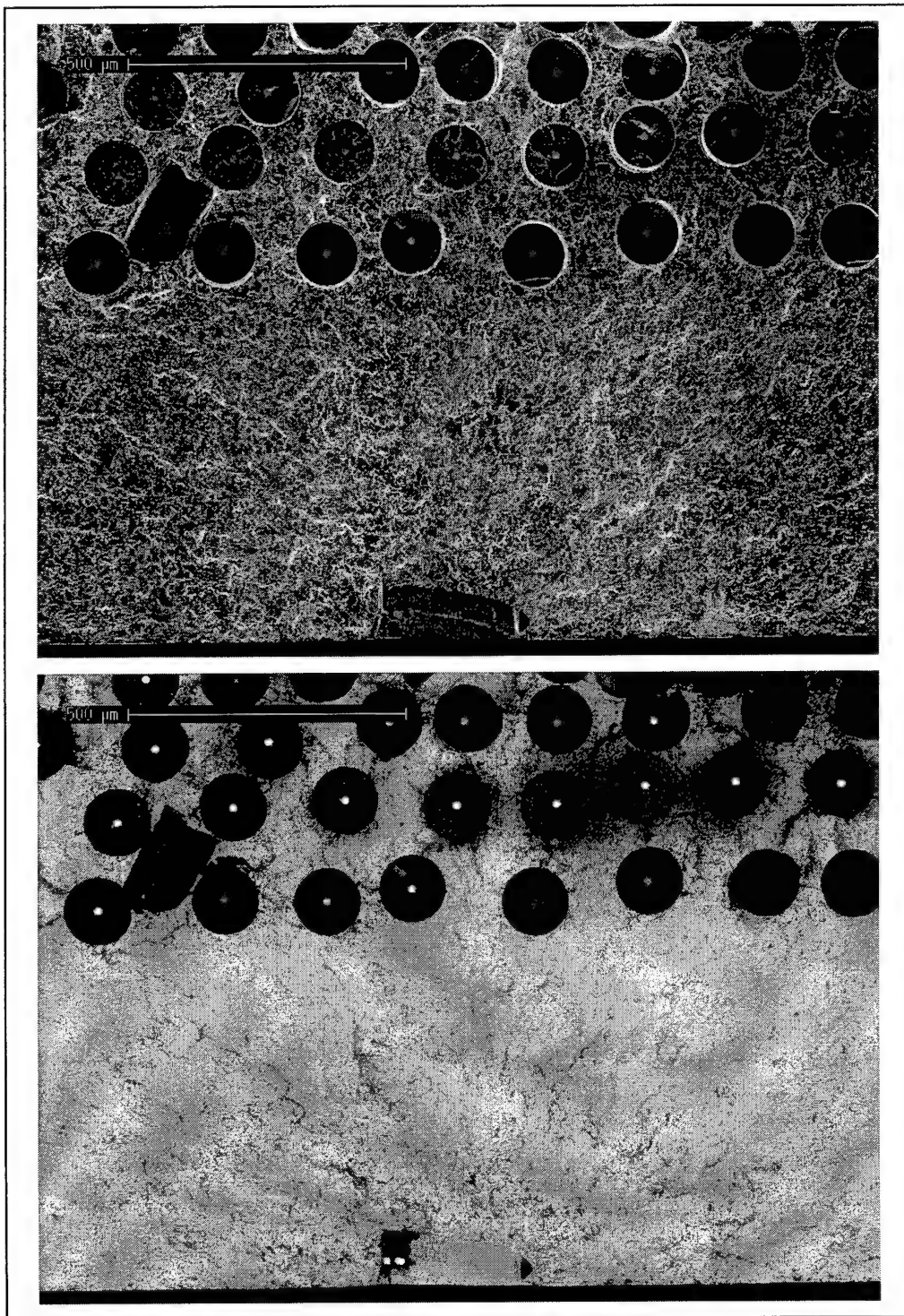


Figure 4.8: Specimen 200 (4:1 F/G) – close-up of the failure-causing flaw (fiber shard)

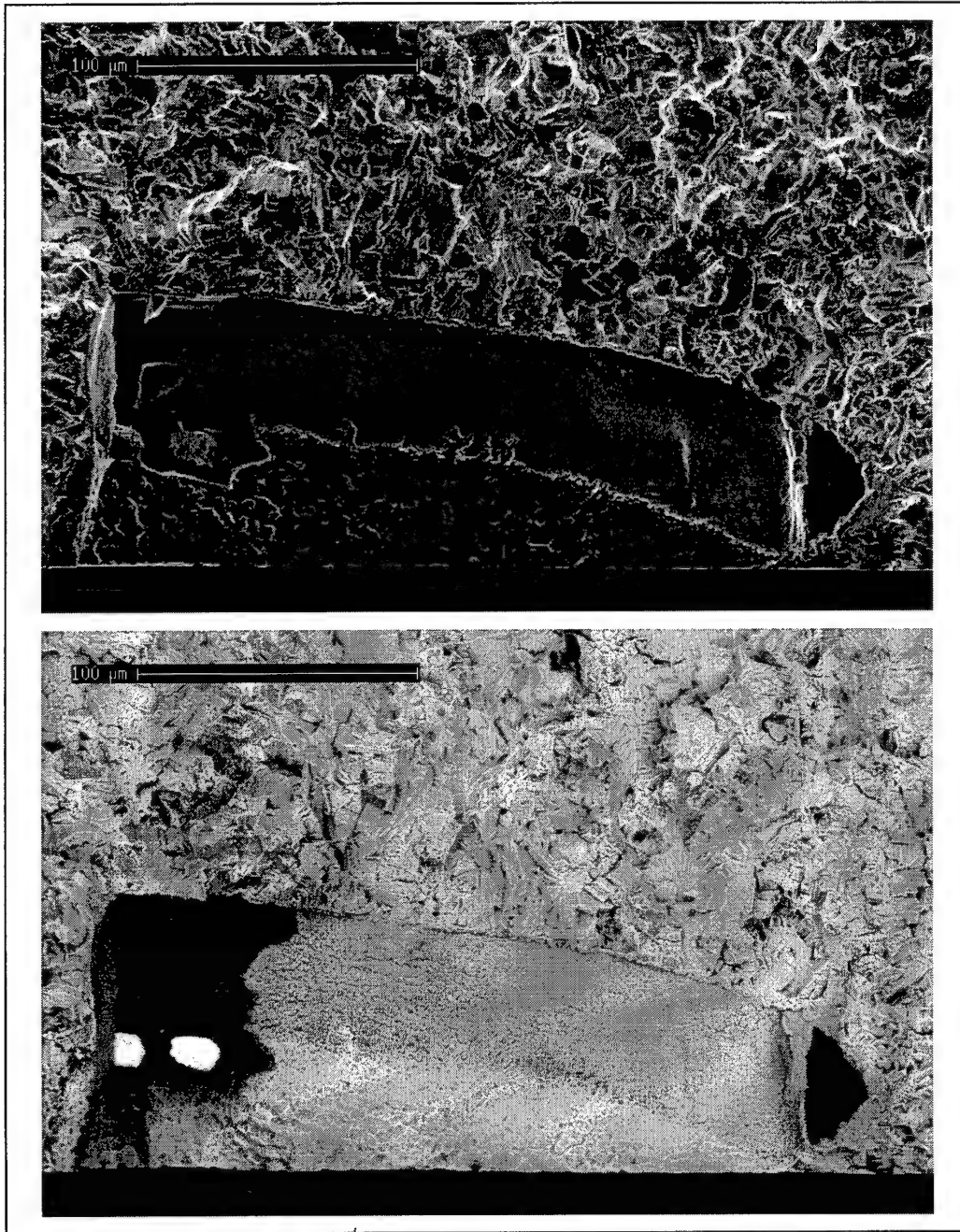


Figure 4.9: Specimen 200 (4:1 F/G) – detail view of the inclusion (the light-colored areas in the RBS image are remnants of the tungsten filament in the Trimarc 1 fiber)

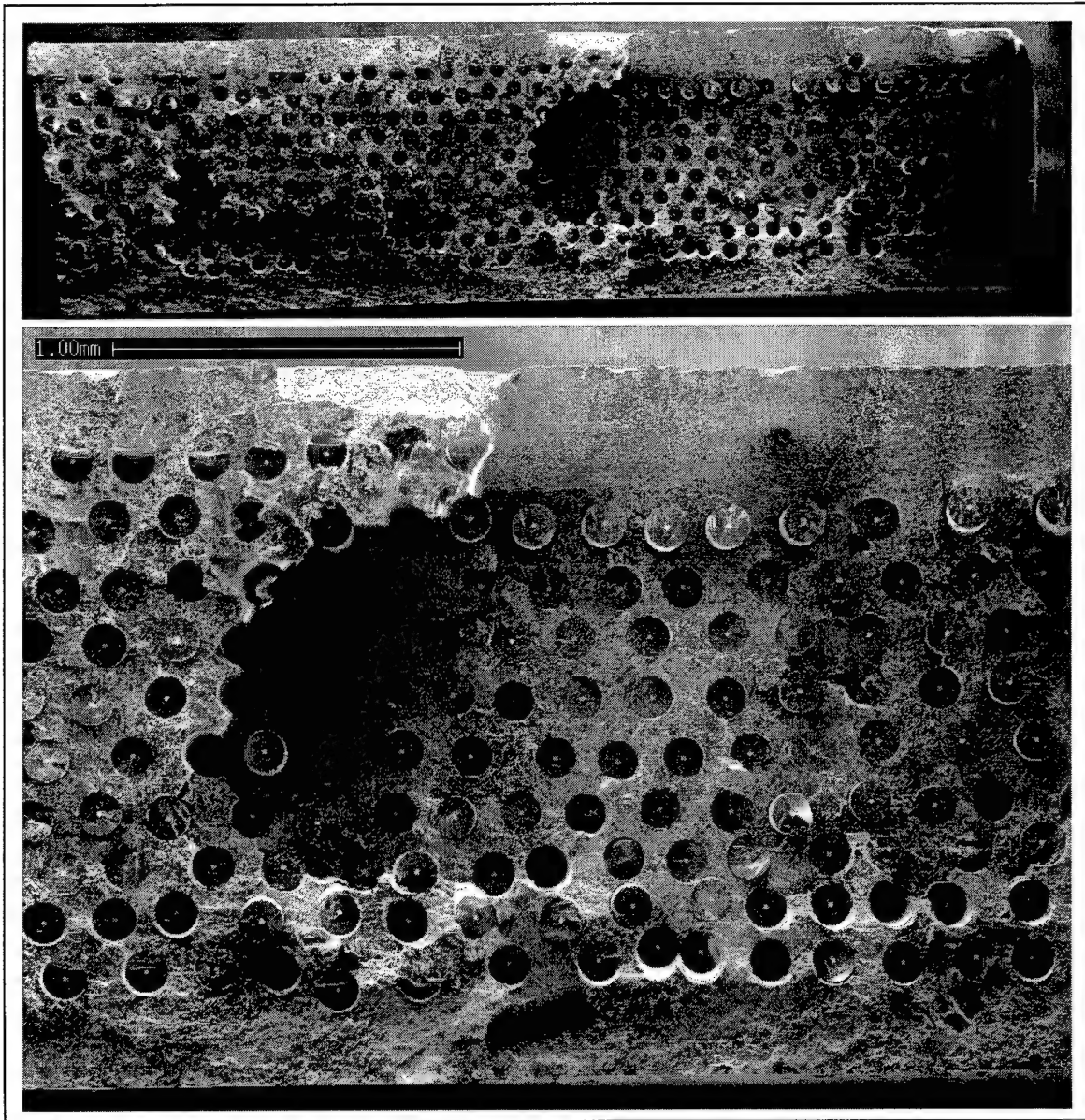


Figure 4.10: Specimen A2 (4:1 F/G) fracture surface. Complete view (above) and close-up view (below). Specimen was subject to tension-tension testing at 360 MPa (52 ksi) and failed at 470k cycles.

testing at 360 MPa (52 ksi) and failed at 470k cycles (see Figure 4.10). Note relative flatness of the monolithic section at upper right, showing little matrix cracking. This indicates that a crack nucleated in the monolithic alloy and propagated into the fiber-reinforced section, totally suppressing matrix cracking. Note fiber bridging effects in the composite section. Note that the bottom edge and left side show more signs of surface roughness associated with matrix cracking. Note fiber shard at lower edge of surface, which may have helped propagate the fracture surface.

4.2.5. Investigation of Premature Failure Source

Elemental Composition: X-ray spectroscopy determined that most of the inclusions consisted of magnesium- or calcium- based substance, or a mix of the two. Their size, along with their composition would indicate that the inclusions are not silicon fiber shards but some other material not ordinarily present during fabrication. As for the fiber shards, they were indeed silicon carbide. For additional information about the composition of the inclusions, and for a copy of the x-ray spectroscopy charts, please refer to Appendix C.

Contamination Source: The origins of the fiber shards are self-evident and will not receive much attention as their remedy involves better handling procedures for the fibers. However, the inclusions in the matrix need further investigation. From the beginning of powder metallurgy processing, researchers identified that “an extreme degree of cleanliness is critical” to the overall performance and acceptance of this fabrication method [43]. In the early eighties, Eyon et al. identified one of the major

contributors to premature crack initiation in titanium powder metallurgy products to be inclusions of “mostly Ca with some Si and Mg.” – identical to the inclusions identified in this study [10]. Many other researchers found similar results as well; the source of these inclusions proved to be airborne particulate matter (dust) [7, 8, 9, 44]. When personally reviewing the fracture surface inclusions found in this study, Dr. Eylon was certain they were dust particles [45].

Explanation: In the mid-1990s, advances in material preparation and fabrication in ultra-clean facilities has essentially eliminated dust as a contamination source [46, 47, 48]. However, due to the immature nature of this new fabrication technique, the manufacturer is still perfecting the fabrication and quality processes. Atlantic Research Corporation (ARC), has evaluated the findings presented above and agrees that the material was contaminated by dust during fabrication [49]. Other all-composite panels fabricated using the same powder but using different techniques showed no signs of inclusions, which would indicate that the starting powder was not contaminated. According to ARC, “this implies that the most likely source of the inclusions is from foreign material being deposited on the surface of the monolithic and fiber reinforced tapecast mats at some point during processing of the panels” [49]. As mentioned in Chapter 3, the fabrication process for this material uses adhesive to ensure the powder binds to the fibers before consolidation. As a result, the surfaces of the lay-up mats are tacky which would also bind fast to any airborne particulates.

Solution: The fabrication method used for these panels employs innovative techniques that ARC had not used previously in quite the same manner. As a result, this

fabrication method exhibits the risk inherent to cutting-edge techniques. It is hoped that this fabrication method will increase in refinement and reliability with time. According to ARC, "Since these panels were fabricated, ARC has modified the filtering system for their clean rooms and instituted procedural changes in their fabrication and storage processes to prevent a reoccurrence of this type of contamination. To date, no other material produced by ARC has shown signs of these inclusions" [49].

4.2.6. Lessons Learned

Although the presence of these inclusions was unfortunate and unwanted, this circumstance nevertheless reveals much about the nature of the joint region. The very fact that inclusions are more detrimental to the fatigue life than the joint region is a very important finding by itself, and would not be intuitively apparent without this experience. The fracture surface of one 20:1 F/G specimen (Specimen B2) provides a poignant illustration of this fact. The fracture surface reveals an inclusion and a short fiber segment (with its accompanying reaction zone) are both exposed. Upon viewing the surface, it is immediately apparent that the inclusion, though much smaller than the fiber segment, nucleated the failure-causing crack and not the fiber or its reaction zone (see Figure 4.1 and Figure 4.2).

This indicates that the inclusions are indeed more detrimental to the F/G fatigue life than is the joint region. Whereas before the fatigue life for the joint was unknown, it is now established that it is better than the well-understood and well-documented situation: Ti 6-4 material with inclusions.

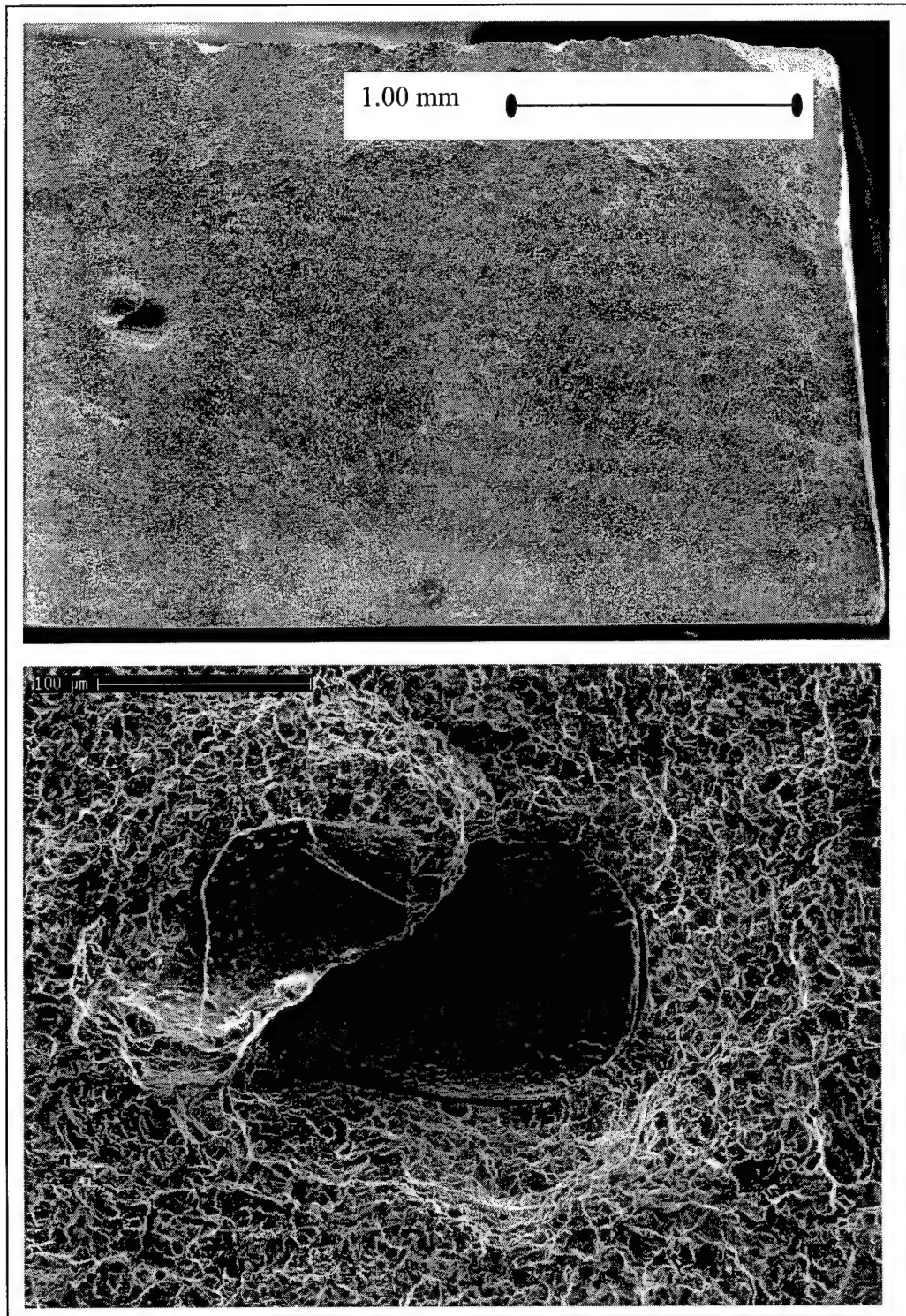


Figure 4.1: Specimen A3 (4:1 taper) – complete view of the fracture surface and close-up view of the fiber shard on fracture surface

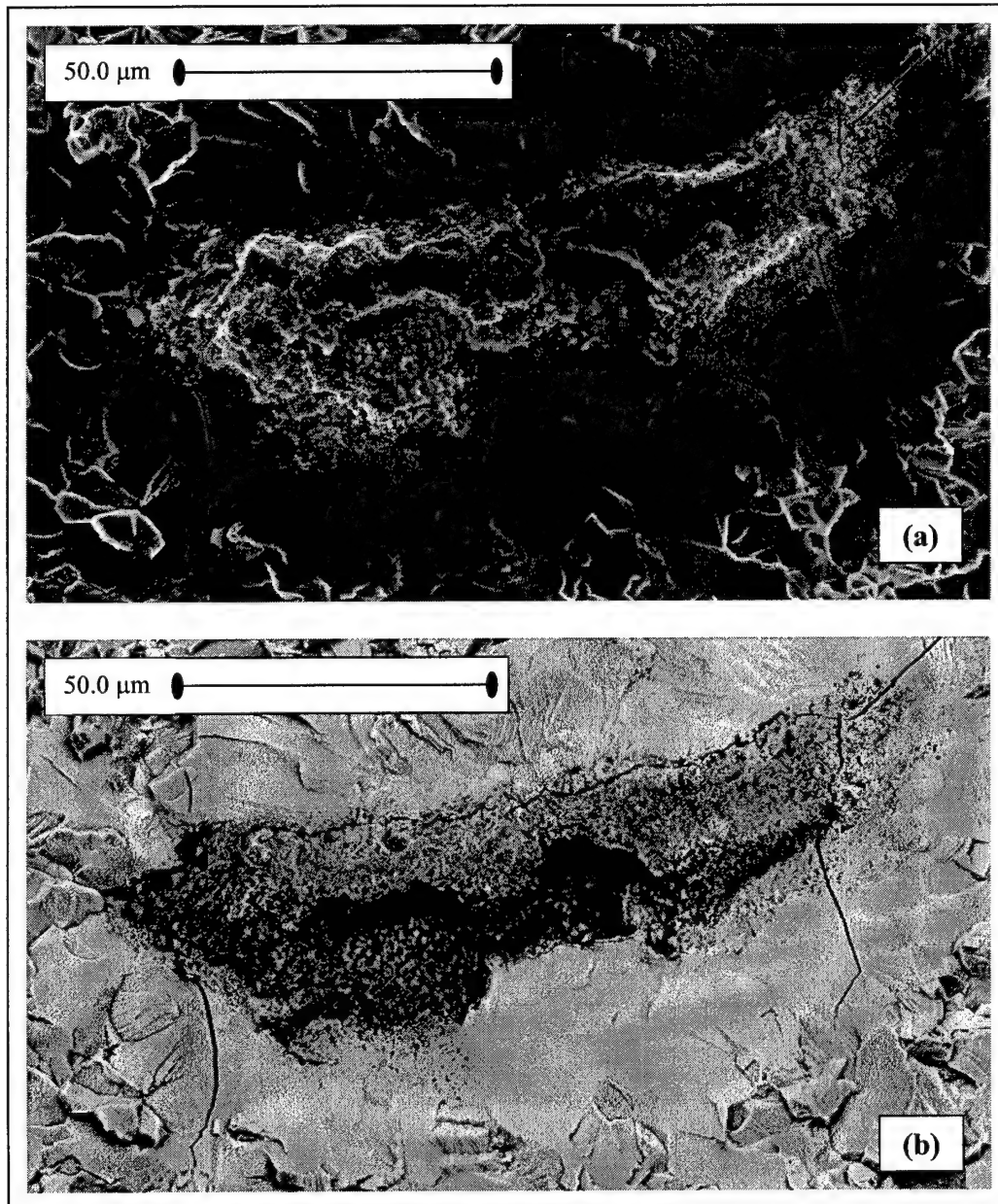


Figure 4.2: Specimen A3 (4:1 F/G) – detail view of the inclusion using (a) secondary and (b) backscattered electron imaging. This enlarged view reveals the sharp, angular nature of the inclusion (dark areas) and the brittle reaction zone that surrounds it.

4.2.7. Determining the Fatigue Life of Functionally-Graded Material

As mentioned in the previous section, the joint region is stronger than the presence of inclusions during fatigue testing. This finding is important because the effect of inclusions on the fatigue life are well-known and well-documented, whereas the effect of the taper joint is not. Since the taper joint is stronger than inclusions in the alloy, this establishes the lower bound for the fatigue life of an F/G TMC without inclusions. And, since the functionally-graded material cannot have a longer fatigue life than that of the titanium matrix composite, the TMC material establishes the upper bound for the fatigue life of an F/G TMC without inclusions. Therefore, the S-N curve for the F/G material will fall somewhere in between the S-N curve for the test samples which failed due to inclusions in the alloy (both F/G samples and the monolithic alloy samples) and the S-N curve for the TMC test samples (see Figure 4.1).

But besides merely bounding the S-N curve, there are other efforts mentioned in Chapter 2 (Previous Works) that may allow an accurate fatigue life prediction to be made for F/G material. This prediction is made on the following premise: *if the inclusions had not been present in the material, the F/G samples would have either (1) still failed in the alloy section due to higher strain values, or (2) failed in the joint region due to the fiber ends.*

To determine which scenario is more probable, two specific research efforts will be employed to this end. The first is by Eylon et al. in characterizing the fatigue life for Ti 6-4 fabricated by powder metallurgy (PM) without inclusions. The second is by

Ramamurty in characterizing the effects on the fatigue life of cladding TMCs with thin layers of monolithic alloy. Both used tension-tension fatigue testing. Therefore, although the inclusions prevent obtaining direct values for the S-N curve, there are possible methods for determining the fatigue life.

4.2.8. Fatigue Life: Lower Bounds (Inclusion-Free Titanium)

Studies have compared the mechanical properties [7] and fatigue life curves [8, 9, 10] of Ti 6-4 using powder metallurgy methods, and the effect of inclusions. Inclusions do not significantly affect monotonic tensile testing [7], but become more critical in tension-tension cyclic loading. The inclusions significantly degrade the fatigue life. Eylon et al. determined an S-N curve showing the effects of calcium- and magnesium-based inclusions in Ti 6-4 test specimens as well as the S-N curve for Ti 6-4 specimens free of inclusions [10]. See Figure D.2 in Appendix D for a copy of the curve they derived.

Superimposing the S-N curve for the alloy with inclusions (from the work of Eylon et al.) onto the combined S-N curve for the test samples that failed due to inclusions (from the current work) shows a nice correlation (see Figure 4.1). This indicates that the S-N curve from Eylon et al. for inclusion-free alloy would be an accurate representation for how the monolithic test samples *would* have behaved if there had been no inclusions.

Making the hypothesis that the joint of the F/G specimens would have been stronger than the inclusion-free monolithic alloy section means therefore that failure

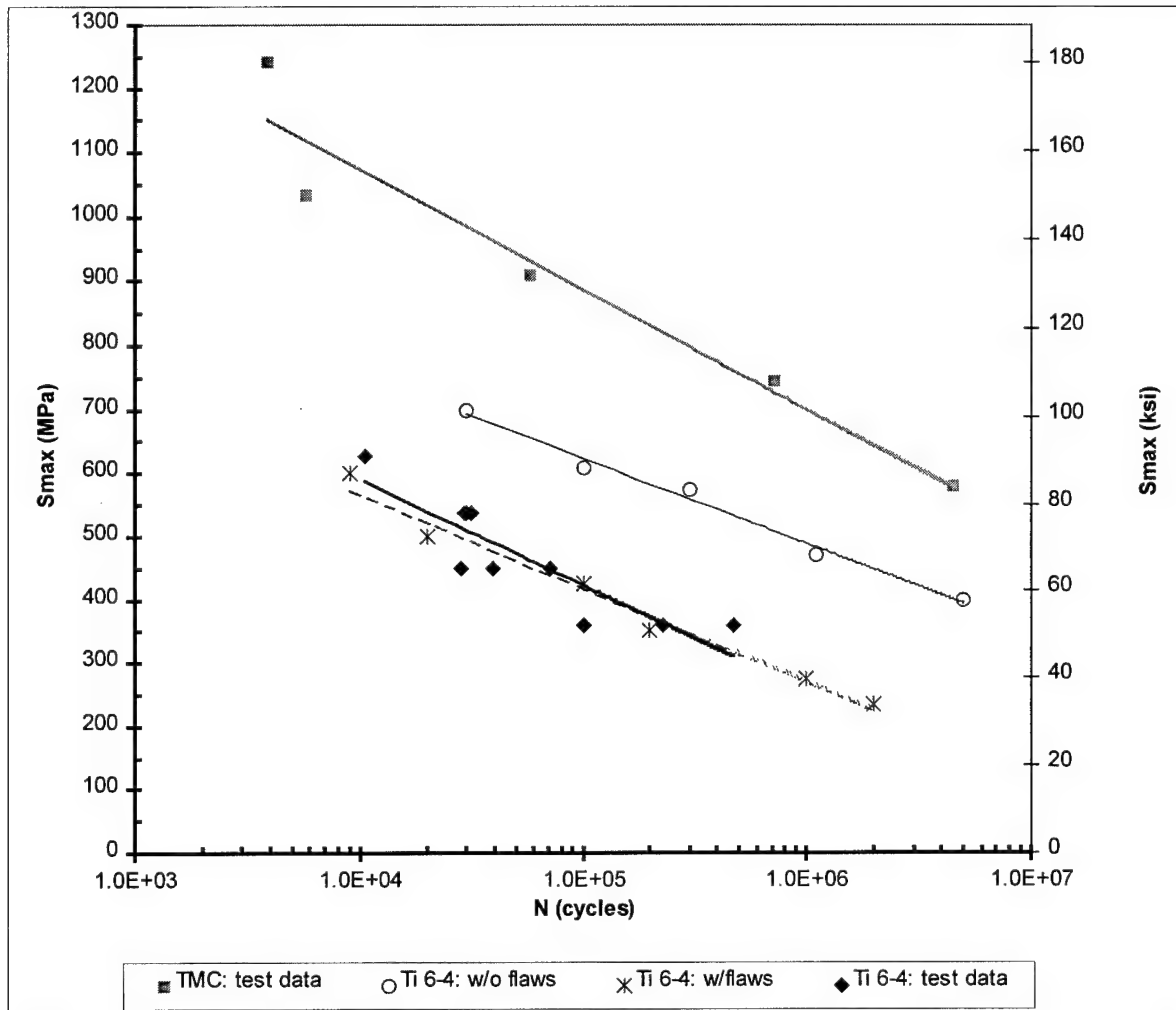


Figure 4.1: Comparison of the S-N curves derived from Eylon et al. (Ti 6-4 material with high levels of contaminants and Ti 6-4 with low level of contaminants)

would still have initiated in the alloy. If this is true, then the S-N curve for inclusion-free alloy from the work of Eylon et al. would also be an accurate representation of the S-N curve for F/G TMC material. This curve is placed alongside that of the upper and lower bounds (the S-N curves for TMC and inclusion-containing alloy, respectively) for the sake of comparison (see Figure 4.1)

4.2.9. Fatigue Life: Upper Bounds (Alloy-Clad Titanium Matrix Composite)

As mentioned in Chapter 2, Ramamurty researched the effects of cladding TMC with layers of monolithic alloy. He studied tension-tension cyclic loading and constructed S-N curves for this material. Although the geometry of Ramamurty's samples was quite different (they did not have a joint region with fiber ends), it is not altogether improper to view this material as having an infinitely long joint region (0:1 taper angle). To review, he found that adding even a small layer of alloy on the surface of the TMC significantly degraded the overall fatigue life of the sample. This is due to several factors, which occur as follows. (1) The clad alloy experiences slightly higher strain values than does the TMC. (2) The alloy therefore nucleated cracks. (3) The cracks in the alloy grew since there were no fiber bridging effects as in the TMC section. Finally, (4) the alloy cracks then extended into the TMC region, entirely suppressing matrix cracking and causing failure.

Ramamurty also baselined this work by testing TMC samples without any cladding, and included the corresponding S-N curve in his report. This S-N curve was

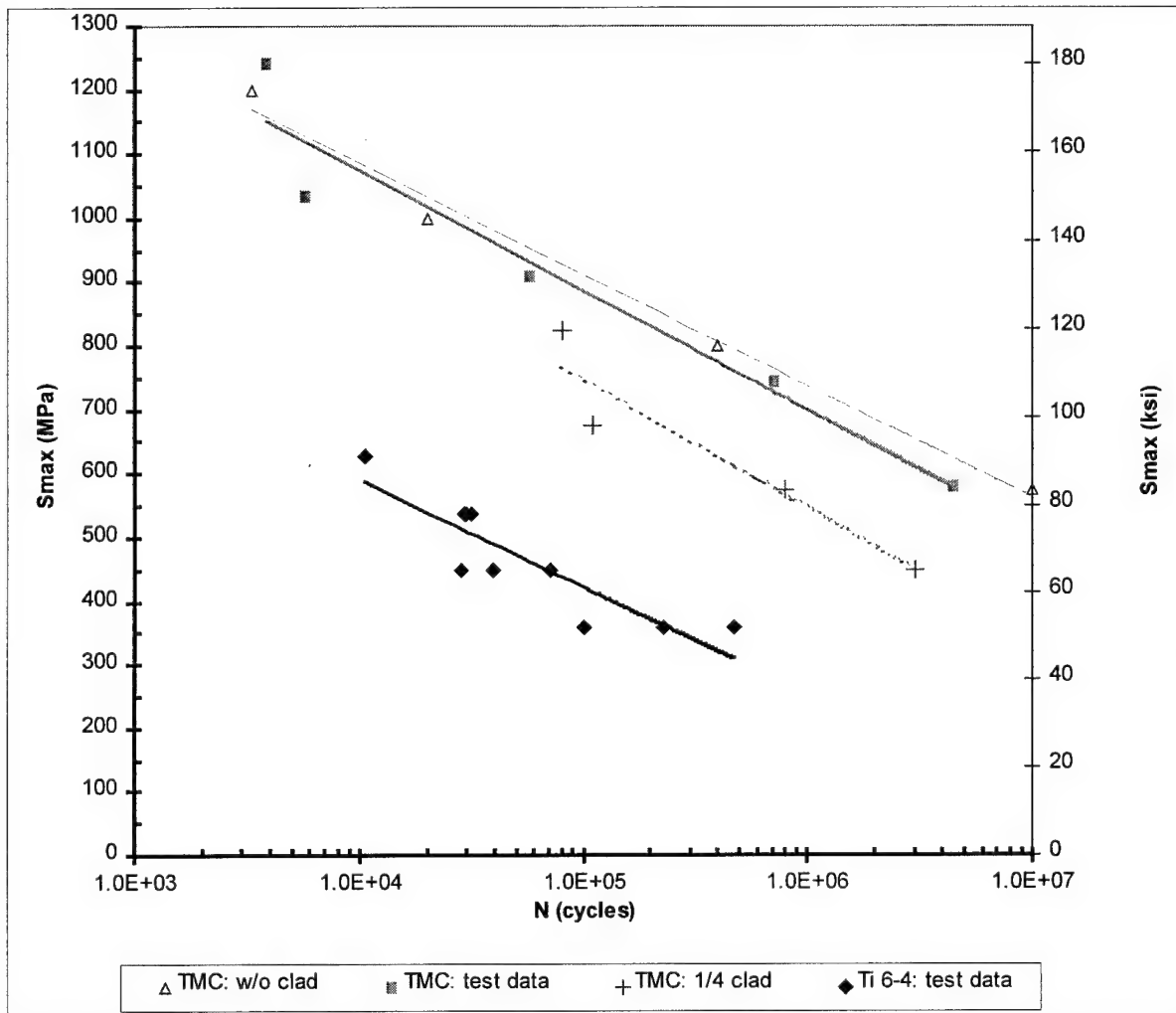


Figure 4.1: Comparison of the S-N curves derived from Ramamurty (TMC and TMC material with a cladding layer 1/8 the thickness of the TMC panel on both sides)

superimposed on the S-N curve for TMC test samples used in the current study (see Figure 4.1). It is evident that there is good correlation between the curves.

Making the hypothesis that the F/G samples would have failed at the joint had they been free of inclusions means that the failure mechanism would have been similar to the cladded material studied by Ramamurty. The one significant difference is the presence of fiber ends: cracks would more likely initiate from the fiber ends and grow simultaneously outward into the monolithic alloy as well as into the TMC section. For the time being, fiber end effects are neglected; as will be explained, this difference does not detract significantly from the hypothesis. With these assumptions in mind, the S-N curve for cladded material indicates what the fatigue life for the F/G samples would have been if there were no inclusions present. This S-N curve is also placed alongside the upper and lower bounds for the fatigue life curve for the sake of comparison (see Figure 4.1).

4.2.10. Comparison and Discussion of S-N Curves

From Figure 4.1, comparing the S-N curve for inclusion-free alloy to that of alloy-clad TMC shows that the fatigue curve for the alloy is appreciably lower than for the cladded TMC. This indicates that for inclusion-free functionally-graded material, the limiting factor for fatigue life will be monolithic alloy. This claim is supported by several factors.

Fiber End Effects: The fiber ends will cause the joint region to have an S-N curve lower than that for the cladded material. This is also true for the monolithic alloy: the

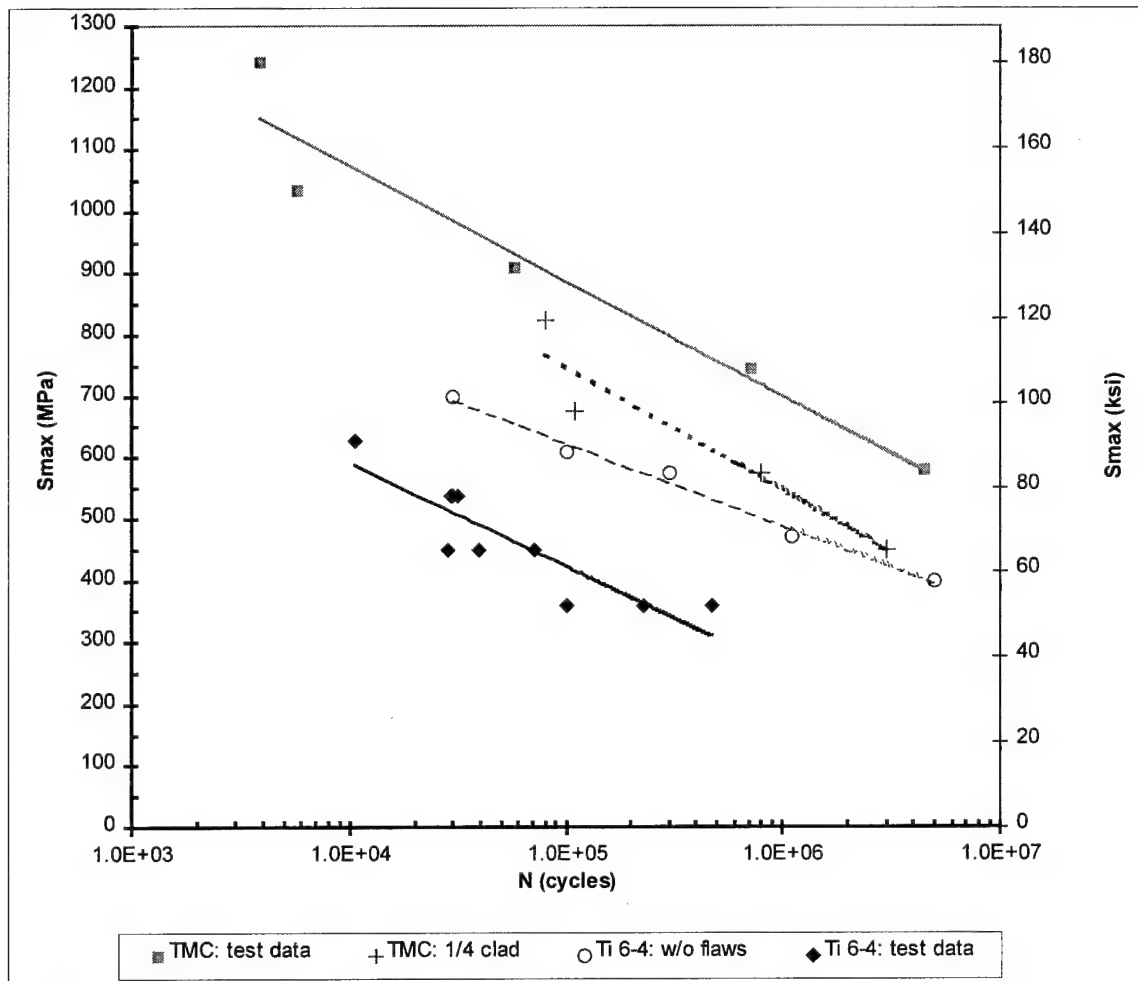


Figure 4.1: Comparison of the S-N curves derived from Ramamurty (TMC with a cladding layer 1/8 the thickness of the TMC panel on both sides) and from Eylon et al. (Ti 6-4 without inclusions) to the results found in this study. It is important to note that the S-N curve for inclusion-free alloy is lower than the curve for the clad TMC, meaning that the functionally-graded specimens used in this study will fail in the alloy section.

“tip” of the scarf joint can be considered as extending into the alloy section. This means that the unreinforced alloy section will have an S-N curve lower than that of the low-contaminant alloy as reported by Eylon et al. The S-N curve for the alloy section should approach (but never attain) the S-N curve for typical titanium due to the presence of fiber ends. Since fiber ends will affect both the joint area and the unreinforced alloy, this study would indicate that the unreinforced alloy section will still remain the weakest part of the material. Therefore, its fatigue life will determine the fatigue life for the entire material.

Strain Effects: During fatigue testing of F/G material, the joint region is stiffer overall than the monolithic alloy. This stiffness varies linearly over the length of the scarf joint. Near the composite section, the stiffness is similar to that of TMC and gradually decreases to the same stiffness as the alloy at the “tip” of the scarf joint. Therefore, the strain value during loading will vary as well. The monolithic section experiences higher strain values than in the composite section or even the joint region. Therefore, the alloy is more sensitive to crack growth due to the higher strain value. In fact, the tip of the scarf joint will experience the same strain value as the alloy section, but with the drawback of having a row of fiber ends present. Strain effect may prove to be the determining factor for fatigue life. Therefore, the maximum strain value could be more important than the maximum stress value in determining other fatigue life properties for F/G TMCs in future testing.

Fracture Location: It then follows that fracture in inclusion-free F/G TMCs should initiate at the tip of the joint region or in the monolithic alloy section adjacent to the tip of

the joint. The joint region and the composite section both benefit from fiber bridging effects and from a lower strain value. Both of these factors act to retard crack growth..

Fatigue Life: Now the bounds for the expected S-N curve for the inclusion-free can be refined. Before, the bounds for the material were the inclusion-containing alloy and the TMC S-N curves, with three orders of magnitude as a gap between them. From the analysis performed above, it is expected that the F/G material S-N curve will fall between that of the inclusion-containing curve derived in this study, and the low-contaminant curve derived from the work of Eylon et al. There is only one order of magnitude between these curves, which is a far better range of resolution than three orders of magnitude. In addition, it is also expected that the inclusion-free F/G S-N curve will approach that of the low-contaminant curve in future testing.

4.3. Fracture Toughness

As a final item of discussion, the inclusions provide an opportunity to determine the fracture toughness of the alloy to verify it matches the values that others have determined for titanium fabricated by powder metallurgy. If for some reason the material used in this study had a lower fracture toughness value, it might invalidate the conclusions stated previously. Therefore, a quick investigation of fracture toughness values is in order. For an embedded circular crack, Sneddon arrived at the following equation to describe the stress concentration factor [50].

$$K_I = \frac{2}{\pi} \sigma \sqrt{\pi a}$$

The shape of the inclusions on most of the fracture surfaces in this study is roughly elliptical rather than circular. Based on the work of Green and Sneddon [51], Irwin derived a useful expression for the stress field around an ellipsoidal cavity [52].

$$K_I = \frac{\sigma\sqrt{\pi a}}{\Phi} \left(\sin^2 \varphi + \frac{a^2}{c^2} \cos^2 \varphi \right)^{\frac{1}{4}}$$

Where a and c are the semi-minor and semi-major axes length of an ellipsoid, respectively, and Φ is an elliptical integral of the second kind, given by

$$\Phi = \int_0^{\pi/2} \left[1 - \frac{c^2 - a^2}{c^2} \sin^2 \varphi \right]^{1/2} d\varphi$$

The elliptical integral can be approximated by taking the first two terms of the expansion series, given by:

$$\Phi = \frac{\pi}{8} \left(3 + \frac{a^2}{c^2} \right)$$

Irwin found that the stress intensity was the largest at the ends of the minor axis (where $\varphi = \pi/2$).

$$K_{I(\varphi=\pi/2)} = \frac{\sigma\sqrt{\pi a}}{\Phi}$$

Approximating the inclusion shapes to be twice as long as they are wide ($a=2c$), then $a^2/c^2 = 4$, and $\Phi = 7\pi/8$. Therefore the max K_I value (at $\varphi=\pi/2$) is equal to

$$K_{I(\varphi=\pi/2)} = \frac{8\sigma\sqrt{\pi a}}{7\pi}$$

Now compare the max K_I evaluated over the length of each inclusion at the appropriate loading value for each sample. This value should be larger than ΔK_{th} for the material if the crack from the inclusion is to propagate through the sample.

Eylon and Froes studied the toughness for titanium powder metallurgy and found ΔK_{th} to be roughly 6.6 to 11 MPa \sqrt{m} (6 to 10 ksi \sqrt{in}), and K_{IC} to be 66 MPa \sqrt{m} (60 ksi \sqrt{in}) [6].

Refer to Figure D.1 in Appendix E for a copy of the diagram used in the Eylon and Froes article. Table 4.1 shows that the toughness values for the alloy at the inclusion sites fall within these values.

5. Conclusions and Recommendations

5.1. Conclusions

Although the characteristics of the functionally-graded titanium matrix composite (F/G TMC) joint region were not determined in as much detail as hoped, this study nonetheless provides valuable insight as to the mechanical properties and behavior of F/G TMCs in general.

- Under tensile loading, the joint region will initiate failure. The deformation mechanism of plasticity in the alloy plays a greater role in failure than does damage in the brittle reaction zone along the fiber ends.
- Although the joint region initiates failure under tensile loading, the properties for the joint are similar to the alloy. Yield and ultimate strength are roughly identical to the monotonic alloy section; whereas the modulus of elasticity is the average of the two parent materials, as determined by the following formula:

$$E_{joint} = c_a E_a + c_c E_c$$

That is, the modulus is equal to the sum of one-half the modulus of the alloy and one-half the modulus of the composite.

- The exact fatigue properties for the functionally-graded titanium matrix composite are bounded by the S-N curves established in this research: fatigue life will not be lower

than the inclusion-filled alloy, and not be higher than for an all-composite material.

In addition, the fatigue life of the monotonic alloy section is expected to determine the overall fatigue life of inclusion-free functionally-graded material.

- The joint region is more robust than was expected. The functionally-graded material is more sensitive to strain values in the monolithic alloy section than to fiber ends in the joint region.
- Since the weakest part of the functionally-graded material is the monolithic alloy section, the taper angle has little effect on the overall properties of the material.

5.2. Recommendations

Some slight design modifications to the test material may prove beneficial to future testing of this material. The current material has the joint at the midsection of the panel. As was demonstrated, even a tiny inclusion anywhere in the length of the monolithic section can propagate failure. A better plate design, having a smaller monolithic section (offset the joint so that the panel is 80% composite, 20% monolithic alloy), will reduce the probability of an inclusion in the monolithic section (see Figure 5.1). This would yield stronger material and allow better examination of the joint area properties.

It may be beneficial to conduct future testing of this material using the strain-controlled condition rather than the load-controlled condition in order to determine if strain effects in the alloy do indeed determine the overall fatigue life of this material.

Although the fatigue life curve was not directly determined due to the effect of inclusions, this study nevertheless revealed basic mechanical properties and behavior for the joint region as well as for the overall material. This study has set the foundation for further research. Will future fabrication improvements or other material vendors yield a more suitable material? Even with better material, will the premise that the alloy section determines the fatigue life (and not the joint region) hold true? And with inclusion-free material, can previous analytical models accurately describe and provide insights onto the behavior of functionally-graded material? Additional research should be conducted to answer these questions.

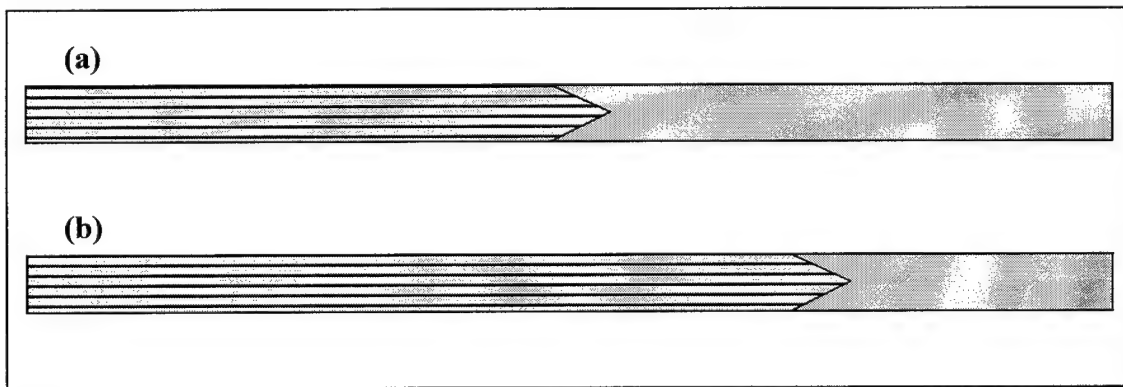


Figure 5.1: F/G TMC Test samples. **(a)** current design, and **(b)** a design less sensitive to inclusions in the monolithic section. Decreasing the volume for the monolithic section also decreases the statistical probability of encountering a failure-causing inclusion.

Appendix A: Additional Graphical Results of Tensile Testing

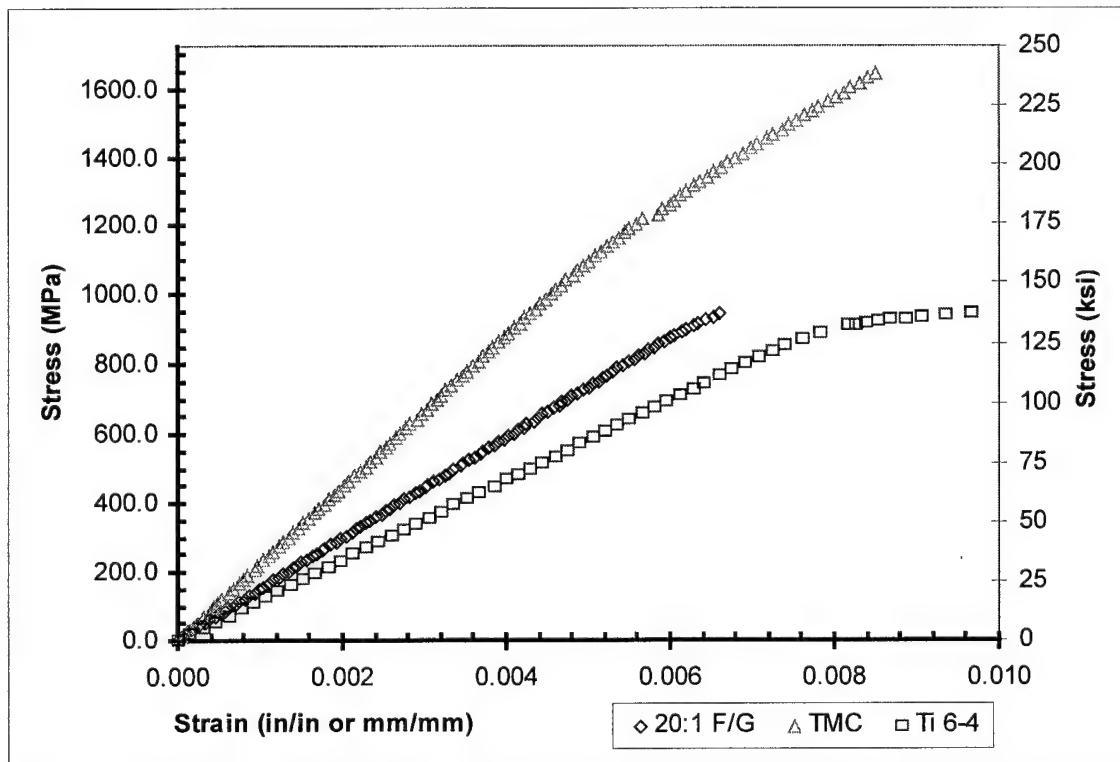


Figure A.1: Stress-strain curve for the 20:1 taper hybrid (Specimen #203) as compared to the stress-strain curves for TMC and monolithic alloy (monotonic tensile testing)

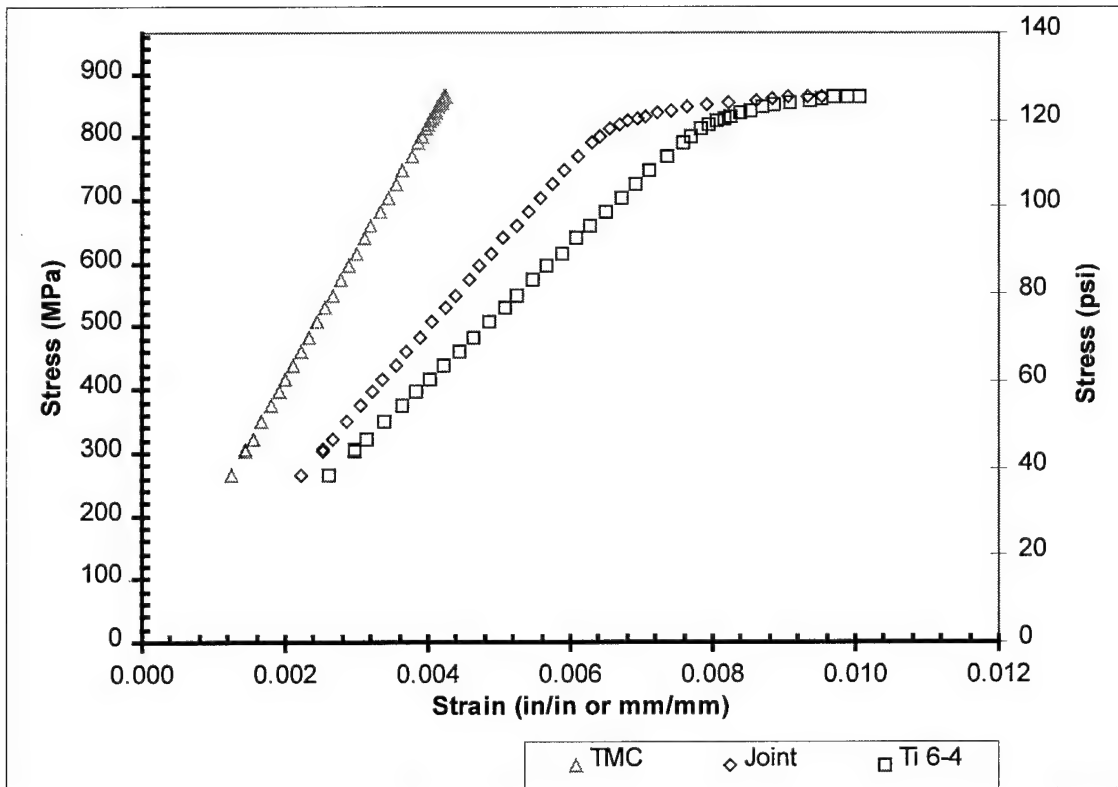


Figure A.2: Stress-strain curve for the 4:1 taper hybrid (Specimen #199). Data was collected from the forth (and final) set of interrupted tensile testing. Strain values for TMC and alloy displayed above were taken from strain gage measurements on the respective sections of the F/G material.

Appendix B: Additional SEM Images of Fracture Surfaces

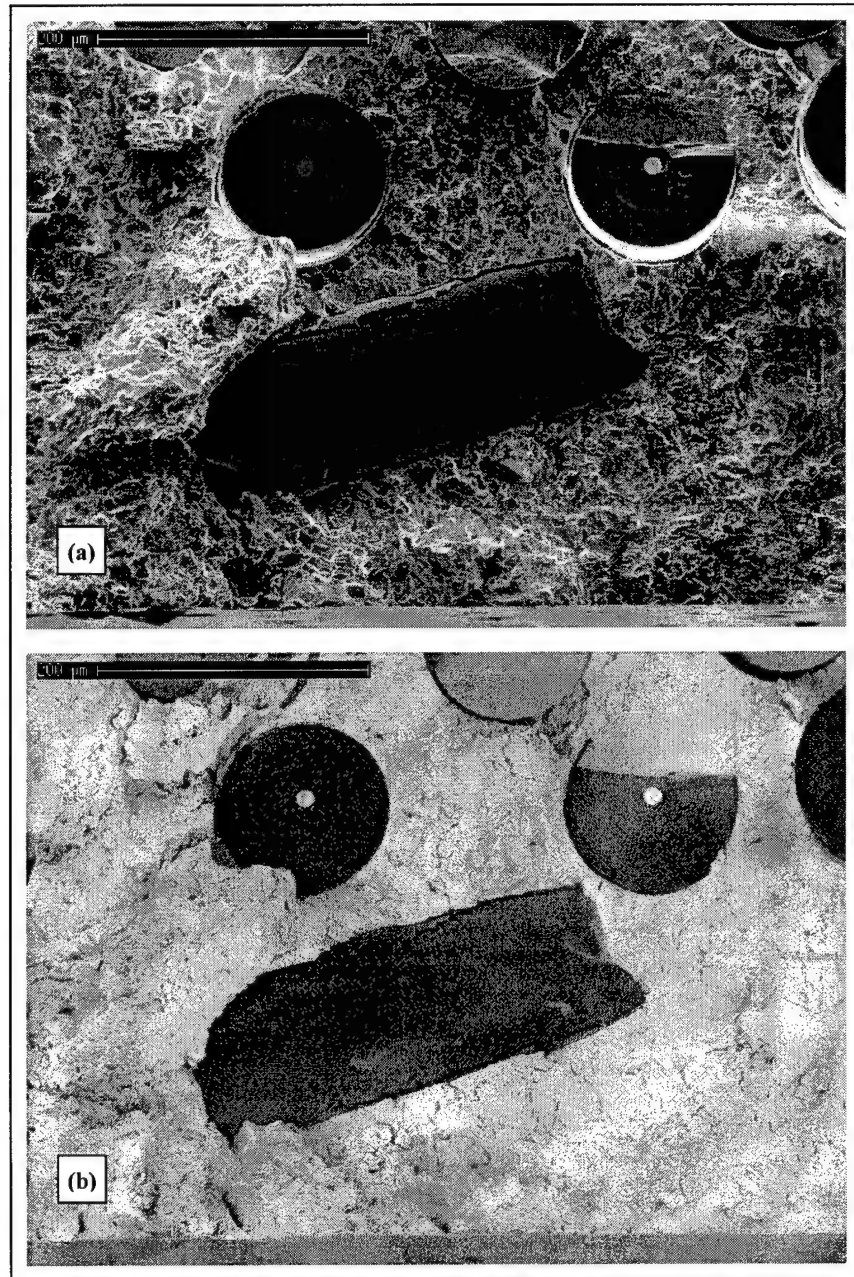


Figure B.1: (a) SEM and (b) RBS Close-up of the silicon shard on the Specimen A2 fracture surface, showing that it did not propagate a single large crack. Note roughness of matrix material, indicating matrix cracking.

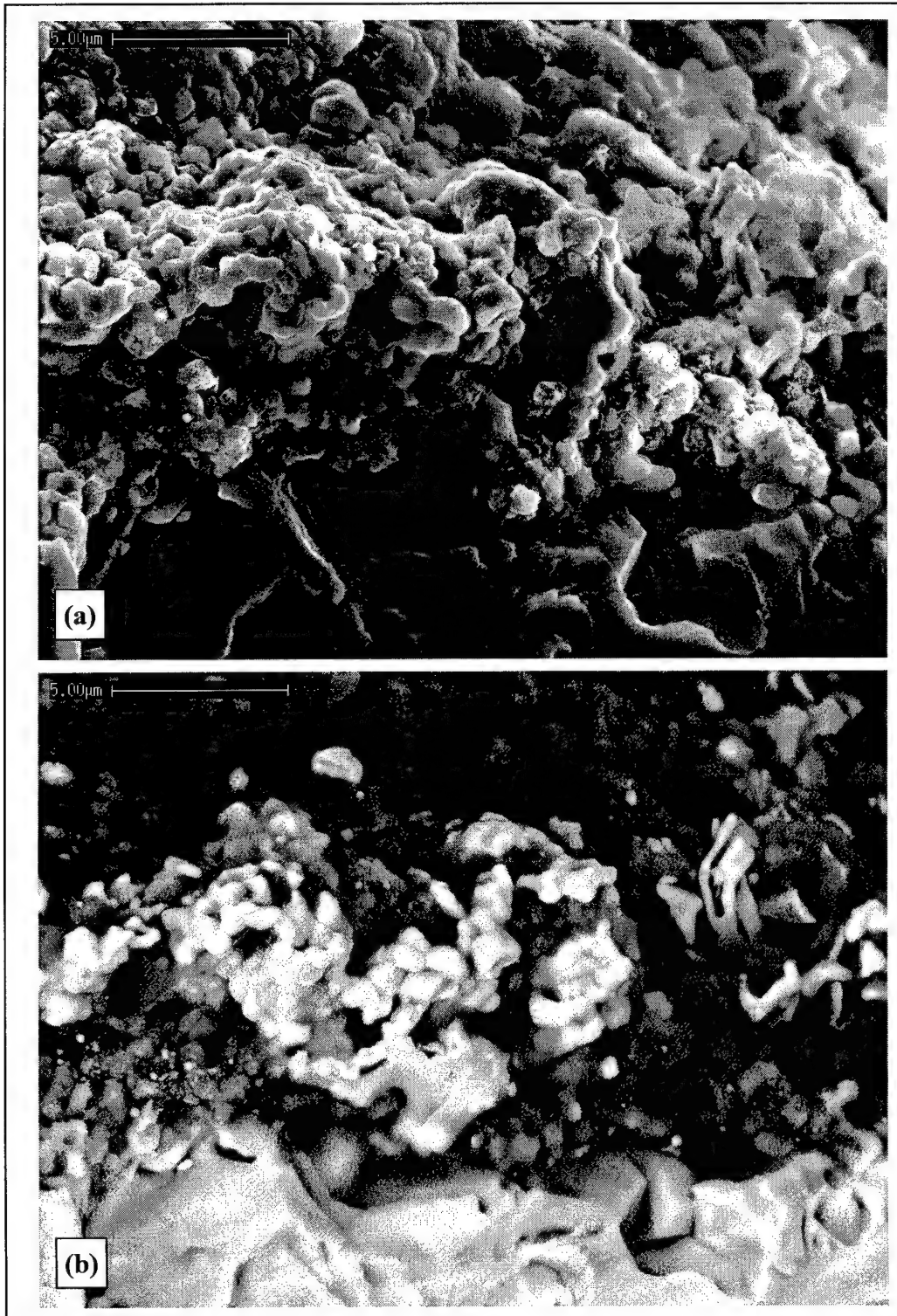


Figure B.2: Close-up of the magnesium-titanium transition region on the Specimen B2 fracture surface flaw under (a) SEM and (b) RBS.

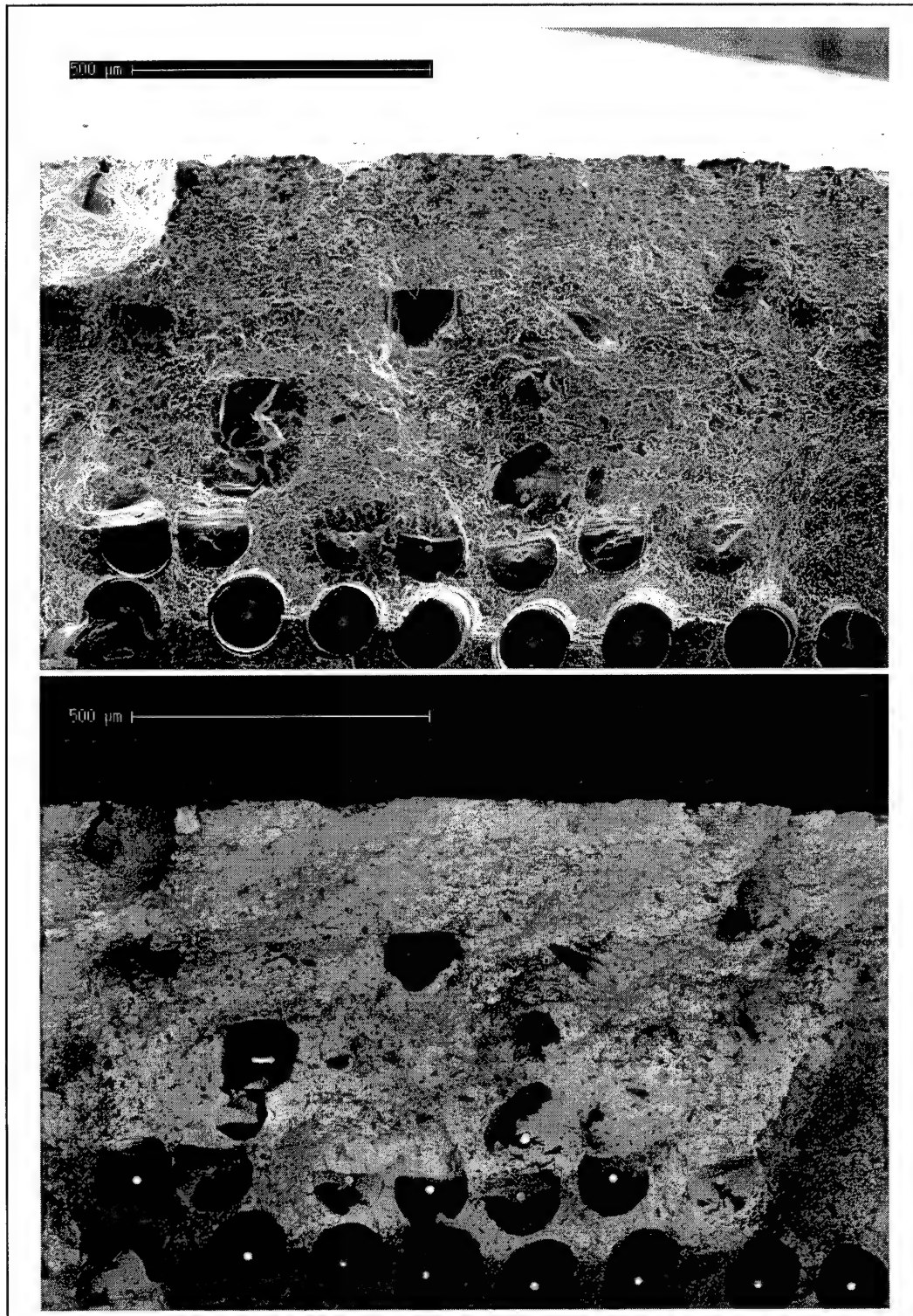


Figure B.3: Detail view of upper right corner of Specimen 200 fracture surface. Note that these fiber shards in the monolithic section did not initiate cracks, as did the other shard, since they were aligned with the loading direction.

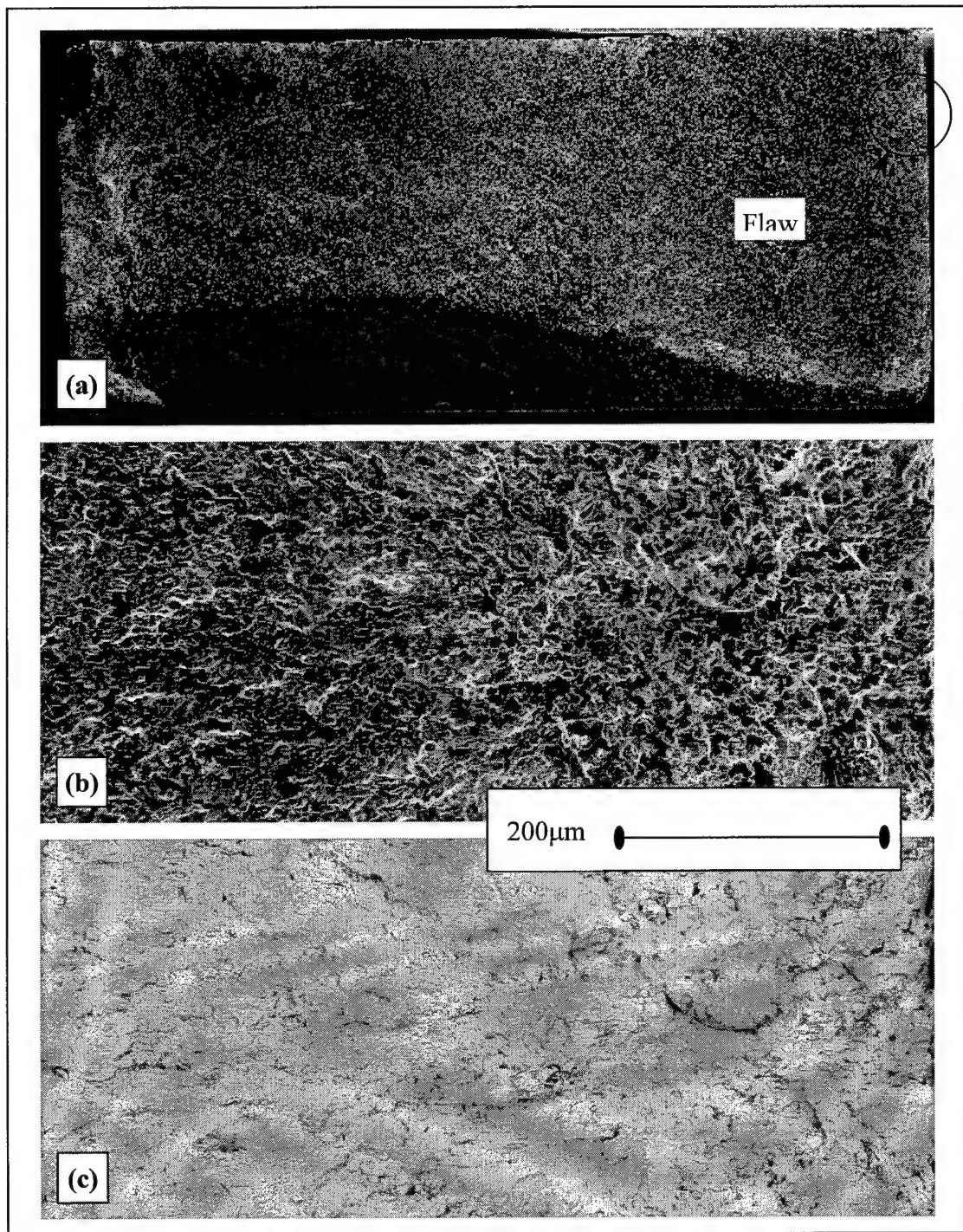


Figure B.4: (a) Overview of Specimen C5 (monolithic alloy) fracture surface. Specimen was fatigue tested at 360 MPa (52 ksi) and failed at 227k cycles. Note crack propagated from near the top right corner. Neither the inclusion site nor crack radiation are markedly apparent in (b) SEM imaging, but both are very noticeable using (c) backscattering imaging.

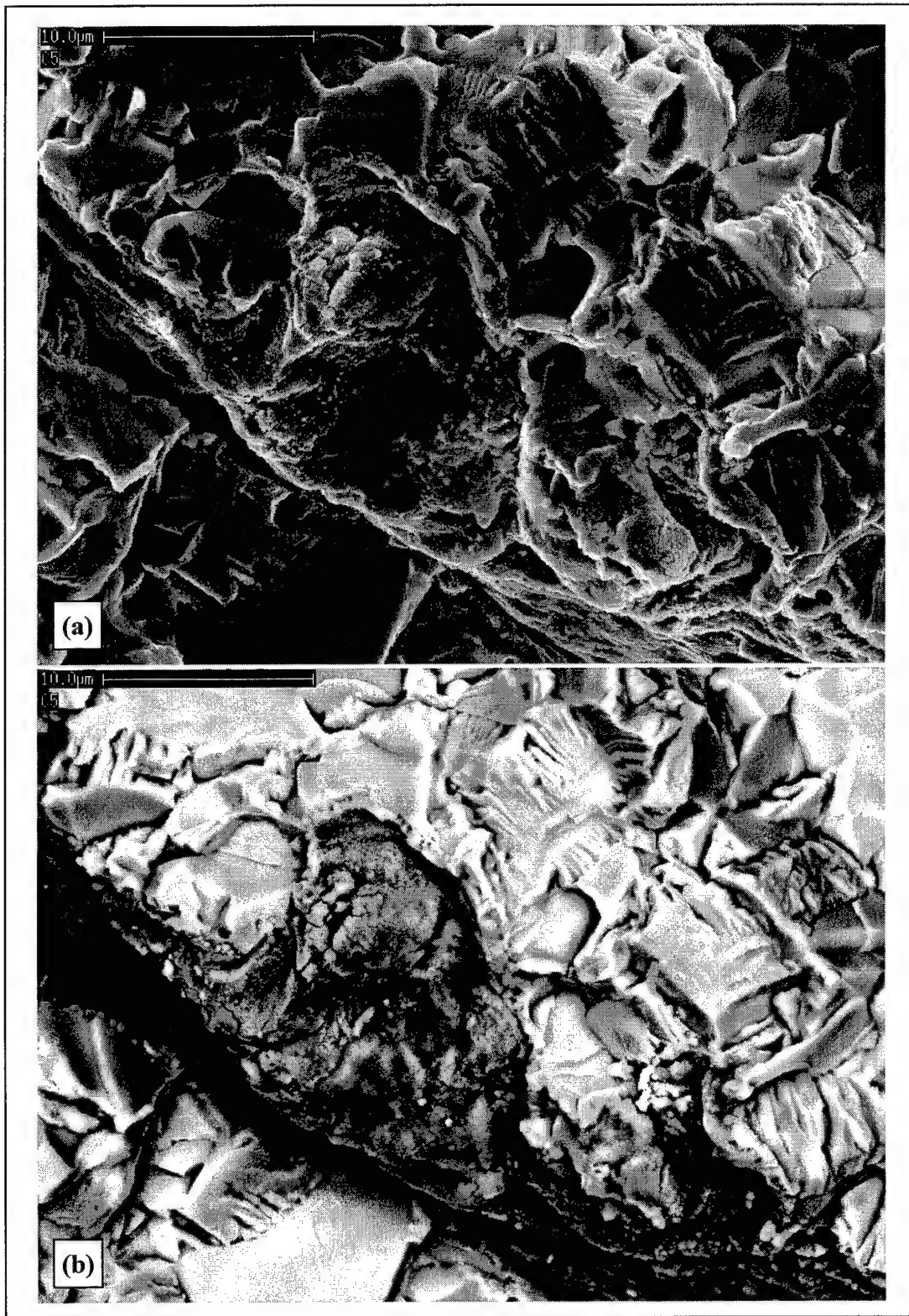


Figure B.5: Close-up of flaw on C5 fracture surface using (a) SEM and (b) RBS imaging. What appears to be a void in SEM is revealed as an inclusion (rough, dark gray area) of calcium. The white flecks in the inclusion are tungsten.

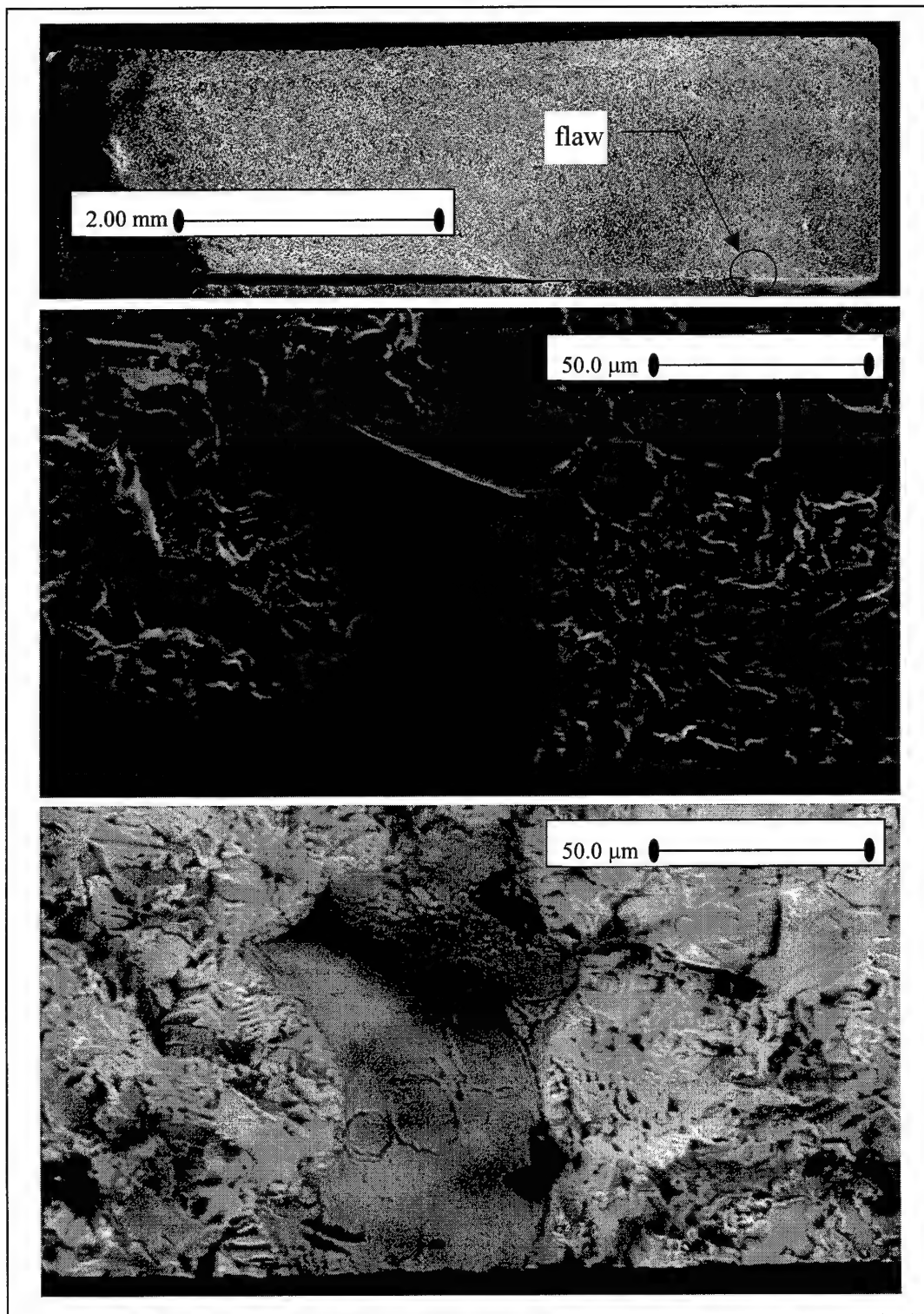


Figure B.6: Overview and detail view of Specimen B1 (20:1 taper) fracture surface, subject to 360 MPa (52 ksi) tension-tension fatigue testing. Failure occurred at 101k cycles. A close-up of the crack nucleation site shows that the conclusion fell out after fracture. Trace amounts of calcium and magnesium were evident in the reaction zone left behind

Appendix C: X-ray Spectroscopy of Inclusions

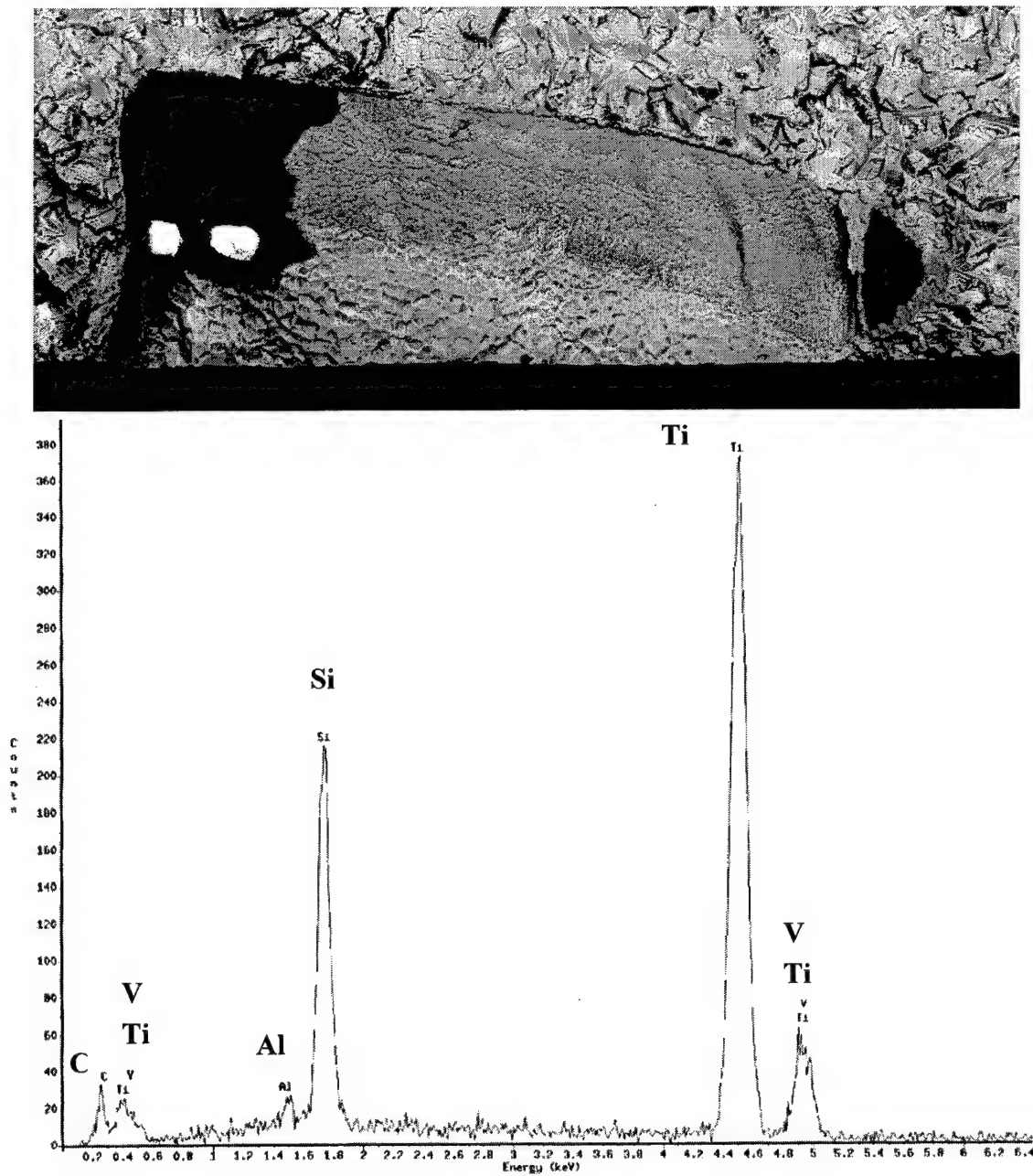


Figure C.1: Reaction zone chemical composition of Specimen 200 inclusion (fiber shard)

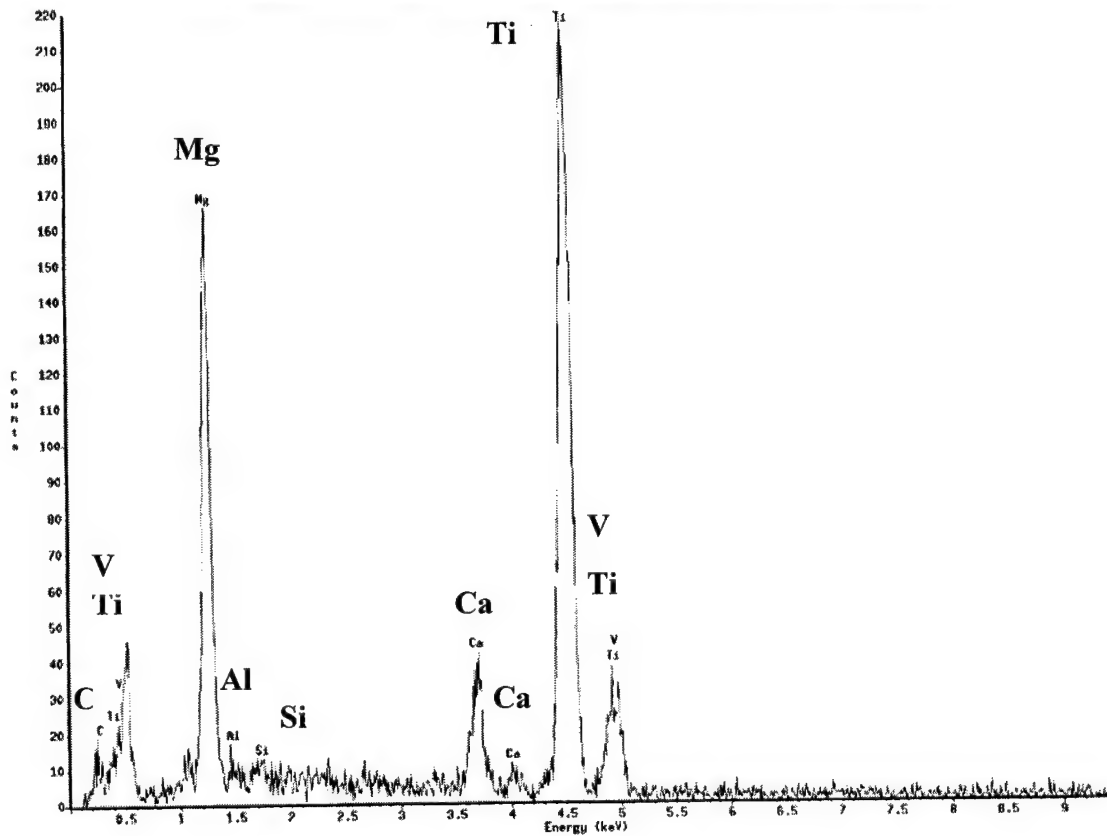
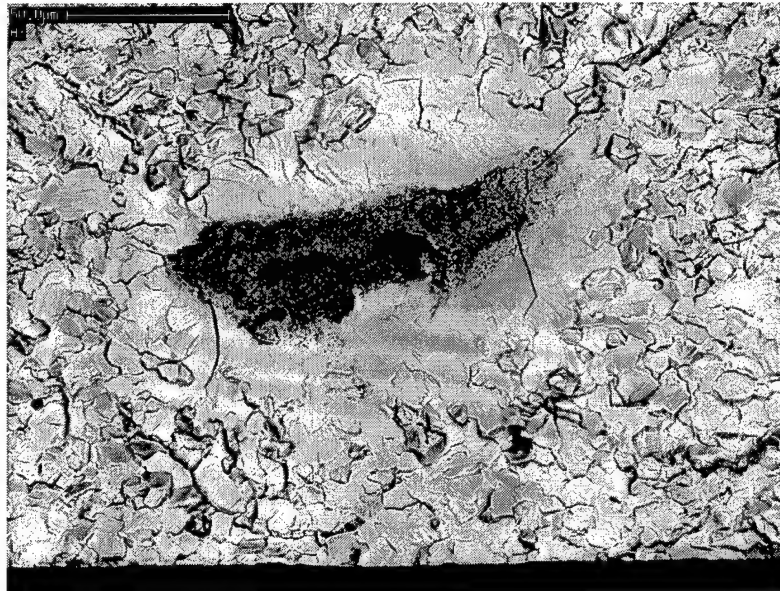


Figure C.2: Specimen A3 inclusion chemical composition

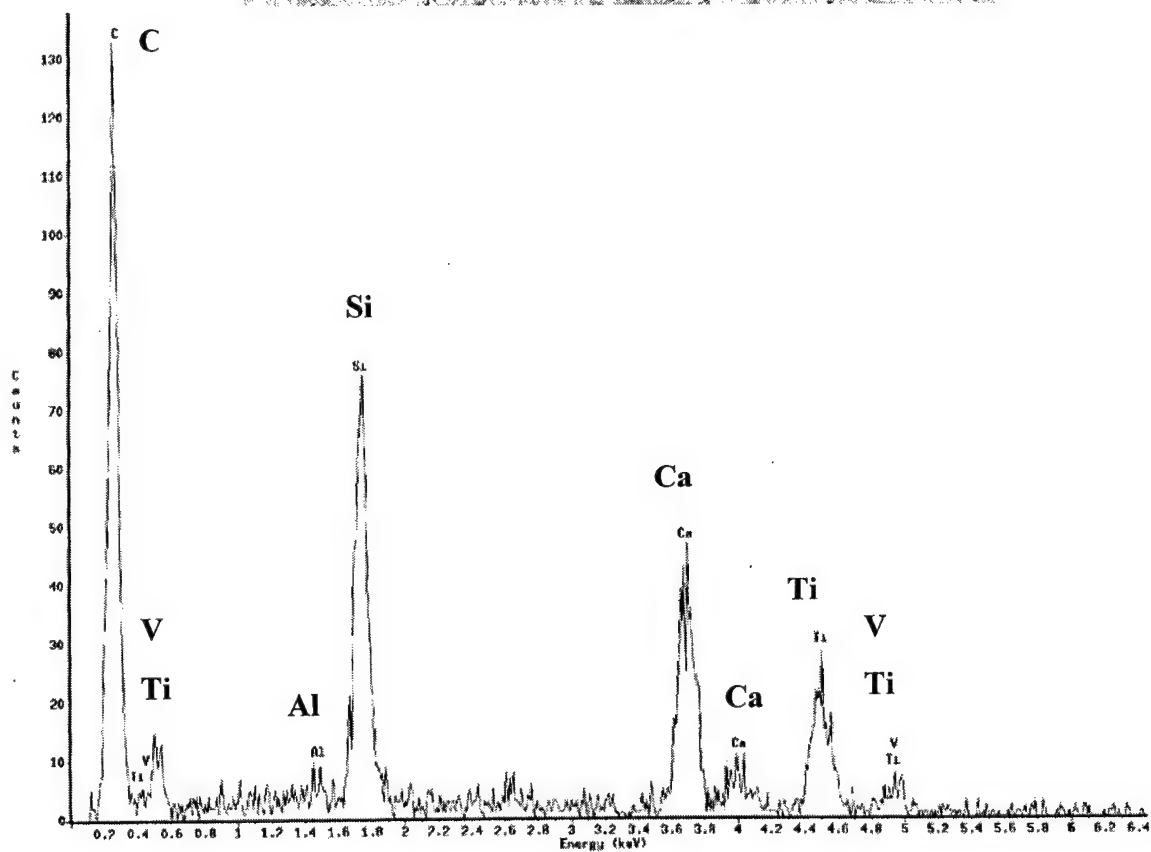
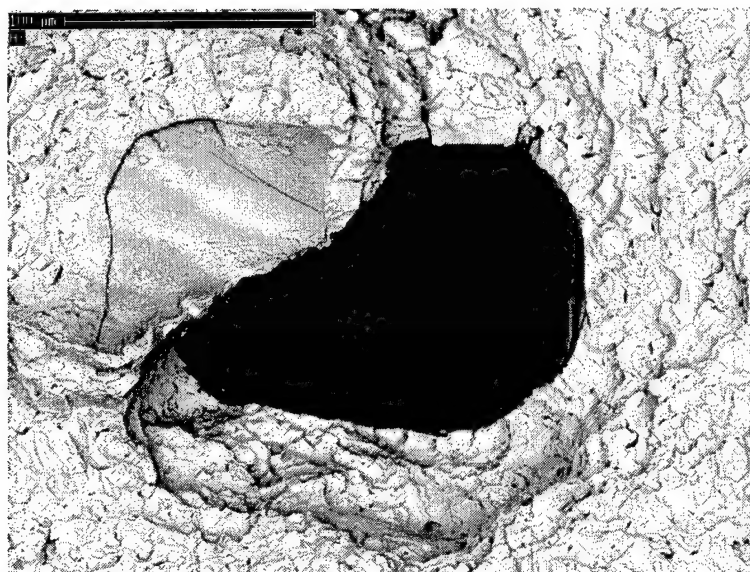


Figure C.3: Specimen A3 fiber shard chemical composition

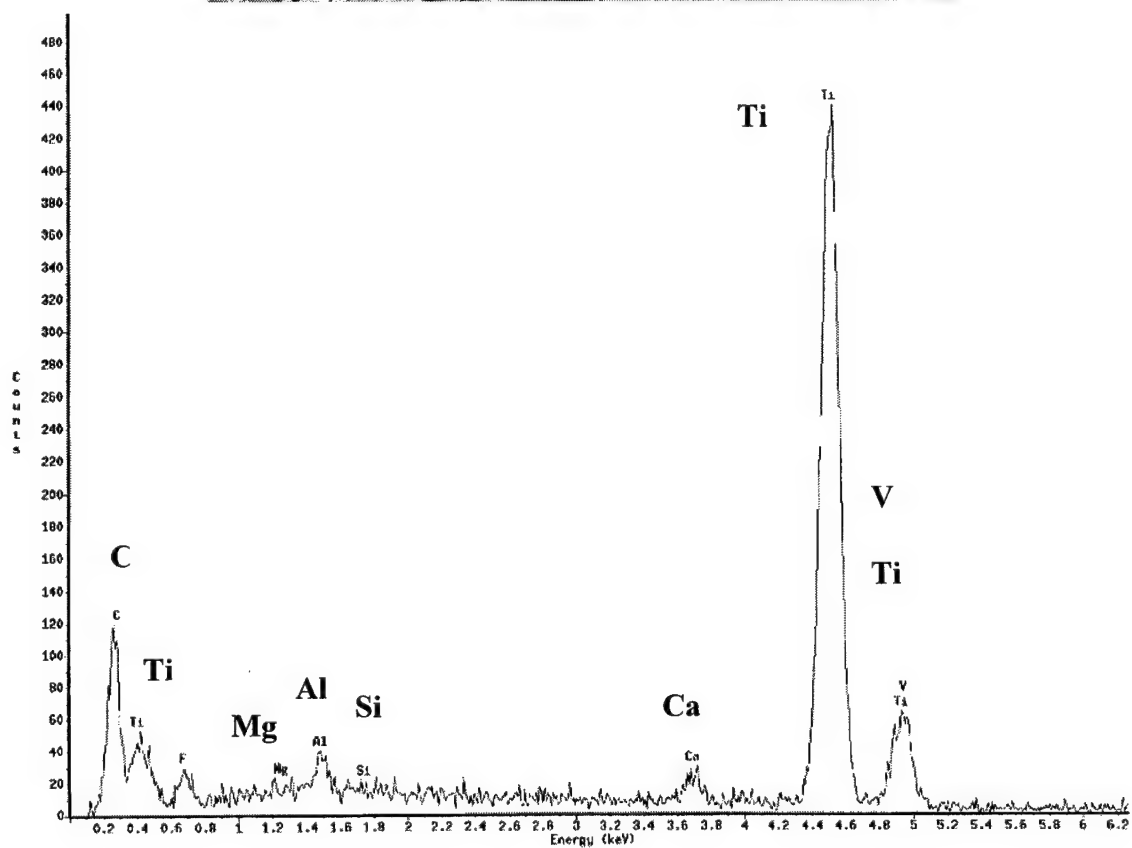
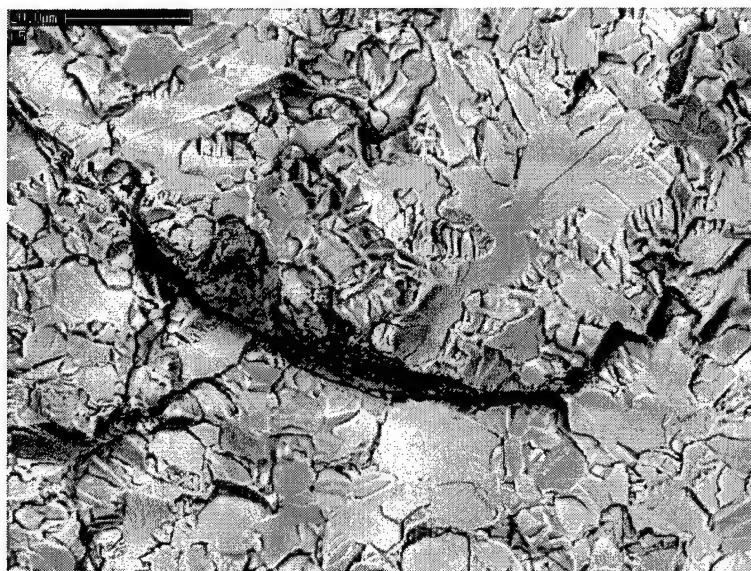


Figure C.4: Specimen C5 flaw chemical composition (inclusion reaction zone).

Appendix D: Comparison of Toughness and Fatigue

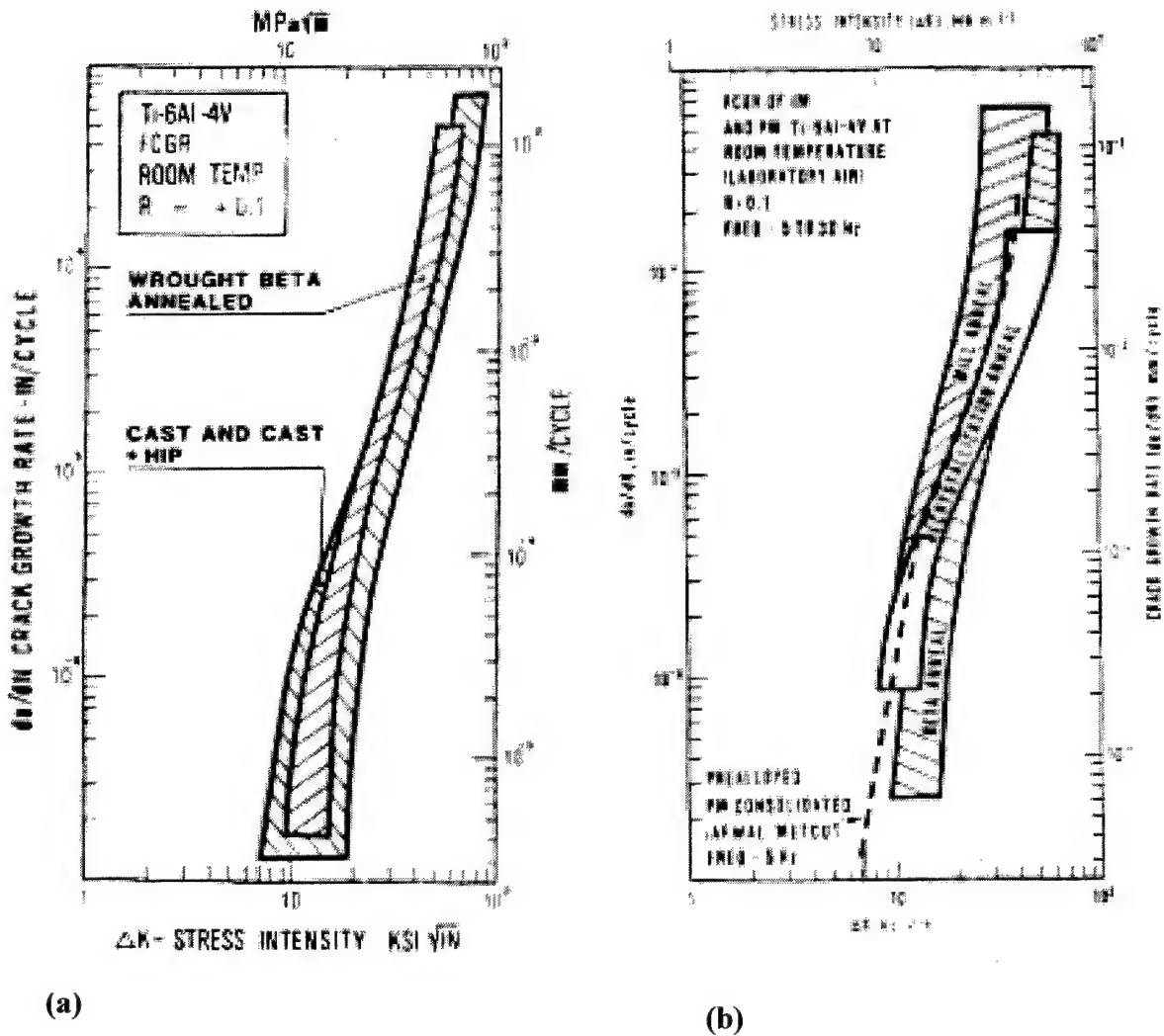


Figure D.1: (a) Scatterband comparison of room temperature fatigue crack growth rate (FCGR) of cast or cast+HIP Ti-6Al-4V with beta-annealed wrought material. (b) Comparison of FCGR of PM PA and IM Ti-6Al-4V (taken from Froes F. H. and Eylon, E, "Application of HIP-ing to Titanium-Based Materials, *Proceedings of 4th International Conference on Isostatic Pressing*, 1990, pp. 16-1 to 16-24).

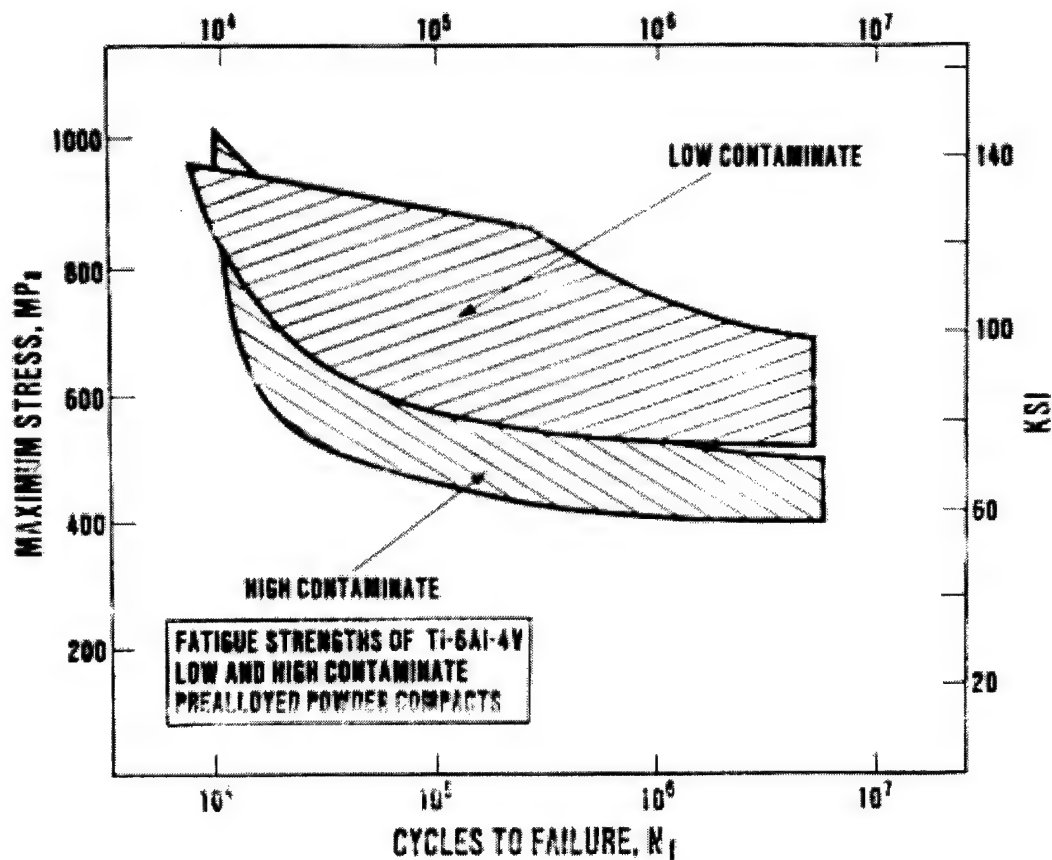


Figure D.2: Comparison of fatigue life of Ti-6Al-4V PA, high and low contaminate (taken from Froes F. H. and Eylon, E, "Application of HIP-ing to Titanium-Based Materials, *Proceedings of 4th International Conference on Isostatic Pressing*, 1990, pp. 16-1 to 16-24).

Vita

Captain G. Brandt Miller was born July 9, 1970 in Lincoln, Nebraska. He graduated from Monticello High School, Monticello, Utah, in 1988, and earned a Bachelor of Science in Mechanical Engineering from Brigham Young University, Provo, Utah in 1995. He received his commission as a Second Lieutenant that same year through the Reserve Officer Training Corps program. His first assignment was at the Air Force Research Laboratory (previously known as Phillips Laboratory) at Kirtland AFB, NM, where he served as a satellite payload engineer and division-level executive officer. He entered the Air Force Institute of Technology, Graduate School of Engineering, in August 1998 and was promoted to Captain in May 1999.

Permanent Address: PO Box 760
Monticello, UT 84535

Bibliography

1. Mall, S. and Nicholas, T., editors, *Titanium Matrix Composites: Mechanical Behavior*, pub. by Technomic Publishing Co., Inc., 1998.
2. Mall, S. and Robertson, D. D., "Mechanics of Integrally Fabricated Joint between Reinforced Titanium Matrix Composite and Monolithic Titanium Alloy," Research Proposal to AFOSR, 1998.
3. Shea, M. A., and Macy, M. A., "The Low Lifecycle Cost Landing Gear, Phase III: Technology Transition Plan," WL-91-3045, July 1991.
4. Mittnick, M. A., "Continuous SiC Fiber Reinforced Metals," *Proceedings of the 35th International SAMPE Symposium*, Covina, CA, 2-5 April 1990, pp. 1372-1382
5. Froes, F. H. and Eylon, D., "Application of HIP-ing to Titanium-Based Materials," *Proceedings of the 4th International Conference on Isostatic Pressing*, 1990, pp. 16-1 to 16-26.
6. Froes, F. H. and Eylon, D., "Powder Metallurgy of Titanium Alloys – A Review," *Titanium Technology: Present Status and Future Trends*, ed. by Froes, F. H. and Eylon, D., and Bomberger, H. B., pub. by Titanium Development Association, 1990, pp. 49-59.
7. Peebles, R. E. and Kelto, C. A., "Investigation of Methods for the Production of High Quality, Low Cost Titanium Alloys," *Powder Metallurgy of Titanium Alloys*, ed. by Froes, F. H. and Smugeresky, J. E., pub. by the Metallurgical Society of AIME, 1980, pp. 47-58
8. DeVillard, J. and Herteman, J. P., "Evaluation of Ti-6Al-4V Powder Compacts Fabricated by the PSV Process," *Powder Metallurgy of Titanium Alloys*, ed. by Froes, F. H. and Smugeresky, J. E., pub. by the Metallurgical Society of AIME, 1980, pp. 59-70
9. Vaughan, R.F. and Blekinsop, P. A., "A Metallurgical Assessment of Ti-6Al-4V Powder," *Powder Metallurgy of Titanium Alloys*, ed. by Froes, F. H. and Smugeresky, J. E., pub. by the Metallurgical Society of AIME, 1980, pp. 83-92
10. Eylon, D., Mahajan, Y., Ontko, N. R., and Froes, F. H., "Fatigue Crack Initiation of Titanium Alloy Powder Compacts," *Powder Metallurgy of Titanium Alloys*, ed. by Froes, F. H. and Smugeresky, J. E., pub. by the Metallurgical Society of AIME, 1980, pp. 93-102

-
11. Mall, S. and Nicholas, T., editors, *Titanium Matrix Composites*, Technomic Pub., 1997, pp. 5-20.
 12. Clyne, T. W. and Watson, M. C., "Interfacial Mechanics in Fibre-Reinforced Metals," *Composites Science and Technology*, Vol. 42, 1991, pp. 25-55.
 13. Boyum, E. A., "Investigation of Tension-Compression Fatigue of a Cross-Ply $[0/90]_{2s}$ Metal Matrix Composite at Room and Elevated Temperature," MS Thesis, AFIT/GAE/ENY/93D-06, Graduate School of Engineering, Air Force Institute of Technology (AU), Wright-Patterson AFB, OH, December 1993.
 14. Kraabel, D. L., "Investigation of Tension-Compression Fatigue Behavior of a Unidirectional Metal Matrix Composite at Elevated Temperature," MS Thesis, AFIT/GAE/ENY/94D-16, Graduate School of Engineering, Air Force Institute of Technology (AU), Wright-Patterson AFB, OH, December 1994.
 15. Pittman, R. N., "Frequency Effects on Fatigue Behavior of a Unidirectional Metal Matrix Composite at Elevated Temperatures," MS Thesis, AFIT/GAE/ENY/95D-20, Graduate School of Engineering, Air Force Institute of Technology (AU), Wright-Patterson AFB, OH, December 1995.
 16. Mall, S. and Ermer, P.G., "Thermal Fatigue Behavior of a Unidirectional SCS6/Ti-15-3 Metal Matrix Composite," *Journal of Composite Materials*, Vol. 25, December 1991, pp. 1668-1688.
 17. Dennis, L. B., "Fatigue Behavior of a Cross-Ply Metal Matrix Composite at Elevated Temperature under Strain-Controlled Mode," MS Thesis, AFIT/GAE/ENY/94D-07, Graduate School of Engineering, Air Force Institute of Technology (AU), Wright-Patterson AFB, OH, December 1994.
 18. Jeng, S. M., Jeng, C. J., and Yang, J. M., "Fracture Mechanisms of Fiber-reinforced Titanium Alloy Matrix Composites, Part I: Interfacial Behavior," *Materials Science and Engineering*, Vol. A138, 1991, pp. 155-167
 19. Jeng, S. M., Jeng, C. J., and Yang, J. M., "Fracture Mechanisms of Fiber-reinforced Titanium Alloy Matrix Composites, Part III: Toughening Behavior," *Materials Science and Engineering*, Vol. A138, 1991, pp. 181-190
 20. Jeng, S. M., Alasoeur, P., and Yang, J. M., "Fracture Mechanisms of Fiber-reinforced Titanium Alloy Matrix Composites, Part II: Tensile Behavior," *Materials Science and Engineering*, Vol. A138, 1991, pp. 169-180
 21. Ochiai, S. and Osamura, K., *Interfaces in Polymer, Ceramic, and Metal Matrix Composites*, ed. By Ishida, H, 1988, pp. 413-423

-
22. Ochiai, S. and Osamura, K, *Metallurgical Transactions A*, Vol. 21, 1990, pp. 971-977
 23. Majumdar, B. S. and Newaz, G. M., "Fatigue of a SCS-6/Ti 15-3 Metal Matrix Composite," Batelle Memorial Institute, Columbus, OH, 1993.
 24. Johnson, W. S., Lubowinski, S. J., and Highsmith, A. L., "Mechanical Characterization of Unnotched SCS-6/Ti-15-3 Metal Matrix Composites at Room Temperature," *Thermal and Mechanical Behavior of Metal Matrix and Ceramic Matrix Composites*, ASTM STP 1032, ed. by Johnson, W. S., pub. by ASTM, 1989, pp. 194-221
 25. Jeng, S. M. et al., "Fracture Mechanisms of Fiber-reinforced Titanium Alloy Matrix Composites, Part IV: Low-Cycle Fatigue," *Materials Science and Engineering*, Vol. A148, 1991, pp. 67-77
 26. Lerch, B. A., "Matrix Plasticity in SiC/Ti-15-3 Composite," NASA TM 103760, July 1991.
 27. Majumdar, B. S. and Newaz, G. M., "A Comparison of Mechanical Response of MMC at Room and Elevated Temperatures," Batelle Memorial Institute, Columbus, OH.
 28. Lerch, B. A. and Halford, G. R., "Fully Reversed Fatigue of a Ti-MMC," *Proceedings of the 17th Annual Conference on Composites, Materials, and Structures (Restricted Sessions)*, January 1993.
 29. Johnson, W. S., Mirdamadi, M., and Bakuckas Jr., J. G., "Fatigue of Continuous Fiber Reinforced Metallic Metals," NASA Langley Research Center, 1993.
 30. Majumdar, B. S. and Newaz, G. M., "Inelastic Deformation of Metal Matrix Composites: Plasticity and Damage Mechanisms," *Philosophical Magazine*, Vol. 66, No. 2, 1992, pp. 187-212.
 31. Nutt, S. R. and Needleman, A., "Void Nucleation at Fibre Ends in Al-SiC Composites," *Scripta Metallurgica*, Vol. 21, 1987, pp. 705
 32. Aveston, J. and Kelly, A., "Theory of multiple fracture of fibrous composites," *Journal of Materials Science*, Vol. 8, 1973, pp. 352-362.
 33. Solti, J. P., Mall, S., and Robertson, D. D., "Modeling Damage in Unidirectional Ceramic-Matrix Composites," *Composites Science and Technology*, Vol. 54, 1995, pp. 55-66.

-
34. Aboudi, J., "Closed Form Constructive Equations for Metal Matrix Composites," *International Journal of Engineering Science*, Vol.25, 1987, pp. 1229-1240.
 35. Newaz, G. M., "Monotonic Response," Titanium Matrix Composites, ed. by Mall, S. and Nicholas, T., pub. by Technomic Publishing Co., 1997, pp.23-66.
 36. Ahmad, J. and Nicholas, T., "Modeling of Inelastic Metal Matrix Composite Response under Multiaxial Loading," *ASME Symposium on Failure Mechanisms and Mechanism Based on Modeling High Temperature Composites*, ASME Winter Annual Meeting, Atlanta, GA, November 1996.
 37. Dvorak, G. J., Bahei-El-Din, Y. A., and Zuiker, J. R., "Micromechanical Theories," Titanium Matrix Composites, ed. by Mall, S. and Nicholas, T., pub. by Technomic Publishing Co., 1997, pp.69-111.
 38. Robertson, D. and Mall, S., "Micromechanical Analysis and Modeling," *Titanium Matrix Composites*, ed. by Mall, S. and Nicholas, T., pub. by Technomic Publishing Co., 1997, pp.397-464.
 39. Anoshkin, N. F., Gelman, A. A., and Pavlov, V. M., "Some Aspects of Formation of Joints of Various Configurations During Diffusion Bonding of Two-Phase Titanium Alloys," *Titanium '92: Science and Technology*, Vol. 2, 1992, ed. by Froes, F. H., and Caplan, I. L., pub. by TMS, pp. 1445-1452
 40. Ramamurty, U., "Fatigue in Selectively Fiber-Reinforced Titanium Matrix Composites," *Metallurgical and Materials Transactions*, Vol. 30A, August 1999, pp. 2237-2248.
 41. Spear, S., E-mail communication, 25 October 1999.
 42. Spear, S., E-mail communication, 13 November 1999.
 43. Roberts, P. R. and Loewenstein, P., "Titanium Alloy Powders Made by the Rotating Electrode Process," *Powder Metallurgy of Titanium Alloys*, ed. by Froes, F. H. and Smugeresky, J. E., pub. by the Metallurgical Society of AIME, 1980, pp. 21-35
 44. Scarich, G. V., Chanani, G. R., Petersen, V. C., and Weaver, D. M., "Relationship between Mechanical Properties, Contaminants, and Fracture Topography of HIP Ti-6Al-4V Powder Metallurgy Products," *Powder Metallurgy of Titanium Alloys*, ed. by Froes, F. H. and Smugeresky, J. E., pub. by the Metallurgical Society of AIME, 1980, pp. 103-114
 45. Eylon, D., Personal communication, 12 January 2000

-
46. Sears, J. W., Itoh, G. and Loretto, M. H., "Spray Forming of Ti-Al-Based Alloys," *Titanium '92: Science and Technology*, Vol. 2, 1992, ed. by Froes, F. H., and Caplan, I. L., pub. by TMS, pp. 987-994
 47. Gerling, R., Schimansky, F. P., and Wagner, R., "A Novel Inert Gas Atomization Facility for the Production of Intermetallic Titanium-Based Alloy Powders," *Titanium '92: Science and Technology*, Vol. 2, 1992, ed. by Froes, F. H., and Caplan, I. L., pub. by TMS, pp. 1025-1032
 48. Yolton, C. F. and Eylon, D., "Effects of Processing and Heat Treatment on Mechanical Properties of Gamma Titanium Aluminide Powder Compacts," *Titanium '92: Science and Technology*, Vol. 2, 1992, ed. by Froes, F. H., and Caplan, I. L., pub. by TMS, pp. 1083-1090
 49. Spear, S., Personal and e-mail communication, 21 January 2000
 50. Sneddon, I. N., "The distribution of stress in the neighbourhood of a crack in an elastic solid," *Proceedings of the Royal Society of London*, Vol. 187A, 1946, pp. 229-260.
 51. Green, A. E. and Sneddon, I. N., "The stress distribution in the neighbourhood of a flat elliptical crack in an elastic solid," *Proceedings of the Cambridge Philosophical Society*, Vol. 46, 1950, pp. 159-164.
 52. Irwin, G. R., "The crack extension force for a part-through crack in a plate," *Transcripts, AMSE Journal of Applied Mechanics*, 1962, pp. 651-654.